PARTICULATE ORGANIC MATTER (POM) EXPORT FROM CATCHMENTS: ROLE OF PARTICLE SIZE, SOURCES, HEADWATER DRAINAGE AREA AND STORM EVENT MAGNITUDE

by

R. Douglas Rowland

A thesis submitted to the Faculty of the University of Delaware in partial fulfillment of the requirements for the degree of Master of Science in Water Science and Policy

Summer 2016

PARTICULATE ORGANIC MATTER (POM) EXPORT FROM CATCHMENTS: ROLE OF PARTICLE SIZE, SOURCES, HEADWATER DRAINAGE AREA AND STORM EVENT MAGNITUDE

by

R. Douglas Rowland

Approved: _____
Shreeram P. Inamdar, Ph.D.
Professor in charge of thesis on behalf of the Advisory Committee

Approved: _____
Shreeram P. Inamdar, Ph.D.
Director of the program of Water Science and Policy

Approved: _____
Mark W. Rieger, Ph.D.
Dean of the College of Agriculture and Natural Resources

Approved: _____
Ann L. Ardis, Ph.D.
Senior Vice Provost for Graduate and Professional Education

ACKNOWLEDGMENTS

Thank you to Dr. Shreeram Inamdar for his mentorship in teaching me to think like a scientist and for his leadership in the operations of our lab group. I'd also like to thank Dr. Thomas Parr for his guidance and many teaching opportunities together. Thank you to my committee member, Dr. Delphis Levia for many insightful comments during our official meetings and our unofficial conversations.

I would also like to thank fellow M.S. students Erin Johnson, Chelsea Krieg and Catherine Winters, Ph.D. student Dan Warner and summer interns Margaret Orr, Caraline Canning, and Shawn Del Percio for their assistance in sediment collection and processing, and for many lively research discussions. Thank you to the Delaware Environmental Observing System (DEOS) for providing climatological data and to the members of the DEVIL, EIGL, UD Advanced Materials Characterization and UD Soil Testing laboratories for their assistance and patience in sample analysis.

This work would not have been possible without the generous funding from the NSF and USDA, grant numbers IIA 1330238 and 2015-67020-23585, respectively. It has truly been a privilege to receive the many great learning and career development experiences during my M.S. research through a subsidized research assistantship.

Finally, I'd like to thank my parents, Rick and Sue, my sister Callie, and all of my friends and colleagues at the University of Delaware and beyond for their support and friendship over the course of my M.S. studies.

TABLE OF CONTENTS

LIST OF TABLES

LIST OF FIGURES

ABSTRACT

High-runoff events can trigger rapid and highly variable fluxes of sediment and ecologically-important solutes from small catchments and these can be difficult to characterize due to their transient nature. We investigated the quantity and sources of particulate organic matter (POM) during storm events in a forested network of first and second order streams in the mid-Atlantic, Piedmont region of the USA. We compared stable isotope ratios (^{13}C and ^{15}N) of three size classes of particulate organic carbon (POC) and nitrogen (PN) to those of potential sediment end members to infer proportional source contributions. Additionally, we explored hydrologic controls on POM source and elemental and isotopic composition using samples from discrete time points along storm event hydrographs. Our findings indicate that plant litter contributes the greatest proportion to the coarse fraction and that valley bottom wetlands consistently contribute to POM. While resuspension of coarser mineral bed sediments dilutes the carbon and nitrogen content of sediments at larger drainage areas, fine POM was increasingly mobilized from the bed. The C:N ratios and isotopic quality of fine particles suggest this pool of POM has undergone aquatic microbial processing. Higher maximum discharges mobilized material from the forest floor O horizon (litter and humus) to the channel, while more intense precipitation flushed stream bed POM. Precipitation events are projected to increase in frequency and magnitude in the northeastern United States under changing climate scenarios. Understanding the potential for hydrologically-driven changes to POM efflux from

headwater sources may help to explain altered biogeochemical cycles within their higher-order watersheds.

Chapter 1

INTRODUCTION

The coupled availability of carbon and nitrogen is a fundamental driver of aquatic ecosystem structure and function and is thus a major water quality concern. Recent studies (Carey *et al.*, 2005, Dhillon and Inamdar 2013, Inamdar *et al.*, 2015, Jeong *et al.*, 2012) indicate that particulate organic carbon (POC) and particulate nitrogen (PN) within the fluvial suspended sediment load can constitute a larger portion of long term loads from headwater systems than dissolved phases of carbon and nitrogen due to disproportionate fluxes during rare high-discharge events. Runoff associated with large and intense storm events mobilizes disproportionate fractions of POM during relatively short episodes, making accurate characterization of long term fluxes difficult (Hope *et al.*, 1994). This is often particularly pronounced in headwater streams (defined as first and second order systems here), which can compose up to half of the longitudinal reach of a watershed network (Leopold *et al.*, 1964) and can contribute disproportionately to basin-scale sediment loads (Wohl *et al.*, 2015). The catchments drained by small but abundant, often high-relief, headwater systems have been suggested to contribute 40-70% of the fluvial POM to larger rivers, which can have important consequences in the composition and relative bioavailability of downstream organic matter (Bianchi and Bauer, 2011). Notably, this allochthonous POM is derived predominantly from terrestrial plants and humified soil organic matter (SOM) with relatively high molar C:N ratios (Kendall *et al.*, 2001) but this may

change substantially with land cover, position within a drainage network, timing within a runoff event, or between seasons and antecedent conditions.

Sediment loads can be exacerbated by human activity and are often an important vector for the delivery and post-depositional release of labile nutrients in sensitive coastal zones (Mayer *et al.*, 1998). Regional analyses have indicated that particulate nutrient loads are increasing even while dissolved loads are being mitigated in some major basins (Hirsh 2012, Zhang *et al.*, 2015). Zhang *et al.* (2015) suggested that while declines in dissolves species are being observed, increases in loads of particulate species is a consistent trend throughout many parts of the Chesapeake Bay Watershed. In addition to serving as a potential nutrient subsidy, the lateral transfer of organic matter through surface waters can strongly influence vertical carbon degassing, in turn affecting regional fluxes as part of global carbon cycling (Cole *et al.*, 2007).

Physicochemical and biotic process can have unique effects on different size fractions of POM, subsequently altering their mobility and bioavailability. Consumers utilize POM as the foundation of lotic food webs, inducing decreases to its size, increases in its mobility, and alteration to its composition in the process (Wallace *et al.*, 1982, 1993). Processes such as post-feeding leaching of coarse POM (Yoshimura *et al.*, 2015), abrasion during high flows (Martilla & Kløve, 2014) or photobleaching (Estapa *et al.*, 2012) can affect the size and elemental content of POM. Colonization of fine POM by heterotrophic microbes has been shown to reduce C:N ratios and to alter POM bioavailability. For example, while fungi often dominate coarse POM colonization and increase respiration rates, bacterial abundance may increase for fine

POM (e.g. Tant *et al.*, 2013). These processes (among others) can interact to induce alterations to POM composition during downstream transport.

Various methods have been deployed over numerous studies to trace the source of sediment and POM in fluvial environments. Studies on the isotopic quality and source of POM have contributed greatly to our understanding of the landscape, biological, and hydro-climatic drivers of lateral fluxes of organic matter and nutrients in many environments. Other researchers have generated insights into various biotic processing and ecological roles of POM across different size classes. However, a disconnect exists in the literature between bulk POM source and such findings that highlight differences in the composition, ecological ramifications, and transport dynamics of various sizes of POM (e.g. Wallace *et al.*, 1982, 1993). A recent review noted the importance of considering variable elemental compositions across particle size gradients in sediment fingerprinting endeavors (Gellis and Makundan, 2013). Here, we investigated three discrete size classes of sediments (>1000 μm, 250-1000 μm, <250 μm) mobilized by storm events along a series of drainage areas in a forested headwater network, asking:

1. How does the total organic C and N content, isotopic quality, and abundance of three discrete particle size classes vary at multiple headwater drainage locations?
2. How does the source of POM to the stream vary among different combinations of particle size and drainage area?
3. How do rainfall intensity and total discharge influence POM source and quality?

Understanding of the controls on POM in forested drainage networks may help to inform changing water-quality drivers as the northeastern United States enters an era of greater climate uncertainty. While several studies have explored the variability

in POM quality along a gradient of particle diameters, there is a paucity of literature explicitly addressing unique catchment sources for different size classes of POM during periods of high yield. Additional work here may help to explain altered nutrient dynamics in downstream receiving waters.

Chapter 2

LITERATURE REVIEW

This review explores the various finding regarding variability in the source, quality and quantity of POM in lotic (i.e. flowing waters such as streams, creeks, and rivers) environments. Specific sections highlight varying ecological roles for POM of different particle size, the effects of hydrology on POM fluxes, and the results of studies tracking POM source within watersheds.

2.1 Definition and ecological significance of POM

POM is operationally defined as the fraction of compounds containing organic carbon that are retained on a 0.2 to 0.7 μm filter, dependent on the study. Organic matter is generated through inorganic carbon fixation by autotrophic organisms, and undergoes subsequent transformation by heterotrophic and/or abiotic processing. Fluvial POM is typically considered as a component of the suspended sediment pool regardless of its origin or degradation state. The organic content of suspended sediments in streams and rivers typically ranges from ~0.5 to 10 percent, with most between 1-5 percent (Wotton, 1994). Under baseflow conditions, POM helps to support aquatic food webs, and it varies widely in bioavailability. Algae, fresh plant litter, and animal tissue typically have higher contents of proteins, carbohydrates and other labile components that serve as bioavailable food sources, and this is commonly estimated by its molar C:N ratio, with lower ratios often associated with greater proportions of labile materials such as amino acids (Wotton, 1994). Aquatic

consumers such as shredders and collectors utilize POM as a foundation for food webs in stream environments and subsequently change its structure, composition, and mobility (Wallace *et al.* 1982). POM subsequently serves as a substrate for colonization by heterotrophic microbes, which has been shown to reduce C:N ratios and alter its bioavailability (e.g. Tant *et al.*, 2013).

While POM can subsidize oligotrophic (i.e. nutrient-poor) systems, POM can serve as an important vector for the transport of excess nutrients and toxic contaminants from contaminated watersheds to sensitive lakes and coastal zones. For example, the sediments delivered to the deltas via major rivers have been shown to release labile nitrogen after deposition (Mayer *et al.* 1998), which can contribute to the eutrophication of coastal water bodies. This is of particular interest in the Mid-Atlantic region of the United States where nutrient enrichment in the Chesapeake Bay and other estuarine bodies is a leading water quality concern. Interestingly, Mayer *et al*. (1998) indicated that "Particulates are probably not important to the Susquehanna-Chesapeake system…because of low sediment delivery rates".

Contrary to the findings in Mayer *et al.* (1998), recent work in the Mid-Atlantic region suggests that particulate-borne nitrogen has been increasing in its relative fraction of rivers' nutrient loads in recent years. For example, Hirsch (2012) reported 65 to 98 percent of measured nitrogen was contained within the particulate fraction during nitrogen maxima sampled during flood conditions on the Susquehanna River, although this increase is predominantly attributed to diminished trapping capacity in local reservoirs such as the Conowingo Dam. Zhang *et al.* (2015) employed a time series modelling effort and calculated increasing trends in the particulate nitrogen (PN) loads of the three largest Chesapeake Bay tributaries

(Susquehanna, Potomac and James rivers), even while dissolved nitrogen concentrations were decreasing. These results underscore the importance in evaluating PN and associated organic carbon exports for watersheds ranging from headwaters to those drained by major rivers in order to understand the changing controls on regional aquatic nutrient and energy flows. Additionally, multiple regional studies (e.g. Donovan *et al.*, 2015, Hupp *et al.*, 2015, Walter and Merritts, 2008) have noted the extensive presence of nutrient-rich "legacy sediment" in Mid-Atlantic floodplains and valley bottoms. These authors indicated that massive topsoil erosion occurred during the 17^{th}-19^{th} centuries after European settlers implemented widespread agriculture, forestry and damming in the region, and that erosion of these sediments from floodplains could contribute to contemporary pollution of surface waters.

2.2 Variability in POM quality among particle sizes

Conflicting paradigms in the study of particulate material in lotic environments have arisen from the measurement of POM as an integral component of the fluvial suspended sediment load. Hydrologists, soil scientists and geomorphologists working at the scale of large drainage basins often base the definition of "fine" sediments on the distinction for silt and clay versus sand, or particles less than 63 microns in diameter (e.g. Horowitz, 2008, Wood & Armitage, 1997). This distinction has several purposes including greater mobility of silts and clays and the preferential association of many chemical constituents of interest with "fines" due to the negative surface charge of clays (Horowitz, 2008).

Aquatic ecologists working in smaller systems have often considered POM in size classes other than the sand-silt distinction noted above. This is largely due to the

observed difference in source, quality, and ecological impact of POM across these different levels of distinction (e.g. Tant *et al.*, 2013, Tank *et al.*, 2015, Yoshimura *et al.*, 2008). Furthermore, the progressive fractionation toward fine sediments in larger systems has been reported in the literature (e.g. Martilla & Kløve, 2015), suggesting work conducted at smaller catchments may seek differentiations between sediments above 63 μm. These can be valuable in exploring biogeochemical differences in POM classes that may experience variable transport dynamics through these environments. Discrete particle size classes may exhibit different response to hydrologic or other drivers as suggested by Atkinson *et al.* (2009) and Wallace *et al.* (1993). While a clear consensus on defining multiple discrete size classes of POM does not exist in the literature, 1000 μm is a common choice in distinguishing coarse (CPOM) fractions from other classes (Table 2.2.1).

Several studies have explicitly discussed the relative carbon and nitrogen content of discrete size classes of fluvial sediments. Akamatsu *et al.* (2011) reported significantly greater total C content, butsmaller C:N ratios in finer POM. Similarly, Atkinson *et al.* (2009) reported higher C:N in coarser particles. Mayer *et al.* (1998) showed positive correlations between nitrogen content and specific surface area (which increases with decreasing particle size) for suspended sediments in several major river basins worldwide. These analyses utilized data sets that extended across multiple flow conditions and catchment scales. Studies on the relative lability or recalcitrance of POM have suggested that although C:N ratios in fine POM (FPOM) may be more amenable to aquatic microbial communities, the organic matter may be composed of more refractory compounds. While Akamatsu *et al.* (2011) reported a lower C:N ratio for FPOM—generally interpreted as indicative of more labile

material—they also used stable isotopes of carbon to show that medium POM (MPOM) and CPOM came from fresher or "higher quality" sources. Jung *et al.* (2012) and Atkinson *et al.* (2009) similarly reported enrichment of heavier stable isotopes of carbon and nitrogen in smaller particles, suggesting this indicated the presence of more degraded organic material. Similarly, Yoshimura *et al.* (2008) found that C:N was lower in biologically-processed FPOM when compared to the CPOM from which it was derived, but that it also had higher content of refractory materials such as lignin. The above studies suggest that greater surface area offered by FPOM allowed for more adsorption of mineralized nutrients such as ammonium and for increased microbial colonization. Tant *et al.* (2013) found that fungal and bacterial biomass dominated CPOM and FPOM colonization, respectively, and that CPOM exhibited enhanced microbial colonization rates in the presence of enriched nutrients. These studies collectively suggest that while greater nitrogen content in finer matter may represent active microbial populations, total organic matter may be greater in CPOM as it is typically closer in composition to fresh terrestrial plant litter.

Table 2.1: Discrete size classifications used in analyses suspended sediments or POM from previous studies.

Study	FPOM (µm)	MPOM (µm)	CPOM (µm)	Notes
Atkinson *et al*., 2009	10-44	45-250	>250	
Akamatsu *et al*., 2011	<100	100-250	250-1000	
Dyer and Manning, 1999	<150	*N/A*	>150	*Micro/macro-flocs in estuary*
Garzon-Garcia *et al.*, 2014	<2	<10	<64	*Stoke's Law used for separation*
Hope *et al*., 1994	53-1000	*N/A*	>1000	*Review;* "VFPOM" = 0.45-53
Horowitz, 2013	<63	*N/A*	>63	*Traditional sand/silt distinction*
Tank *et al*., 2010	45-1000	*N/A*	>1000	*Review*
Tant, *et al*., 2013	<1000	*N/A*	>1000	
Wallace *et al*. 1995	<4000	*N/A*	>4000	*Definition in part due to artifact*
Webster & Meyer, 1997	<1000	*N/A*	>1000	*Review*
Yoshimura I. 2010	100-250	250-500	>1000	

2.3 Sources of POM in lotic environments

POM in headwater streams is composed predominantly of plant litter but also contains animal detritus and waste, microorganisms, humified soil organic matter (SOM), and dissolved organic matter (DOM) adsorbed to mineral surfaces, and varies accordingly in composition. In higher-order rivers and estuaries, POM sources are qualitatively and topologically diverse (Bianchi & Bauer, 2011). While ecological communities are adapted to capitalize on upstream communities' processing inefficiencies (Vannote *et al.*, 1980), autochthonous organic matter production tends to reach its maximum in at middle (approximately fifth order) reaches of a basin. Studies attempting to differentiate POM source at very large scale often consider broad categories such as uplands and riparian regions, C3 and C4 plants (and their associated soils), plankton, algae, and macrophytes and anthropogenic waste (Kendall *et al.*, 2001). Small catchment studies allow for a more detailed exploration of the processes controlling POM source, but they are inherently spatially limited and tend to focus on allochthonous sources.

The effect of land use/land cover on POM mobility and composition

The speciation, concentration, composition, and mobility of fluvial organic matter have been explored as a function of source region within a watershed, with studies yielding complex results. For example, the relative importance of POC to DOC in total carbon export can be explained in part by catchment land use characteristics. A study in a small agricultural catchment in the southeastern U.S. found that POC constituted a lesser fraction of carbon export than DOC under tropical storm conditions (Caverly *et al*., 2013), contrasting with observed POC dominance in storm exports from higher-relief forested catchments (Dhillon & Inamdar 2014, Jeong

et al., 2012). Conversely, Bass *et al.* (2014) proposed increased POC mobilization from tilled soils in an agricultural catchment in Australia and Jung *et al.* (2014) found higher POC concentrations in an agricultural versus a forested tributary of the same watershed in South Korea during a storm event.

Land use can also impact the proportional organic matter and nutrient content of sediments and the composition of POM. For example, Hancock and Revill (2012) and Laceby *et al.* (2014), reported higher organic carbon and nitrogen in stream channel banks than in material from upland erosion. Nitrogen and phosphorus exports associated with POM were found to increase rapidly relative to dissolved phases during stormflow in a Mid-Atlantic cropland catchment, where exports from a nearby forested catchment contained a greater fraction of dissolved organic nutrients (Correll *et al.*, 1999). Although agricultural land use increases fluvial sediment loads and has generally been shown to lead to increases in the nutrient content of sediments, some studies suggest this is associated with lower quality or less labile carbon. Jung *et al*. (2014) found more recalcitrant POM in agricultural runoff when compared to forested environments. Similarly, Ford *et al.* (2015) suggested FPOM mobilized to the channel by large events in an agricultural system shifted the benthic matter toward degraded, recalcitrant organic matter. Martilla and Kløve (2014) found transport of denser, finer POM from agricultural sites compared to that in natural systems. These results have important implications for nutrient cycling and aquatic metabolism in receiving systems. While urbanization has also been shown to increase sediment loads to streams, some studies (e.g. Larsen *et al*., 2015) have suggested decreased organic fractions in streams draining urban environments. However, the remaining POM may

bear a more bioavailable and autochthonous signature as suggested by Lu *et al.* (2014).

Residence within different watershed compartments, particularly the riparian corridor and stream bed, has been shown to considerably alter the carbon and nutrient content of exported POM. Atkinson *et al*. (2009) interpreted shifts in stable isotope signatures and C:N ratios as evidence of higher quality POM introduced from the floodplain at high flows. Similarly, Jung *et al*. (2014) suggested that microbial consumption of labile components from terrestrially-derived POM during downstream transport can be at least partially replenished by the introduction of fresh POM from the floodplain.

Estimates of POM source

Sediment fingerprinting is a complex field with a rich body of literature in catchment hydrology and geomorphology. Rather than providing a detailed description of the chemical and statistical methods involved in tracing sediment in fluvial environments here, readers are directed to comprehensive reviews by Davis *et al.* (2009), Mukundan *et al.* (2012) and Gellis and Mukundan (2013). Here, instead, the focus is placed on the use of stable isotopes of carbon and nitrogen in addition to some of the concepts underlying the use of molecular fluorescence and structural biomarkers for allocating sources of organic fractions of sediments to their respective sources among organisms and soils across relevant watershed compartments.

Studies at various watershed scales have extensively leveraged stable isotopes and elemental ratios to trace POM source. Briefly, isotopic enrichment refers to preferential retention of the less abundant, heavier stable isotopes of carbon and nitrogen (i.e. ^{13}C and ^{15}N) versus the lighter, more abundant forms (^{12}C and ^{14}N),

whereas relatively depleted organic matter has a lower abundance of these heavier isotopes and is generally associated with fresh plant material. An important theme in the literature is enrichment of nitrogen and especially carbon isotopes during decomposition of plant matter to humus, SOM in a mineral soil matrix, or benthic sediments. Preferential respiration of lighter carbon by heterotrophic microbes typically leads to a small isotopic enrichment of carbon in soils relative to their parent plants, and can be used to infer decomposition state (Natelhoffer & Fry, 1988). Nitrogen is also abundant in organic matter, so its isotopic signature can be employed in conjunction with that of carbon to refine interpretations of POM source. This signature is conventionally expressed relative to atmospheric N_2 and varies less predictably than carbon due to the complexities of nitrogen cycling between inorganic and organic forms (Sharp, 2007). However, $\delta^{15}N$ typically enriches when moving up trophic levels, and can display large enrichments in response to specific natural processes such as denitrification or anthropological activities such as spreading manure for agricultural fertilization. Although slightly less common, some studies also employ stable isotope analysis of sulfur and oxygen in tracing organic matter.

A spatially and temporally extensive study on the variability of stable isotopes and elemental C:N ratios by Kendall *et al.* (2001) emphasized that C:N greater than fifteen can be used to allocate POM source to vascular plants and their soils as opposed to aquatic production. They also interpreted positive correlations between $\delta^{13}C$, flow, and turbidity, as mobilization of degraded soil carbon with runoff. Similarly, a study in an agricultural catchment in Korea (Jung *et al*., 2012) inferred the erosion of deeper, mineral-bound POM over the course of intense storm events by comparing progressively enriching $\delta^{13}C$ and $\delta^{15}N$ in stream sediments over the course

of the event to measured enrichment with depth in soil profiles. Fox and Papincolaou (2007) applied a Bayesian simulation to the $\delta^{13}C$, $\delta^{15}N$, and C:N of sediments to validate a physical erosion model in a small agricultural catchment. They concluded that the physical model underestimated floodplain erosion with respect to upland, tilled soil erosion, when compared to mixing model. Work in an Australian catchment (Garzon-Garcia *et al*., 2014) suggested that $\delta^{13}C$ values in POC indicated 40 to 70 percent of C from silt-sized sediments was from tree litter, and suggested these values might be greater in coarser fractions of sediments. It is worth noting that the tight coupling of POM mobility with that of mineral sediments in some environments has permitted the use of bulk sediment chemistry to trace dynamic POM sources. For example, Dhillon and Inamdar (2014) developed a multivariate mixing space using sediment cations and metals and interpreted increased variability above a precipitation intensity threshold as the erosion of a more diverse pool of distal POC sources. In addition to the elemental and isotopic tools discussed above, a number of complex biochemical and molecular methods have been used for characterizing POM in lotic, lacustrine and marine environments; a review by Bianchi and Bauer (2011) offers an in-depth description of these methods.

It is worth noting that techniques in optical fluorescence that have been widely applied for rapid characterization of bulk DOM pools via excitation-emission measurements with subsequent PARAFAC modelling in the last decade (e.g. Cory & McKnight, 2005) may be applied to extracts of POM to characterize its fluorescent, soluble fractions and as an environmental tracer (e.g. Osburn *et al*., 2012). Larsen *et al.* (2015) introduced a novel technique in comparing eroded POM sources between a managed and an unmanaged urban watershed. They fit a PARAFAC model to

excitation-emission matrices from DOM leached from fluvial POM and subsequently performed a mixing model analysis on the relevant presence of different fluorophores. They found that a "general allochthonous" fluorophore was the dominant component in samples from both systems, but were able to distinguish a higher presence of their stream bed end member in the unrestored system as opposed to a greater presence of soils in the managed system measured under high discharges. Interestingly, they noted that "organic matter within the bed undergoes distinctive transformations that differentiate its fluorescent signature from that of the parent material, regardless of the type of parent material", toward a more humic-like specific-fluorescence. Such results demonstrate the application of these methods developed for DOM in drawing inference about POM source and quality.

2.4 Catchment hydrology and POM fluxes

Hydrologic conditions are a principal driver of the magnitude, source, and quality of POM fluxes in lotic environments. The terrestrial POM that often dominates the loads of low-order streams is mobilized via erosive processes strongly coupled with those affecting mineral sediments (e.g. Carey *et al.* 2005, Caverly *et al.* 2013, Dhillon & Inamdar, 2014). Therefore, hillslope-scale processes such as runoff generation and interill erosion combine with in-stream geomorphic processes to explain POM flow response. Both sediment and total organic carbon (TOC) yields have been shown to decrease with increasing catchment size, while runoff to precipitation ratios increase (Mutema *et al.*, 2015). This meta-analysis attributes decreasing yields to several factors, with re-deposition of particles and oxidation and outgassing of organic carbon most strongly affecting long-term TOC yields. While it is well-documented that smaller catchments exhibit "flashier" hydrology, a recent

review (Alvarez-Cobelas *et al.*, 2010) showed that smaller catchments also show wider variability in TOC exports and that POC is especially unpredictable. These findings raise important questions about to the control on POM mobilization and retention when moving from headwater sources to higher-order streams.

Storm events and POM export

Relatively infrequent stormflows contribute disproportionate quantities of organic carbon to catchments' long term fluxes (Raymond *et al.*, 2015). Transport of particulates is also sporadic, with suspended matter in most streams exhibiting less predictable behavior over event hydrographs when compared to dissolved phases. For example, in a mid-Atlantic Piedmont catchment Dhillon and Inamdar (2014) measured comparable POC:DOC export during several high-discharge events, and found POC dominated TOC export by as much as 92 percent above a precipitation threshold of approximately 75 mm. The authors noted that precipitation intensity was an important variable in explaining suspended sediment and POC export and that successive strong storms resulted in lower percent organic carbon in mobilized sediments, suggesting this resulted from a depletion of available pools of POC. A follow up study (Inamdar *et al.* 2015) highlighted the importance of PN mobilization in total nitrogen exports, showing that between 39 and 87 percent of the N load exported over a series of storm events was in the particulate form and that a single tropical storm exported nearly a third of the catchment's annual nitrogen load as mostly PN. Similarly, Jeong *et al.* (2012) employed high-frequency sampling techniques to show that POC flux rapidly outpaced that of DOC beyond a precipitation threshold on the rising limb of storm events. However, POC concentrations under high flow conditions were highly variable, which the authors attributed to changes in the flowpaths along convergent

catchment zones that contribute to erosion. Bass *et al.* (2011) reported that a tropical catchment exported 84 percent of its TOC during 9 percent of their data record, although DOC contributed more to exports than POC under all flow conditions in this case.

Particulate concentrations often peak prior to the event hydrograph (Hope *et al.*, 1994) following a "first-flush" transport pattern of fine or easily mobilized particles. This can be examined using hysteresis plots, or concentration-discharge relationships in a bivariate space, to estimate an analyte's source region within a watershed. A clockwise relationship suggests a source of an analyte (such as POC) proximal to the stream, where anticlockwise relationships suggest more distal sources. While proximal sources associated with the "first flush" response are common, many catchment or event-specific processes can alter the timing of maximum suspended sediment and POM flux. For example, anticlockwise hysteresis after breakup of bed armoring and subsequent release of fine sediments was reported by Lawler *et al.* (2006). Landers and Sturm (2013) propose another process in which the transport of coarser bed sediments is capacity limited but can respond quickly to increases in stream power whereas finer sediment responds to activation of hillslope erosion later in a runoff event. Dhillon and Inamdar (2014) found shifts from clockwise hysteresis in POC patterns during higher flows as more complex assemblages of flowpaths were activated. Similarly, in a larger catchment in Thailand, Ziegler *et al.* (2014) noted shifts from clockwise to anticlockwise or complex hysteresis patterns during "spottier" storms outside of the typical monsoon season, suggesting activation of disparate sub-catchments with unique sediment dynamics as an explanation. While deviations from the "first flush" timing of POM flux due to catchment hydrology have been observed,

there is a general consensus in the literature that POC exports increase nonlinearly over storm hydrographs under catchment-specific thresholds (Bass *et al.* 2014, Dhillon & Inamdar, 2013).

Recent syntheses have highlighted the need for more work in understanding hydrologic controls on organic carbon dynamics moving from the small catchment to the basin scale. In the "pulse-shunt concept" proposed by Raymond *et al.* (2015), organic matter exports from headwaters are highly episodic and the bulk of mass fluxes are explained by infrequent events. The authors suggest that decreases in residence time driven by stream velocity and changes in water temperature accompanying high discharges reduce the capacity for OM processing, and "shunt" much terrestrial matter to high-order rivers. While the proposed theory explicitly addresses DOM, other findings (e.g. Dhillon and Inamdar, 2013, Jeong et al. 2012) indicate that POC transport is even more episodic in nature, suggesting that this theory may be extended to the particulate pool. However, POM retention dynamics may differ with catchment morphological features, drainage scales and important differences in connectivity to downstream systems driven by watershed functional units (Raymond *et al*., 2015).

High discharge events can alter the source, quality, and magnitude of POM fluxes, with important potential consequences for aquatic ecosystems. Ford *et al*. (2015) generated a metric from stable isotopes of carbon and used this to show that a high-intensity storm promoted connectivity that transported more POC from upland sources to the channel. This influx was sufficient to shift benthic carbon stocks from a signature reflective of autochthonous production to that of relatively recalcitrant, degraded, terrestrial soil matter for approximately one year after the event and to

suppress seasonal fluctuations in the isotopic signature of benthic POC. Jung *et al.* (2012) similarly found enrichment in $\delta^{13}C$ with increasing total suspended solids (TSS) and POC concentrations at peak flows, suggestive of more degraded soil carbon inputs from deeper in the soil profile. However, they noted that differences in POC quality observed between particle size classes at low flows were homogenized at high flows and that $\delta^{13}C$ was correlated to precipitation but not to discharge. Conversely, in a follow up study at a larger catchment scale the authors found that monsoon rainfalls replenished depleted labile fractions of POM with fresh floodplain material along a downstream gradient, suggesting the terrestrial source of POM is critical in shaping runoff-induced changes to POM quality (Jung *et al.* 2014),. Bass *et al.* (2011) similarly interpreted depletion of POM $\delta^{13}C$ and increases in C:N during flood conditions as fresher surficial soil organic matter mobilized by runoff. Fox and Papanicolaou (2007) used stable isotopes of carbon and nitrogen in paired framework of statistical models to show that slight differences in hydrologic conditions in two subsequent storm events mobilized POM from different catchment storage compartments. One event had slightly higher total precipitation and contributed more recalcitrant upland agricultural sediments to the channel while a second event mobilized proportionally more floodplain material. Such variations in sediment quality can ultimately affect aquatic biogeochemical cycles; for example, Guenet *et al.* (2013) showed that soil matter from terrestrial sources exhibits enhanced mineralization in aquatic environments, resulting in greater efflux of carbon dioxide to the atmosphere.

Wet-dry cycles

Antecedent and seasonal hydrologic conditions can also affect POM fluxes and quality. Ambient warm, moist conditions can increase rates of organic matter accumulation in terrestrial environments, with subsequent flushing of dissolved C and N from soils observed during rewetting pulses following extended droughts (Borken & Matzner, 2009). This review suggests that net total mineralization of OM under drought conditions is smaller compared to that in soil at optimum moisture conditions. This raises important questions pertaining to C and N losses to aquatic systems via alternate, particulate-dominated (i.e. erosional) pathways following periods of drought and intense, subsequent precipitation.

The surficial soil pools of POC accumulate in forested catchments during warm, dry conditions may be readily mobilized when large storm events occur. Dhillon and Inamdar (2014) noted that "flow-weighted mean POC concentrations decreased for closely-spaced sequential storms, suggesting an exhaustion of the POC pool, whereas the same pattern was not replicated by DOC". A complimentary interpretation is offered in Garzon-Garcia *et al.* (2014), in which there were significant differences in N export at different catchment drainage scales during dry years, but not during wet years. The authors suggest that during dry periods integration of more plant material into sediments can explain higher observed percent N content in sediments along an increasing drainage gradient. Bass *et al.* (2011, 2014) observed an elevated "flush" of both DOC and POC at the inception of precipitation in the absence of a notable hydrograph response and attributed this to "prolonged dry spells" prior to the event.

Alteration to POM along drainage network gradients

Several studies have stressed the role of downstream transport, or variation in drainage areas within a catchment, in altering the quality and quantity of mobilized POM. Such alterations to the bulk POM pool can result from deposition and remobilization, or from biotic alteration during lateral transport. For example, Jung *et al.* (2015) found a decrease in lignin and carbohydrates—interpreted as "forest like" organic matter—in POM moving downstream, suggesting a fraction of POM is retained within relatively undisturbed environments and that labile components are metabolized by aquatic microbiota during transport. However, the authors also noted a replenishment of some labile fractions resulting from connection with floodplains, suggesting a dynamic interplay between biotic and abiotic factors in altering the bulk POM quality during transport. Atkinson *et al.* (2009) suggested higher quality seston in downstream reaches of a fifth order stream at baseflow was the result of primary production within the system. Akamatsu *et al*. (2011) similarly found decreases in C:N and increases in periphyton contributions to POM downstream and interpreted these as indicative of greater autochthonous production and detachment of benthic algae with higher discharges. In Garzon-Garcia *et al.* (2014), PN concentrations increased at downstream locations in an Australian catchment during drier years, and the authors cited fractionation against heavy mineral particles during transport and increased contributions from N-rich bank sediments as possible causes. A study in a southeastern Australian catchment (Smith and Dragovich, 2008) suggest that a rapid transition from hillslope processes to the dominance of "subsurface", or bank, erosion, occurs when moving downstream in a system with observed bank incision. While this finding was determined from a mixing model of fallout radionucleotides applied to bulk sediment, the results may extend to rapid transitions in POM source in similar

systems. Together, these results suggest that alteration to POM quality along a given reach may vary widely based on a given system's physicochemical and biological characteristics such as stream order, dissolved nutrient concentrations, geomorphology and flow regime. These in turn can affect erosion-deposition dynamics and biological processing.

Chapter 3

STUDY SITE AND METHODS

3.1 Study watershed characterization

This study was conducted in a 79 ha watershed (Figure 3.1.1) in the Piedmont physiographic province in Cecil County, Maryland (Inamdar *et al*., 2015; Dhillon and Inamdar, 2013,, Dhillon and Inamdar, 2014), which drains to the Big Elk Creek and subsequently to the Chesapeake Bay. The watershed is predominantly forested (mean stand age of approximately 60 years), with pasture along the outer periphery. Dominant canopy species including *Fagus grandifolia* (American beech), *Liriodendron tulipifera* (yellow poplar), and *Acer rubrum* (red maple), with some thorny underbrush including *Rosa multiflora* (multiflora rose) and prominent *Symplocarpus foetidus* (eastern skunk cabbage) in the valley-bottom wetlands. Bedrock formations consist of metamorphic gneiss and schist and soils are coarse loamy, mixed, mesic lithic inceptisols on slopes and oxyaquic inceptisols present in saturated valley bottoms. Mean annual precipitation from 1981 to 2010 in this region was 1173.5 mm, with late spring and late summer as the wettest and driest periods, respectively, and mean annual temperature is 13.06 º C (Delaware State Climatologist Office Data Page).

Watershed monitoring and instrumentation

Climatological data was obtained from a local station maintained by the Delaware Environmental Observing System (DEOS) approximately 450 m from the

79-ha catchment outlet. This consists of temperature and tipping-bucket rainfall measurements which can be obtained at hourly intervals online. Additional tension wire gage (GEONOR) rainfall measurements were obtained at hourly intervals upon request and were used for the analyses and figures in this study due to their higher precision compared to tipping bucket measurements.

Intensive monitoring locations exist at nested 12 ha and 79 ha watersheds, which have served as the basis for several studies (Dhillon and Inamdar 2013, Dhillon and Inamdar 2014, Inamdar *et al.* 2015; Singh *et al.*, 2013). Stream discharge estimates were obtained at 20-minute intervals using a Parshall flume at the 12 ha location and a rating curve calculated from paired pressure transducer and acoustic Doppler velocity meter measurements in a culvert at the 79 ha location.

Samples were collected for analysis of suspended sediment and POM at the 1 and 79 ha drainage locations using automated samplers (6712C, Teledyne ISCO, Lincoln, NE, U.S.) triggered either from a rain gage set point (> 0.15 - 0.20" precipitation hr^{-1}) for unpredictable convective systems or manually for more predictable frontal systems. ISCOs were programmed to collect 400 mL of stream water which was filtered to separate particulates. Filter retentate was analyzed for suspended sediment and POM at discrete points on the storm event hydrograph and are thus referred to as discrete sediment samples (DSS) henceforth.

Three additional suspended sediment sampling locations were added for this study, at 4.5 ha and 30 ha drainage locations above and below the 12 ha site, respectively, and at the outlet of a 44 ha tributary catchment. The 30 and 44 ha systems are drained by first order streams and converge approximately 200 meters upstream of the 79 ha monitoring location. Sediment traps composed of capped PVC

piping perforated with 1.5 cm diameter holes beginning several centimeters above baseflow stage were placed at these locations in addition to the intensive watershed monitoring locations (Figure 3.1). During periods of elevated discharge, stream stage rose above the perforations and suspended sediment transported in streamflow settled out as it entered the sampler, collecting composite sample integrated over the course of the storm event for a given drainage location. All samples were retrieved within 24 hours of the end of an event; dried ISCO samples were refrigerated at 4 ° C and samples from sediment traps (hereafter referred to as composite sediment samples, or CSS) were frozen prior to processing and analysis.

Geospatial analysis of watershed attributes

The five sampled subcatchments differ notably in several important parameters that may affect sediment mobility and quality (Table 3.1.1). Notably, the 12 ha and to a lesser extent the 30 ha sites drain a significant portion of the Galla series, an organic-rich, perennially-saturated valley bottom loam. Topography and slopes were calculated using 2005 coastal LiDAR data (NOAA Office for Coastal Management). The topographic wetness indices (TWI) were also calculated in ArcGIS 10.1 from a digital elevation model of the watershed using the equation:

$$TWI = \ln(a/(tanB)) \quad (1)$$

for each two-meter cell, where 'a' is the contributing drainage area and 'b' is the local slope. While subject to some uncertainty the TWI can serve as a useful indicator as higher values (site-dependent, but typically above 5-7) can indicate hydrologic and biogeochemical hotspots. Analysis of probability density function indicated slightly decreasing median values of TWI with increases in drainage area (Appendix C),

indicating a larger proportion of upland areas drained by larger subcatchments (Table 3.1.1). However, heavy right hand tails were observed for TWI in the 4.5- and 12-ha sampling locations. These suggest the presence of permanently or episodically-saturated regions that may exhibit hydrologic connection to the channel and could contribute to POM. A subsequent buffer analysis of percent soil coverage, slope distributions and TWI distributions was conducted for the riparian zone, estimated as a 50-meter radius of the stream, was conducted and is included in (Appendix B). Unsurprisingly, TWI was higher in the riparian corridor and slopes were higher as well. Silty-loam soil series (i.e. Baile and Galla) are more prevalent in the riparian corridor and generally coincided with shallower slopes and higher TWI values, where well-drained inceptisols (i.e. Manor loam) occurred more on upland hillslopes.

Sampling for characterization of watershed end members

Seven potential sediment sources were sampled to identify POM end members within the catchment following Dhillon and Inamdar (2014). These included the stream bed, exposed stream bank A and B horizons, valley-bottom wetland surficial soils, forest floor litter and humus, and the upland A horizons. Sampling was conducted during the summer of 2015. Four replicates of 500-750 g of each end member were sampled using an ethanol-cleaned trowel or auger from both of the main tributary branches of the watershed (Figure 3.2). Stream beds were sampled from areas without major backwatering or pooling and were composited along a three by three-point grid within the channel. Bank sediments were collected from exposed incised banks with three points composited from the A horizon and B horizons. Forest floor litter and humus samples were composited from five points along 20 m transects in low gradient locations below mixed canopies to avoid species-specific bias in litter

composition. Similarly, upland A horizons were collected from five points along 20 m transects along forested backslopes using an ethanol-sterilized auger and composited.

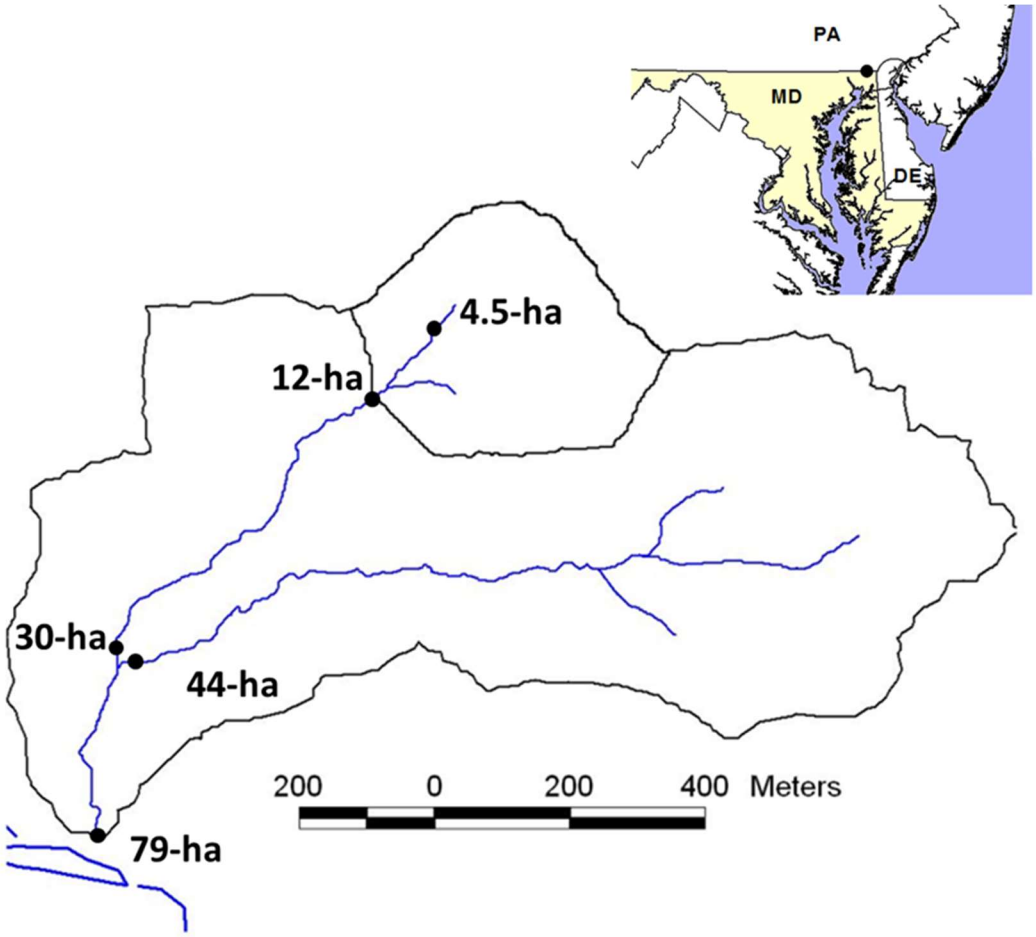

Figure 3.1 Location of the study watershed in Maryland, within the Chesapeake Bay Watershed. The five composite suspended sediment sampling locations are indicated, while discharge and discrete suspended samples were recorded at the 12- and 79-hectare locations.

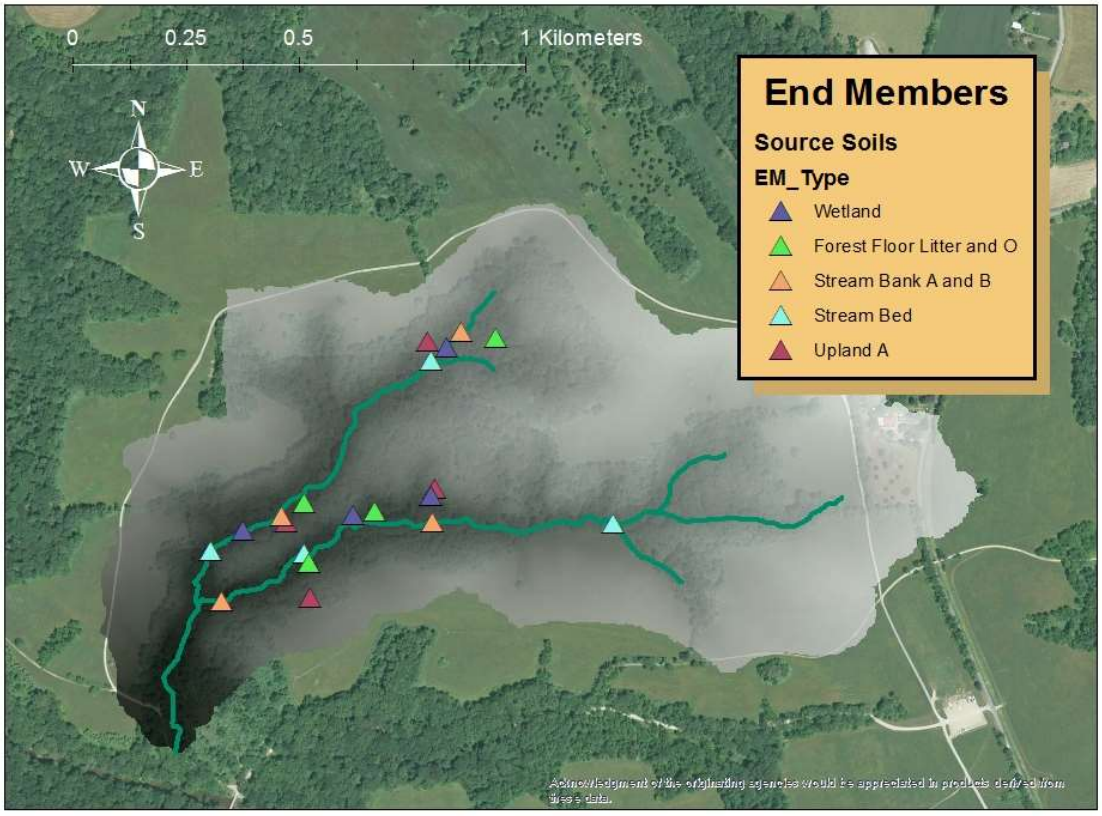

Figure 3.2 End member sediment sampling locations within the study catchment.

Table 3.1: Geospatial analysis of catchment attributes potentially related to POM supply and transport.

	4.5 ha	**12 ha**	**30 ha**	**44 ha**	**79 ha**
Topographic Wetness Index					
10 %	5.09	5.11	4.84	4.86	4.84
50 % (med)	6.61	6.39	6.10	6.24	6.18
90 %	8.61	8.43	8.13	8.21	8.18
Slope (%)					
10 %	1.96	2.37	2.58	2.31	2.43
50 % (med)	4.42	5.36	6.54	5.64	6.10
90 %	10.53	11.99	15.30	13.72	14.50
Soil series coverage (%)					
Baile	28.51	5.02	16.41	14.68	10.65
Galla	*NA*	13.34	3.48	*NA*	2.19
Glenelg	19.00	39.69	14.02	33.80	28.43
Gg	5.88	9.75	3.39	3.03	2.13
Hw	*NA*	*NA*	*NA*	*NA*	1.41
Manor	46.61	32.21	62.70	48.49	55.19

3.2 Hydrologic characterization of sampled events

A total of six high discharge events were selected based on precipitation totals, intensity, seasonal timing, runoff and suspended sediment masses for elemental, isotopic and particle size analysis of passive storm composite samples. Hydro-climatic attributes of the selected events are summarized in Tables 3.2 and 3.3. The sampled events ranged from 31.14 to 148.94 mm of total precipitation and captured a wide range of moderate to high-intensity rainfall conditions and seasonal occurrence, with two events in the spring and autumn, one in the winter, and one in the summer.

The event of May 1, 2014 exhibited the highest total precipitation (148.94 mm), and runoff (25.23 mm, measured at the 12 ha catchment outlet) and resulted in extensive flooding throughout the catchment and surrounding region. However, this event was only ranked fourth in rainfall intensity out of the six sampled events. The July 3, 2015, September 30, 2015, and April 21, 2015 exhibited the three highest maximum hourly precipitation intensities. While the January 19, 2015 event had a relatively lower maximum rainfall intensity of 7.32 mm hr-1, it produced the highest runoff ratio observed in the study period (0.82), presumably due to wet and frozen soils in the study catchment.

Table 3.2: Storm event attributes for the six events collected for analysis of CSS and DSS for all but event number one. API7 is a metric for antecedent moisture conditions indicating the previous seven days' total rainfall.

#	**Collection date:**	**Total rainfall (mm)**	**Rainfall duration (hours)**	**API7 (mm)**	**Max 1-hr rainfall (mm)**
1	*May 1, 2014*	148.94	64	9.70	19.87
2	*Jan. 19, 2015*	31.14	7	16.55	7.38
3	*Apr. 21, 2015*	43.94	12	10.41	19.99
4	*July 03, 2015*	97.36	36	68.21	31.31
5	*Sept. 30, 2015*	40.12	7	0	20.22
6	*Oct. 3, 2015*	59.47	50	41.06	6.99

Table 3.3: Hydrologic data for the six events collected for analysis of CSS and DSS for all but event number one.

#	Collection Date:	Max runoff (mm hr^{-1})	Total runoff (mm)	Runoff ratio	POC yield (kg ha^{-1})
12-ha					
1	*May 1, 2014*	4.50	25.23	0.17	*N/A*
2	*Jan. 19, 2015*	2.02	11.30	0.36	1.75
3	*April 21, 2015*	2.05	11.96	0.27	4.64
4	*July 03, 2015*	2.62	14.80	0.15	20.80
5	*Sept. 30, 2015*	0.47	1.49	0.04	0.28
6	*Oct. 3, 2015*	0.30	2.92	0.05	0.18
79-ha					
1	*May 1, 2014*	*N/A*	*N/A*	*N/A*	*N/A*
2	*Jan. 19, 2015*	3.50	25.39	0.82	*N/A*
3	*April 21, 2015*	3.21	13.15	0.30	2.19
4	*July 03, 2015*	2.63	12.96	0.13	3.55
5	*Sept. 30, 2015*	0.16	0.15	0.01	0.02
6	*Oct. 3, 2015*	0.16	0.46	0.01	0.03

3.3 Sample processing and analysis

CSS were processed for analysis for the six selected high discharge events presented in Tables 3.2 and 3.3, while discrete suspended sediment samples were taken from a total of eight events. Given our sampling methods, it was difficult to obtain the requisite mass for isotopic analysis in DSS so we included auxiliary events beyond those selected for analysis of CSS to increase our sample set used in assessing within-event shifts in the POM concentrations and source. Nineteen auxiliary events were sampled and are included in Table 3.4. Ten of these were submitted for isotopic analysis. Of these, the events analyzed for CSS in addition to four auxiliary events on June 22, 2015, July 27, 2015, August 12, 2015, and February 16, 2016 produced multiple isotopic measurements over the event hydrograph.

Suspended sediment concentrations (SSC) were determined gravimetrically for DSS by drying filters for 1 hour at 105°C, although protocols were changed to 12 hours at 60°C to maintain the integrity of samples for stable isotope and molecular biomarker analyses later in the study period, and concentrations were recorded in mg L^{-1}. Samples with sediment retentate > 100 mg were saved for isotope analysis.

Both end member sediment samples and CSS were dried in acid-cleaned Pyrex dishes in an oven at 45°C. Oven-dry CSS samples were homogenized and partitioned into 2 mL vial aliquots for bulk size fraction analyses. The remaining sample was then partitioned into coarse (CPOM) >1000 μm, medium (MPOM) 1000-250 μm and fine (FPOM) < 250 μm size classes via dry sieving. Dry masses were recorded for particle size class from which the fractional mass percent was calculated for each class in each CSS sample. End member samples were not partitioned into particle classes prior to analysis, but were pre-sieved at 2 mm to remove large organic debris such as

roots. Aliquots in 2 mL vials were lyophilized overnight and preserved in a desiccator cabinet until encapsulation for elemental and isotopic analysis.

CSS and end member samples were ground to a powder-like consistency using an ethanol-rinsed ceramic mortar and pestle and homogenized. DSS samples were obtained by scraping material from glass fiber filters using a sterilized spatula. Care was used to minimize removal of filter material and any visible pieces were removed from the material for encapsulation using sterilized forceps. Filters were pre-combusted to remove organic material. All samples were then weighed to the closest 0.01 mg according to expected ranges of carbon and nitrogen content to optimize elemental and isotopic analysis and subsequently enclosed in 5 x 9 mm tin capsules in duplicate or triplicate wherever sufficient sample was available. End-member samples were encapsulated as a whole (un-sieved) sample in analytical triplicates. A total (not accounting for replication) of 28 end member samples, 19 CPOM, 26 MPOM, 29 FPOM, and 38 discrete time suspended sediment samples (i.e. filter retentate from ISCO samples, not size partitioned) were analyzed.

Elemental and isotopic analysis for carbon and nitrogen

Percent carbon and nitrogen and stable isotopic ratios were determined simultaneously via coupled elemental analysis and isotope ratio mass spectrometry (EA-IRMS). Analyses were performed at two labs: the Environmental Isotope Geochemistry Lab (EIGL) at the University of Delaware and the Duke Environmental Isotope Lab (DEVIL) at Duke University. Five samples for cross comparisons and an International Humic Substances Society organic matter standard (Suwanee River NOM) were submitted to both analytical facilities to ensure cross comparability of results in addition to their respective quality assurance procedures. Carbon and

nitrogen stable isotope ratios were reported in standard delta notation (‰) relative to Vienna pee dee belemnite and air, respectively. Atomic C:N ratios were calculated by first dividing the mass percent carbon and nitrogen by their respective molar masses, then dividing moles of carbon by nitrogen.

Particle size characterization by laser diffraction

In addition to determining the percent by mass of each discrete size class in CSS, particle size distributions were determined via laser diffraction on a Beckman-Coulter LS-13320 in the Advanced Materials Characterization Laboratory at the University of Delaware. Passive samples were thoroughly homogenized and resuspended in deionized water at a concentration of 1000 mg L^{-1} in order to obtain sufficient obscuration of light for accurate determinations of particle size distribution. Suspensions were analyzed in triplicate using the universal liquid module for the instrument. The mean distribution of triplicate runs was reported in order to account for inconsistencies in particle shape following Martilla and Kløve (2014) as the instrumental Fraunhofer method assumes a spherical particle. Particle size density probability density functions were reported in the range of diameters from 0.38 to 2000 μm.

Table 3.4: All events for which DSS were submitted for elemental or elemental and isotopic analysis. More suspended sediment points were measured than the number given for chemical analyses, and the temporally-closest carbon and nitrogen values were applied to those points.

Date	*n* samples 12 ha	*n* samples 79 ha	Isotope analysis
August 13, 2014	4	3	No
September 25, 2014	5	0	No
November 18, 2014	2	1	No
January 19, 2015	2	1	Yes
March 10, 2015	1	3	No
April 21, 2015	4	3	Yes
June 22, 2015	1	2	Yes
June 29, 2015	1	4	Yes
July 1, 2015	0	7	Yes
July 27, 2015	2	3	Yes
August 12, 2015	3	0	Yes
September 30, 2015	2	4	Yes
October 3, 2015	2	1	Yes
November 20, 2015	0	2	No
December 23, 2015	2	4	No
February 16, 2016	1	1	Yes
February 25, 2016	3	1	No
May 7, 2016	3	4	No
May 31, 2016	3	0	No

3.4 Data analyses

Catchment yield calculations

Stream flow POC yields were calculated at both the 12 and 79 ha outlets for five of the six storm events sampled for CSS (Table 3.2.2). The May 01, 2014 event did not have DSS samples upon which to base these calculations, and discharge data was compromised at the 79 ha catchment outlet, and was thus excluded from analysis. Similarly, only one DSS point on at the 79 ha catchment outlet was measured for the January 19, 2015 event, so yields were only calculated for the 12 ha catchment.

Measured SSC values were interpolated to the 20 min time step of discharge measurements by fitting LOESS curves to the sampled points across the hydrograph and assumed concentrations of 0 mg L^{-1} before storm flow inception and after hydrograph recession. Resulting suspended sediment concentrations were multiplied by the percent C and N of the temporally-closest sample that was submitted for elemental analysis to generate POC and PN concentrations (mg L^{-1}). These were then multiplied by discharge in liters second $^{-1}$for each timestep and summed to calculate a flux estimate for the event (reported in kilograms). Finally, fluxes were normalized by catchment area (in hectares) to generate a yield estimate in kg ha^{-1}.

Multivariate statistics

A multivariate analysis of variance (MANOVA) was performed to test for significant differences in the total suspended POM pool (TPOM) and for each size class at the five sampled drainage areas using percent carbon, percent nitrogen, C:N, $\delta^{13}C$ and $\delta^{15}N$. Values of each parameter for analysis of TPOM were determined by averaging the values of each chemical parameter measured for each size class, weighted by the observed mass percent of that class in each CSS sample. Box's M-

test was used to test for inhomogeneity of covariance matrices. Significant results indicated inhomogeneity exists, and could violate assumptions of MANOVA. Extensive negative values existed in the dataset due to delta-reporting standards for stable isotopes, so the data could not be log transformed. Instead, Pillai's trace test statistic was selected as the test statistic for MANOVA as it is more resistant to departures from assumptions of equal variance and normal distributions, although it is less powerful than alternatives (e.g. Wilk's Lambda).

Mixing model analysis

A statistical mixing model was implemented to generate quantitative estimates of the fractional contributions of the sampled end members at each sampled drainage location. We selected SIMMR (version 0.3, Parnell, 2016), a new ecological modelling tool developed from the previous mixSIAR which uses a Bayesian JAGS ("just another Gibbs sampler")-Markov chain Monte Carlo (MCMC) framework to generate probability distributions of different end members' contributions to a given sample. A Bayesian model was deemed preferable to a linear mixing model in this case to quantify the variability in end member contributions in addition to values representing measures of central tendency. Trophic enrichment factors were omitted from the model. The model was implemented in R version 3.2.3 for each particle size class to assess changes in source contributions to different sizes of POM along the network. Gelman diagnostic statistics were reviewed to ensure MCMC convergence after a model run, and these were all found to be sufficient (close to 1).

In order to assess changes to the total POM pool, elemental and isotopic content for total POM was aggregated by a weighted average across the three size classes. Weightings were determined from the mass proportion of each class recorded

after sieving samples, or by values from the laser-diffraction aliquots in a few instances where their masses were not available. C:N was included as a third parameter in the model after graphical analysis revealed its potential to further resolve differences between end members and to decrease uncertainty of modeled posterior distributions without introducing major alterations to their measures of central tendency.

Modes of posteriors were selected as the preferable measure of central tendency for each model run because these represent the "most probable" contribution of a given end member to POM, or the value observed most commonly over simulated sampling. The mean was considered to be less representative of posterior distributions in this case because it is sensitive to outliers and we observed several highly skewed distributions (Appendix D). Finally, 95 percent credible intervals (or highest density intervals) were calculated for each posterior distribution using the coda package in R.

Chapter 4

RESULTS

4.1 Elemental and isotopic composition of potential POM end members

Of the seven POM end members (Table 4.1.1), forest floor litter samples had the highest mean percent C content, followed by forest floor humus, wetland soils, stream bank A horizons, upland A horizons, stream banks B horizons, and stream beds. Mean percent N content followed a similar pattern, with the exception that the value for the upland A horizon was slightly higher than that of the stream bank A horizon. Mean atomic C:N ratios ranged from 16.33 to 34.14 and exhibited a slightly different pattern with lowest values observed in stream bank A horizons, followed by humus, stream beds, wetlands, stream bank B horizons, upland A horizons, and litter (Table 4.1.1). Although forest floor litter and humus samples had higher standard deviations for total C and N content, stream beds, stream banks and wetlands had higher coefficients of variation (i.e. standard deviation relative to their mean). C:N was highest in the forest floor litter, upland A and wetland end members, but had higher coefficients of variation in in stream beds and stream banks. Stable isotope ratios were negatively correlated with C and N content in end member samples (linear model; $p < 0.01$) and indicated a trend toward isotopic enrichment in samples with proportionally less C and N. Forest floor litter had the most depleted $\delta^{13}C$ and $\delta^{15}N$ while stream banks (A and B horizons) were the most enriched in both isotopes. MANOVA analysis indicates significant differences exist between end members

(Pillai's trace statistic, $p < 0.01$) and significant differences for specific parameters are enumerated in Table 4.1.

Table 4.1 Mean elemental and isotopic content across end member replicates. Standard deviation are given in parentheses and letters indicate significant differences by ANOVA with post-hoc Tukey's HSD. Calculation of atomic C:N is included in section 3.3.

	% C	**$\delta^{13}C$**	**% N**	**$\delta^{15}N$**	**C:N (atomic)**
Forest Floor Litter	46.11 (2.82, *A*)	-29.53 (0.38, *C*)	1.74 (0.06, *A*)	-4.50 (0.44, *D*)	31.83 (2.27, *A*)
Forest Floor Humus	11.40 (2.97, *B*)	-28.27 (0.30, *ABC*)	0.80 (0.12, *B*)	-2.08 (0.95, *CD*)	19.25 (1.25, *B*)
Wetland	5.07 (2.60, *C*)	-28.82 (0.71, *BC*)	0.25 (0.13, *C*)	-0.02 (0.46, *BC*)	22.51 (2.25, *B*)
Upland A	1.90 (0.68, *CD*)	-27.74 (0.43, *AB*)	0.09 (0.03, *D*)	3.42 (0.82, *A*)	23.04 (2.48, *B*)
Stream Bank A	2.14 (0.94, *CD*)	-27.02 (0.65, *A*)	0.06 (0.05, *D*)	3.92 (1.24, *A*)	17.52 (0.18, *B*)
Stream Bank B	1.02 (0.31, *D*)	-27.68 (0.31, *AB*)	0.05 (0.02, *D*)	4.96 (1.70, *A*)	22.54 (3.12, *B*)
Stream Bed	0.73 (0.96, *D*)	-28.72 (0.68, *BC*)	0.02 (0.01, *D*)	1.03 (0.96, *B*)	20.44 (5.10, *B*)

4.2 Changes in sediment particle size along the stream network

The median diameter (d_{50}) of CSS increased with catchment drainage area (Figure 4.1). The d_{50} of each sample obtained from laser diffraction analyses was fit to drainage area with a linear model ($p < 0.01$, $R^2 = 0.25$, $\beta_1 = 4.15$). Linear models fit to the 10th and 90th percentiles of sediment diameter showed increasing particle diameter with drainage area when analyzed over multiple events ($p = 0.01$ and < 0.01, respectively). The slope parameter was highest for the 90th percentile ($\beta_1 = 6.55$), suggesting mobilization of the coarsest material downstream explains much of the increases in particle size distributions.

Proportions of the three discrete particle size classes obtained from masses after size class partitioning of composite samples are indicated in Figure 4.2 and also suggest increases in sediment particle size at larger drainage scales. These were analyzed for five of the six events in the study period, and showed that proportions of fine and medium size fractions did not change significantly at different drainage areas (ANOVA, $p = 0.48$ and 0.99 respectively). Coarse sediment changed significantly with drainage area ($p = 0.04$), as a result of significant higher proportions at the 79 ha compared to other drainage locations (Tukey's HSD). General observations by event suggest that relationships between proportions of the fine and medium size classes and drainage area were highly variable, whereas proportions of coarse sediment were consistently highest at the 79 ha location (Figure 4.2). This analysis is consistent with the observation that mobilization of the coarsest particles at the largest drainage scales drives increasing trends in particle size downstream as noted above.

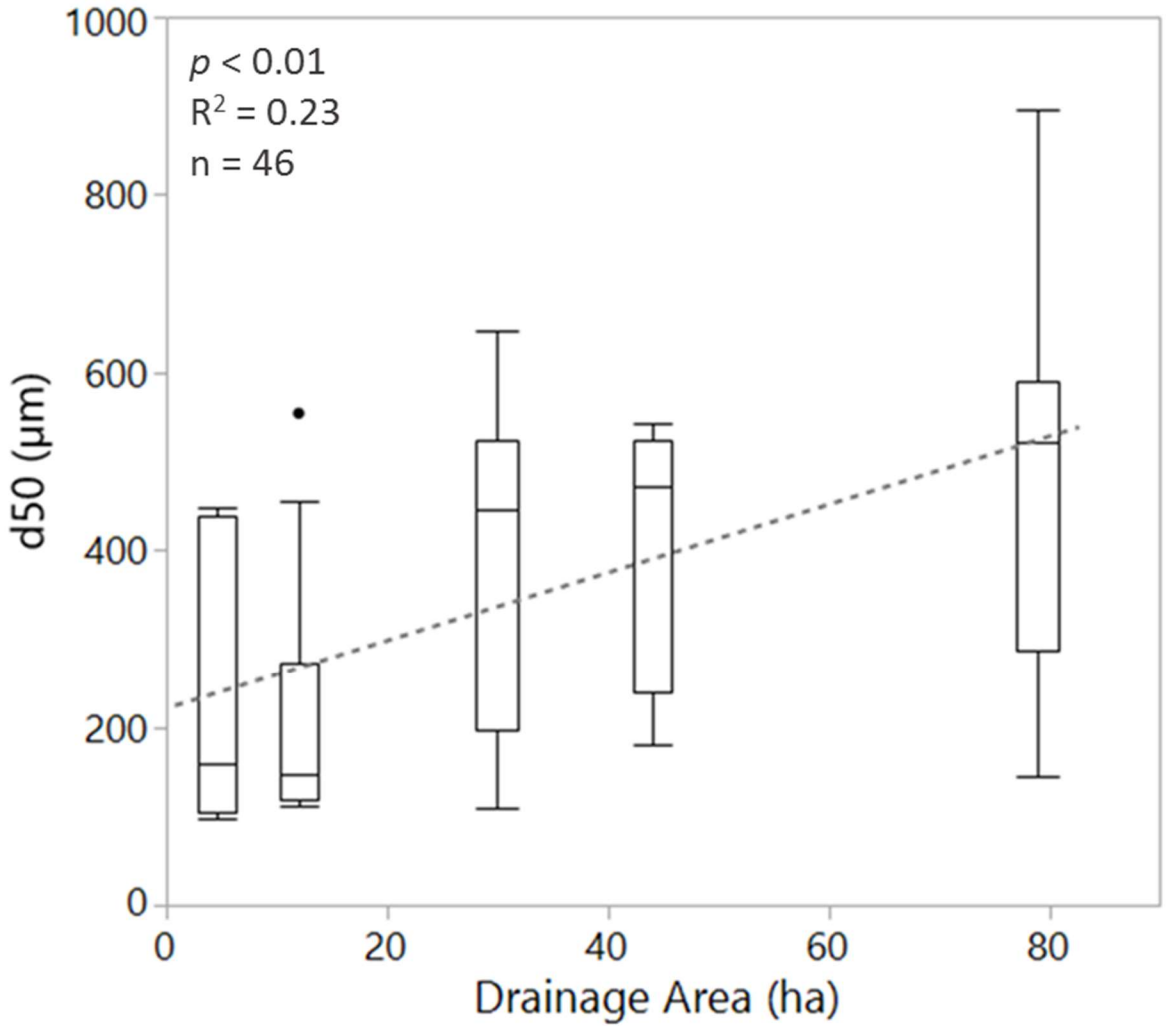

Figure 4.1 Increasing particle size in CSS at larger drainage areas measured by laser diffraction. The generally increasing pattern was consistent for individual events and for quantiles other than the median (i.e. 10th and 90th percentiles). The linear model was significant at $p < 0.01$.

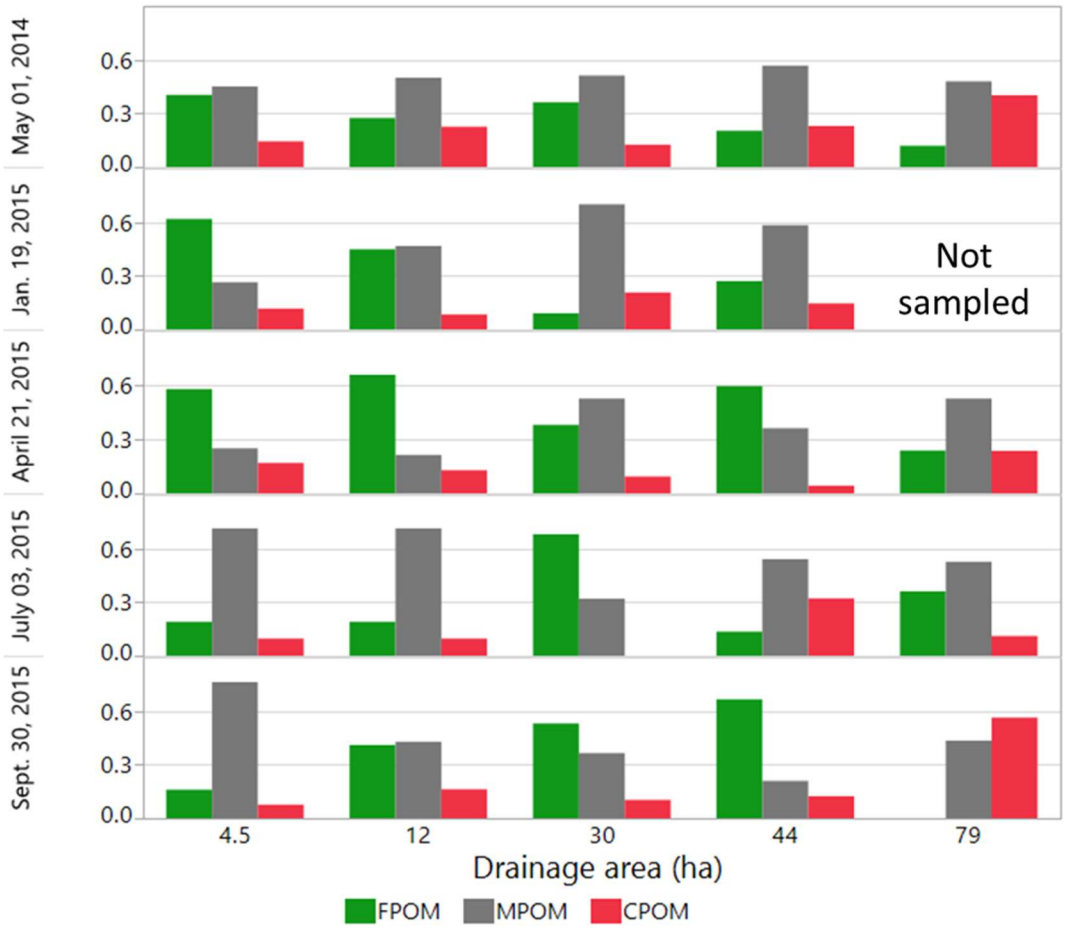

Figure 4.2 The proportion of each POM size class measured by mass after sieving for each event.

4.3 C and N content and isotopic composition with particle class at stream drainage locations for CSS

Linear models to determine significant trends in POM parameters with drainage area ($\alpha = 0.05$). Percent C decreased with drainage area for CPOM, percent C and N and C:N decreased while $\delta^{13}C$ enriched (increasingly positive values) in MPOM, and all of the above trends plus enrichment in $\delta^{15}N$ were observed in FPOM. Percent nitrogen and C:N exhibited a complex relationship with drainage area in CPOM (Figures 4.3 and 4.4). It is important to note that deviations from linear trends were observed in POM from the sampling location draining the smallest (4.5-ha) subcatchment, which appeared more similar to POM from the 30 ha, 44 ha, and 79 ha sampling locations in terms of percent C and N and $\delta^{13}C$ than it did to the intermediate 12 ha sampling location (Figures 4.3 and 4.4). This spatial pattern decreased the strength (R^2) of linear correlations between drainage area and the observed elemental and isotopic content of samples. While $\delta^{15}N$ only enriched at larger drainage areas for FPOM, it varied consistently by particle size class (Figure 4.4), and was significantly more enriched in FPOM than in the other size classes (ANOVA, $p < 0.01$). Similarly, C:N displayed a consistent separation by particle size class, with lower values observed in fine particles (ANOVA, $p < 0.01$). Percent elemental content and $\delta^{13}C$ had more variable relationships with particle size class, and did not exhibit statistically significant trends when assessed across the entire drainage network.

MANOVA analysis performed on TPOM, CPOM, MPOM, and FPOM, and returned p values of <0.01, 0.69, 0.08, and < 0.01, respectively. This indicates that significant differences with drainage area in the TPOM pool over multiple events are result of changes in the fine (< 250 μm) fraction, where CPOM and MPOM may not change significantly.

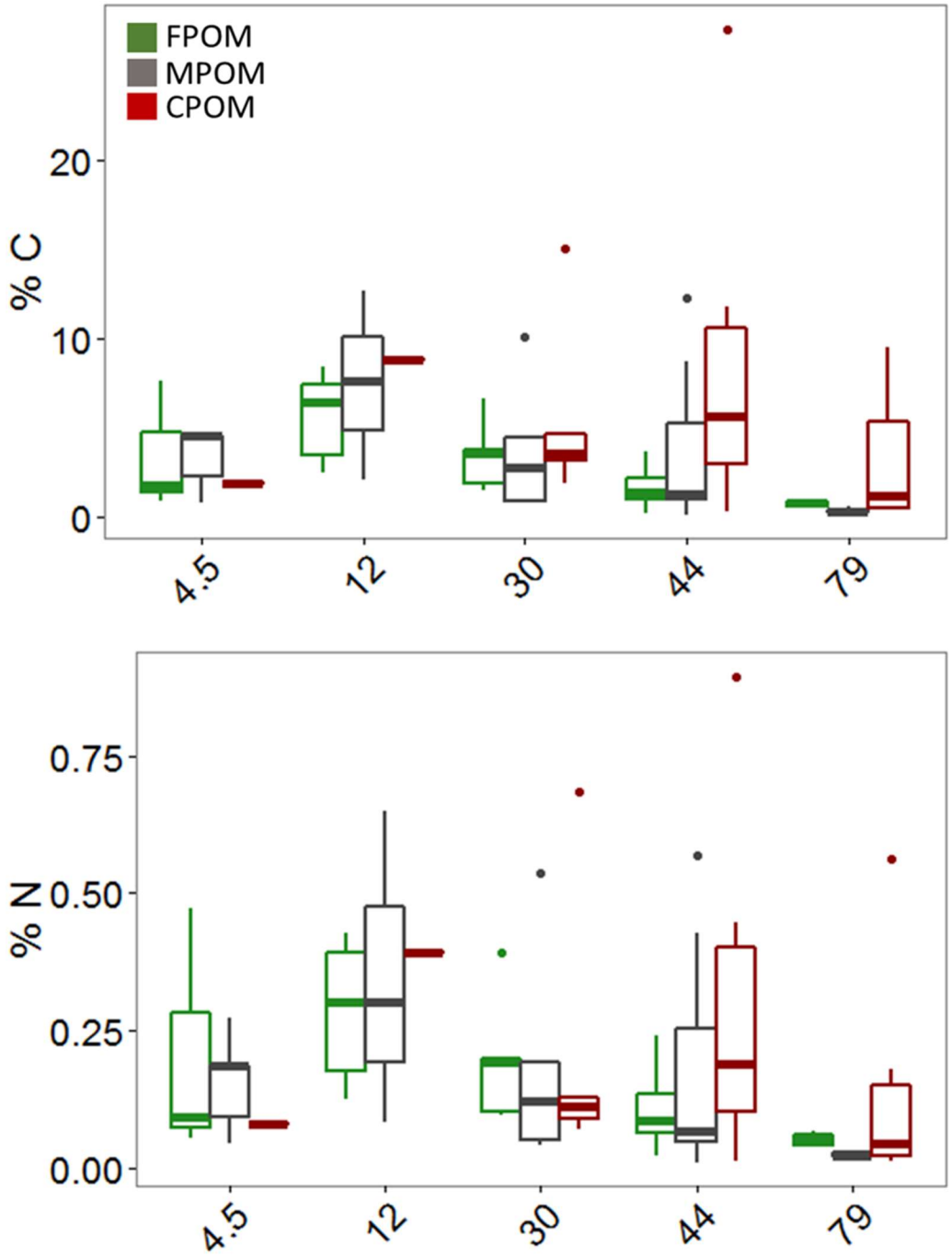

Figure 4.3 Downstream variability in sediment C and N content by particle size classes.

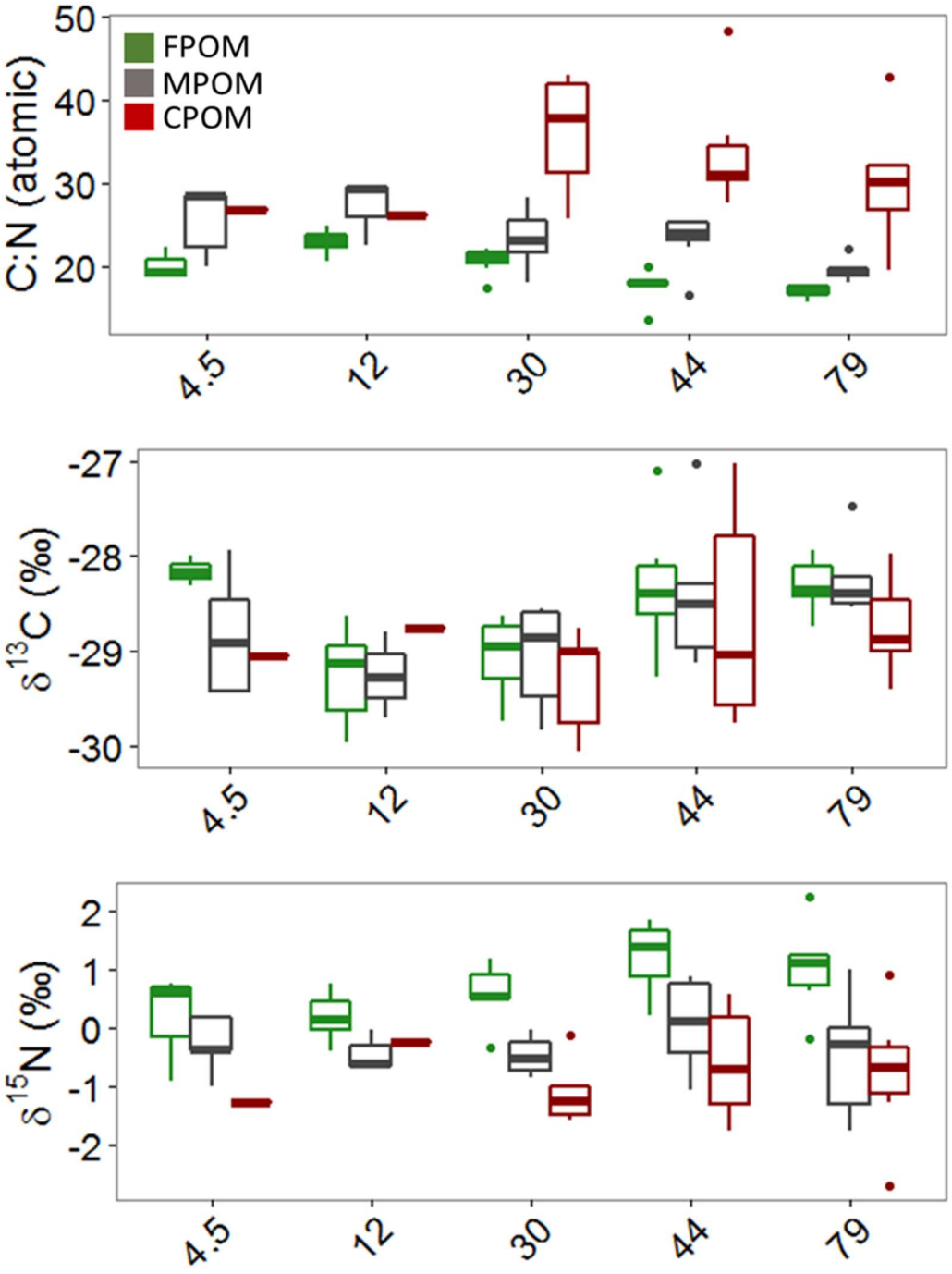

Figure 4.4 Downstream variability in sediment C:N ratio, $\delta^{13}C$ and $\delta^{15}N$ by particle size classes.

Table 4.2: Mean POM data for all composite suspended sediment samples, by size class and drainage location.

	Drainage area (ha)	**% C**	**$\delta^{13}C$**	**% N**	**$\delta^{15}N$**	**C:N (atomic)**
Coarse	*4.5*	1.85	-29.05	0.08	-1.30	26.90
	12	8.77	-28.77	0.39	-0.27	26.22
	30	5.67	-29.32	0.22	-1.10	35.95
	44	8.88	-28.66	0.31	-0.61	34.05
	79	3.22	-28.75	0.14	-0.78	30.28
Medium	*4.5*	3.41	-28.83	0.16	-0.27	25.79
	12	7.46	-29.26	0.34	-0.45	27.28
	30	3.60	-29.05	0.18	-0.49	23.48
	44	3.74	-28.46	0.18	0.07	23.38
	79	0.37	-28.23	0.02	-0.48	19.76
Fine	*4.5*	3.45	-28.16	0.21	0.14	20.27
	12	5.68	-29.25	0.28	0.18	23.11
	30	3.29	-29.05	0.18	0.59	20.82
	44	1.66	-28.31	0.11	1.22	17.89
	79	0.76	-28.31	0.05	1.02	17.22

4.4 Evaluation of CSS versus POM sources in the mixing model space

Potential POM end members and CSS samples were evaluated by particle class, sampling location, and storm magnitude (using maximum event runoff and maximum precipitation intensity) in mixing model space defined by $\delta^{15}N$, $\delta^{13}C$ and C:N ratio (Figures 4.5 through 4.13). Stream bank A and B horizons were combined as one end member ("stream banks") in the conceptual mixing space because of their similarity in stable isotope and atomic C:N ratios (Table 4.1). Considerable overlap was also observed in the conceptual mixing space for the error ranges of wetlands with those of stream bed and between those of upland A horizons and stream banks (e.g. Figure 4.5). Many of the CSS samples were proximal to wetlands and stream beds in the mixing space, and plotted to either side of these end members. Most of these samples were much further from the region within the mixing space defined by the error ranges of upland A horizons and the combined stream bank end members. This suggests that distinction between wetlands and stream beds may be possible, while uplands and banks are indistinguishable using this model (Table 4.1.1).

Overall, the greatest separation between sources and CSS samples was observed in the mixing space defined by $\delta^{13}C$ and C:N. However, enrichment in $\delta^{15}N$ for finer particles suggest this parameter is also useful when distinguishing sources for various particle size classes. Qualitative observations of CSS samples in the mixing space suggest that forest floor litter contributed a considerable amount to CPOM at all drainage locations (Figure 4.5). Litter appears to continue to contribute a notable fraction to MPOM at the 4.5 and 12 ha drainage areas, whereas wetlands are a likely contributor at the 30-ha location and stream banks and forest floor humus appear to have a stronger influence at the 44 and 79 ha drainage areas (Figure 4.6). The means for FPOM samples plot predominantly within the error ranges of the wetland and

stream bed end members, suggesting these are the primary contributors to these size classes of POM. Low C:N values observed at the 44 and 79 ha drainage areas suggest forest floor humus may also contribute to FPOM at these locations (Figure 4.7).

POM for various particle classes was also evaluated in the mixing space (Figures 4.8 through 4.13) for individual storm events of various magnitudes. For these plots means for POM were aggregated across catchment locations. These plots suggest that higher runoff (in mm hr^{-1}) increased litter contributions to CPOM. We observed an altered pattern in MPOM and FPOM, with the highest runoff event (Event # 1; May 1, 2014) shifted toward the humus, stream bank and upland A horizon end members. Despite being of only moderate precipitation intensity, this event produced the highest total rainfall (148.98 mm) and maximum runoff (4.5 mm hr^{-1} at the 12-ha location) and extensive flooding was observed throughout the catchment. Patterns with maximum runoff were also considered using data exclusively from the 79 ha location, and were found to be similar.

Maximum recorded rainfall intensity was considered as a potential hydrologic driver of POM source in addition to maximum runoff as it has been shown to exert a strong control on POM fluxes (Dhillon and Inamdar, 2014). CPOM followed a similar trajectory to that observed for maximum runoff, with higher-intensity events shifted further toward the litter end member (Figure 4.11). MPOM and FPOM, however, plotted close to the center of the space enclosed by the stream bed and wetland end members for the events with the highest maximum precipitation intensities while lower intensity events were shifted toward humus, litter, or stream banks (Figures 4.12 and 4.13). These high-intensity storms events were sampled on April 21, 2015 (#3), July 3, 2015 (#4), and September 30, 2015 (#5).

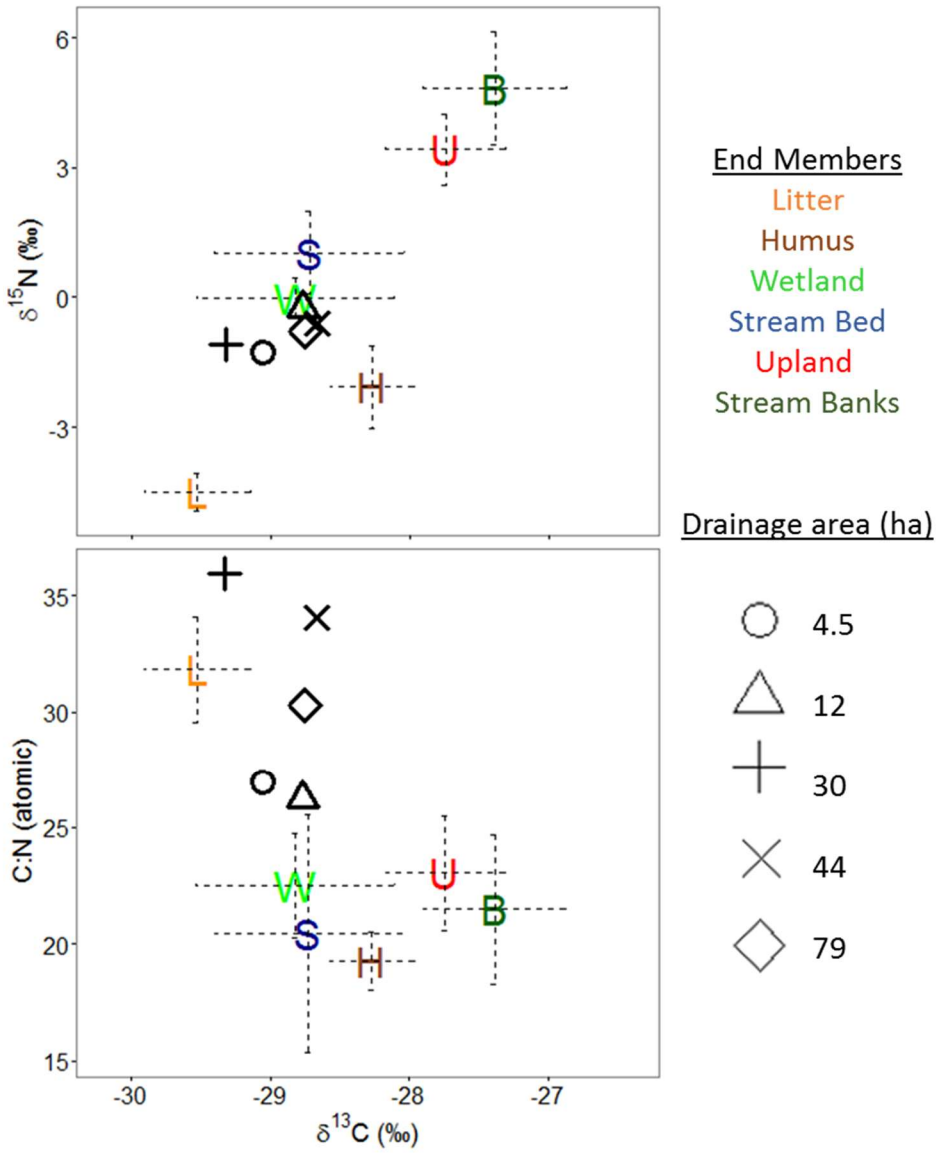

Figure 4.5 Mixing space plots for CPOM, averaged by drainage location across the six sampled events. Error bars represent standard deviations.

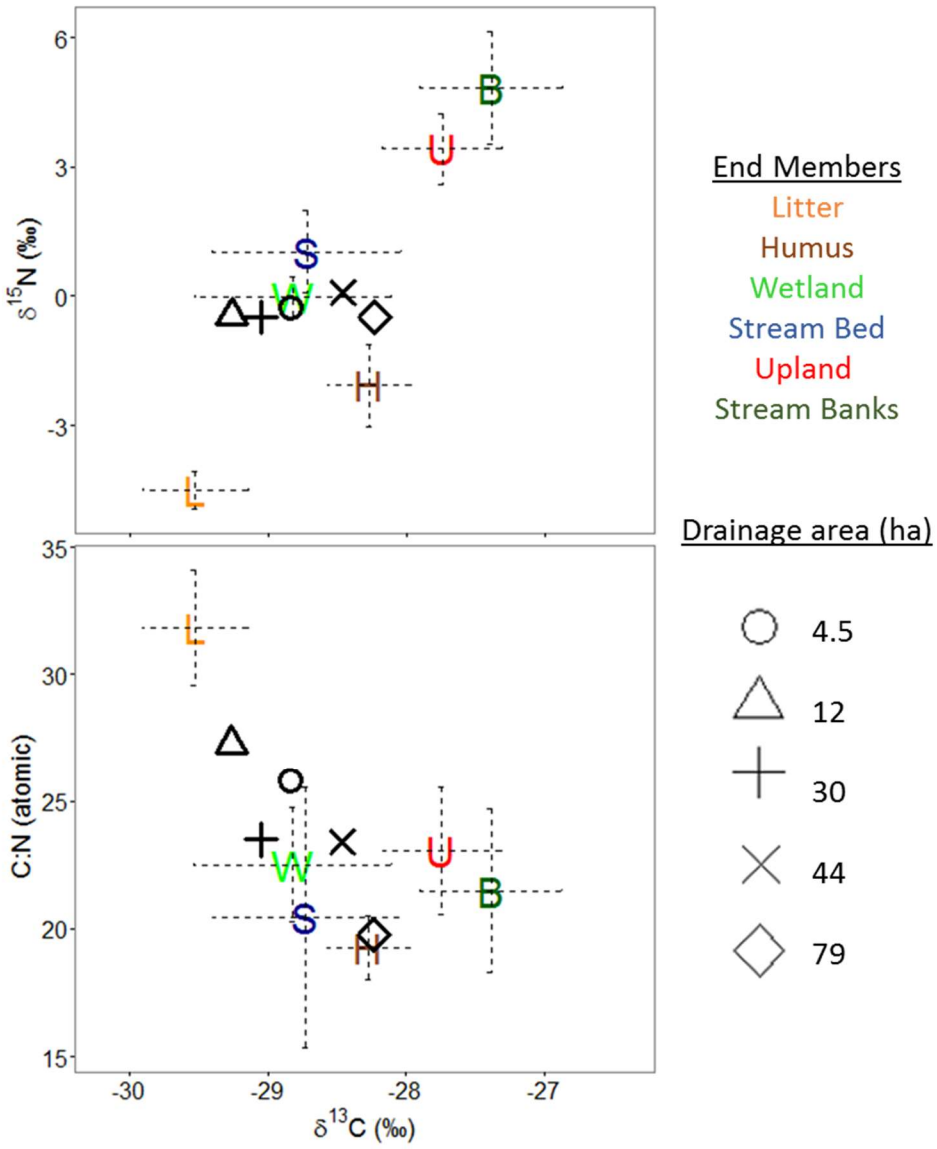

Figure 4.6 Mixing space plots for MPOM, averaged by drainage location across the six sampled events. Error bars represent standard deviations.

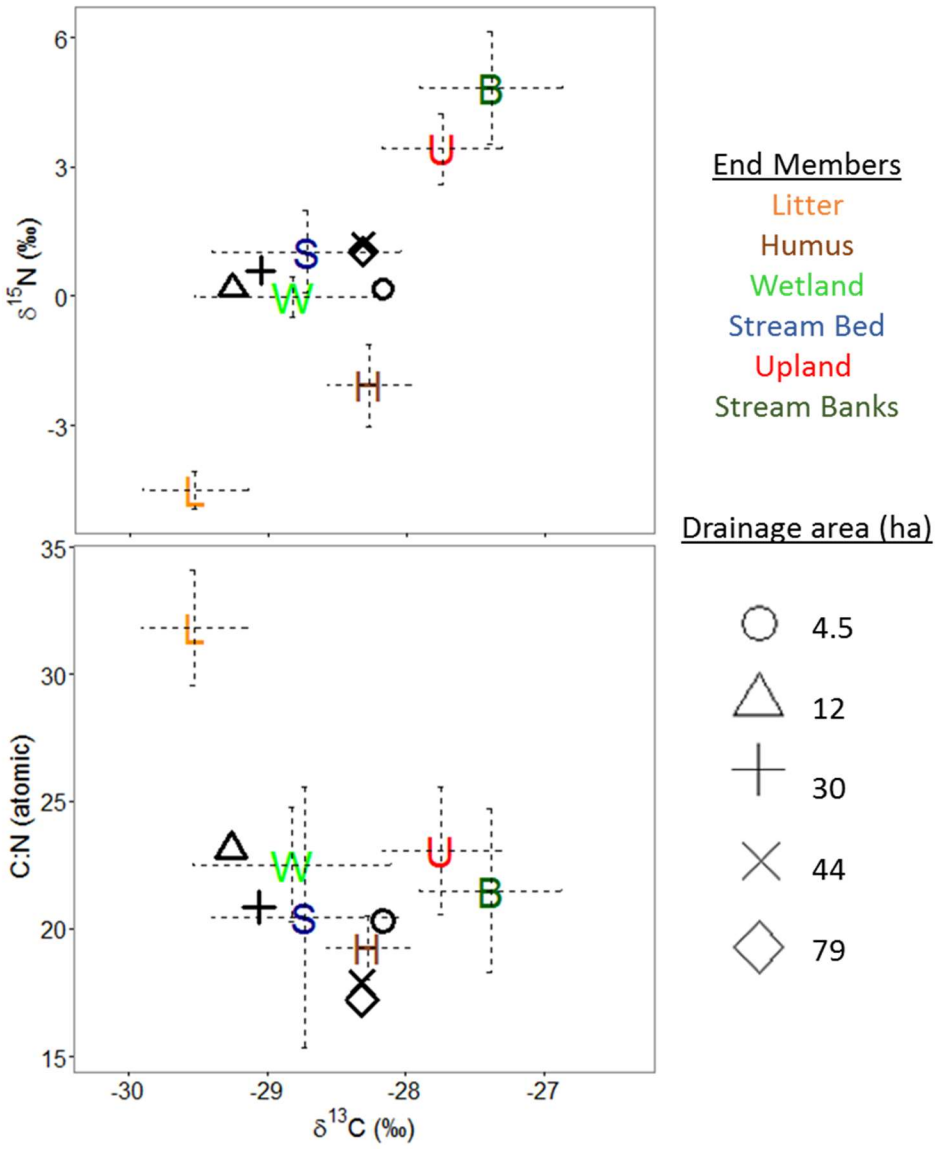

Figure 4.7 Mixing space plots for FPOM, averaged by drainage location across the six sampled events. Error bars represent standard deviations.

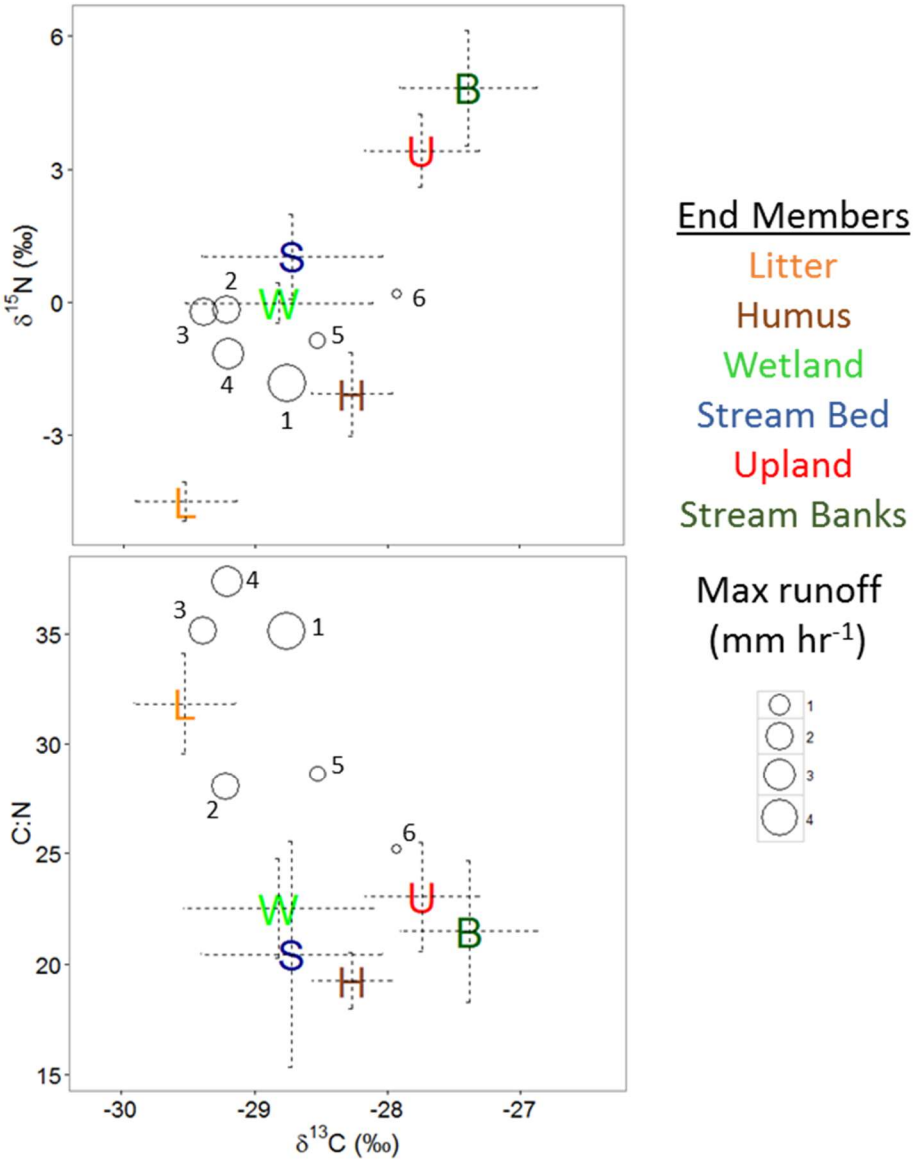

Figure 4.8 Mixing space plots for CPOM, averaged by event across the five sampled locations and sized by maximum recorded runoff. Runoff maximums were taken from the 12 ha catchment because a more robust rating curve exists at this location. These are intended to show relative differences between events. Events are numbered chronologically according to numbers in Table 3.2 and 3.3. Error bars represent standard deviations.

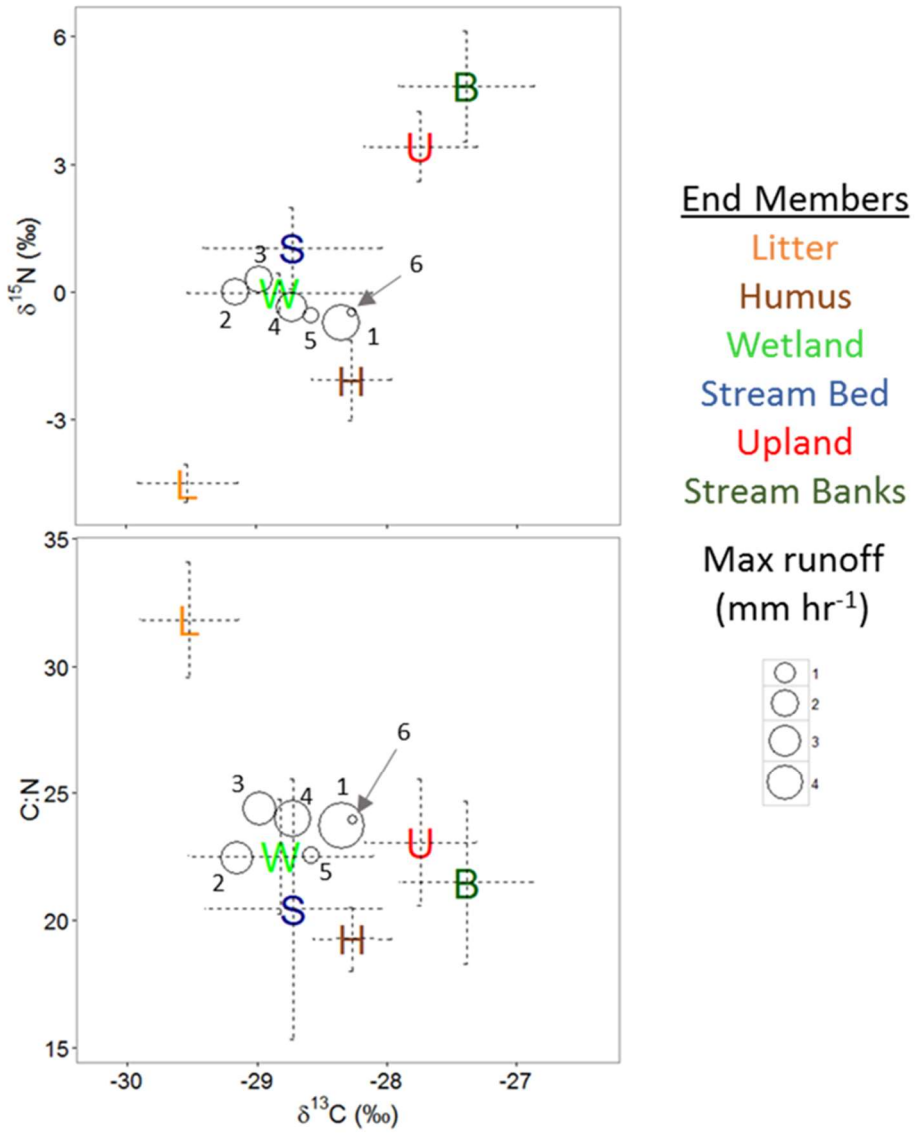

Figure 4.9 Mixing space plots for MPOM, averaged by event across the five sampled locations and sized by maximum recorded runoff. Runoff maximums were taken from the 12 ha catchment because a more robust rating curve exists at this location. These are intended to show relative differences between events. Events are numbered chronologically according to numbers in Table 3.2 and 3.3. Error bars represent standard deviations.

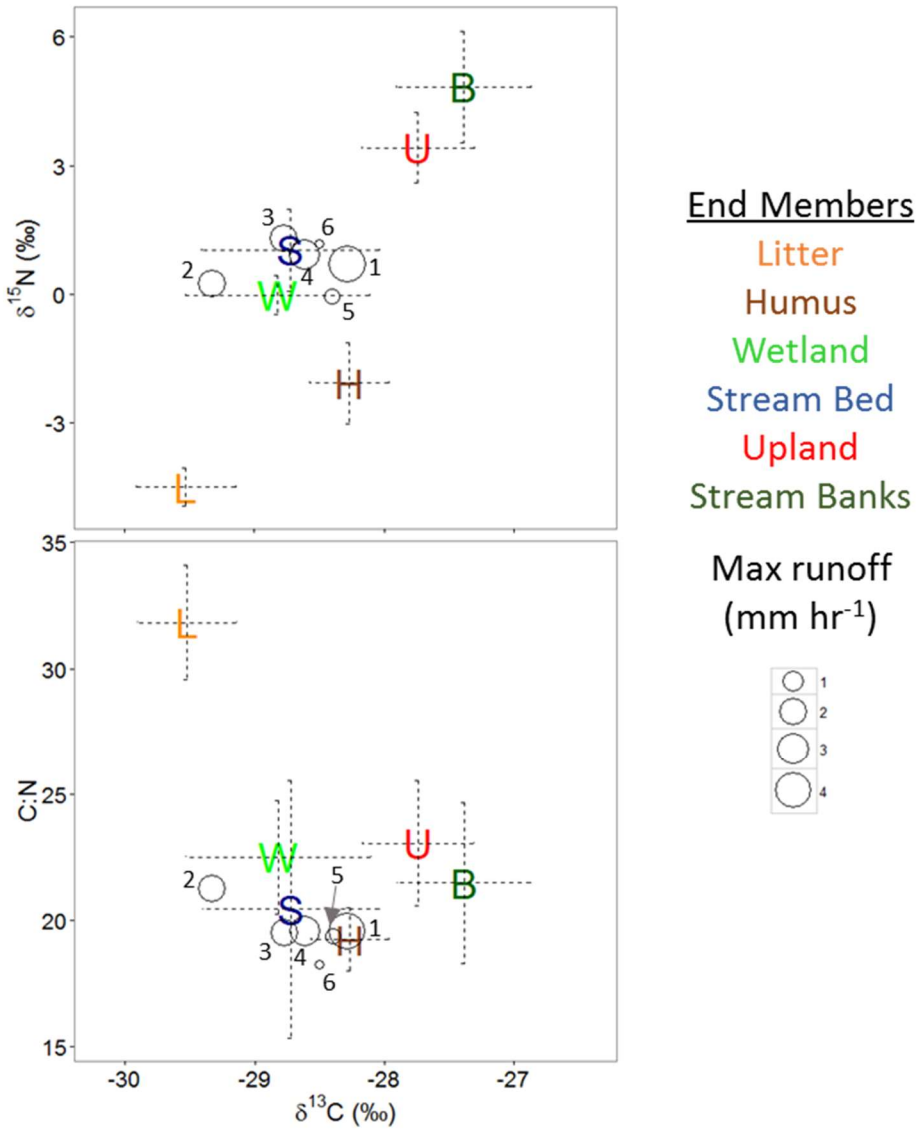

Figure 4.10: Mixing space plots for FPOM, averaged by event across the five sampled locations and sized by maximum recorded runoff. Runoff maximums were taken from the 12 ha catchment because a more robust rating curve exists at this location. These are intended to show relative differences between events. Events are numbered chronologically according to numbers in Table 3.2 and 3.3. Error bars represent standard deviations.

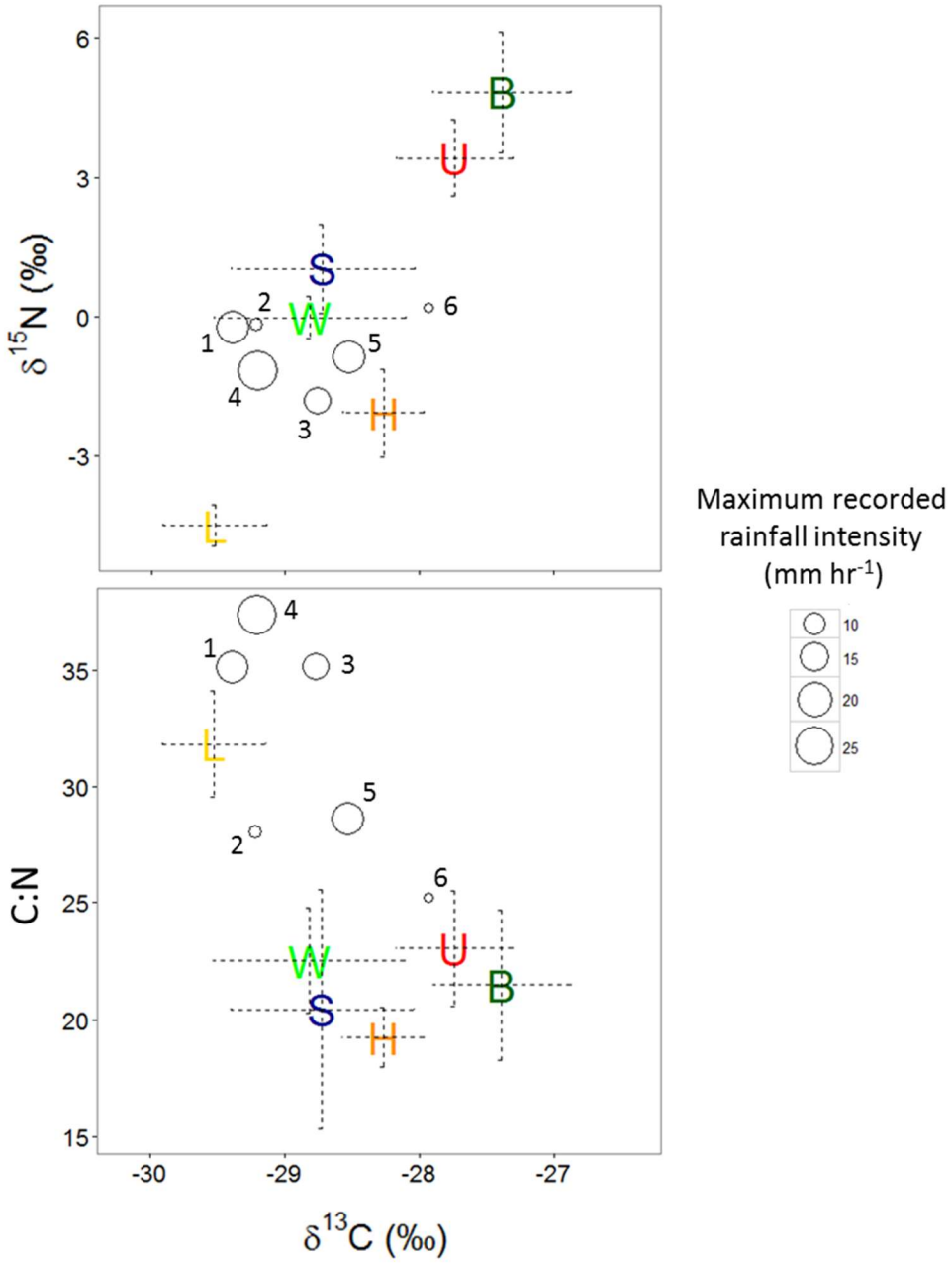

Figure 4.11 Mixing space plots for CPOM, averaged by event across the five sampled locations and sized by maximum precipitation intensity. Events are numbered according to numbers in Table 3.2 and 3.3. Error bars represent standard deviations.

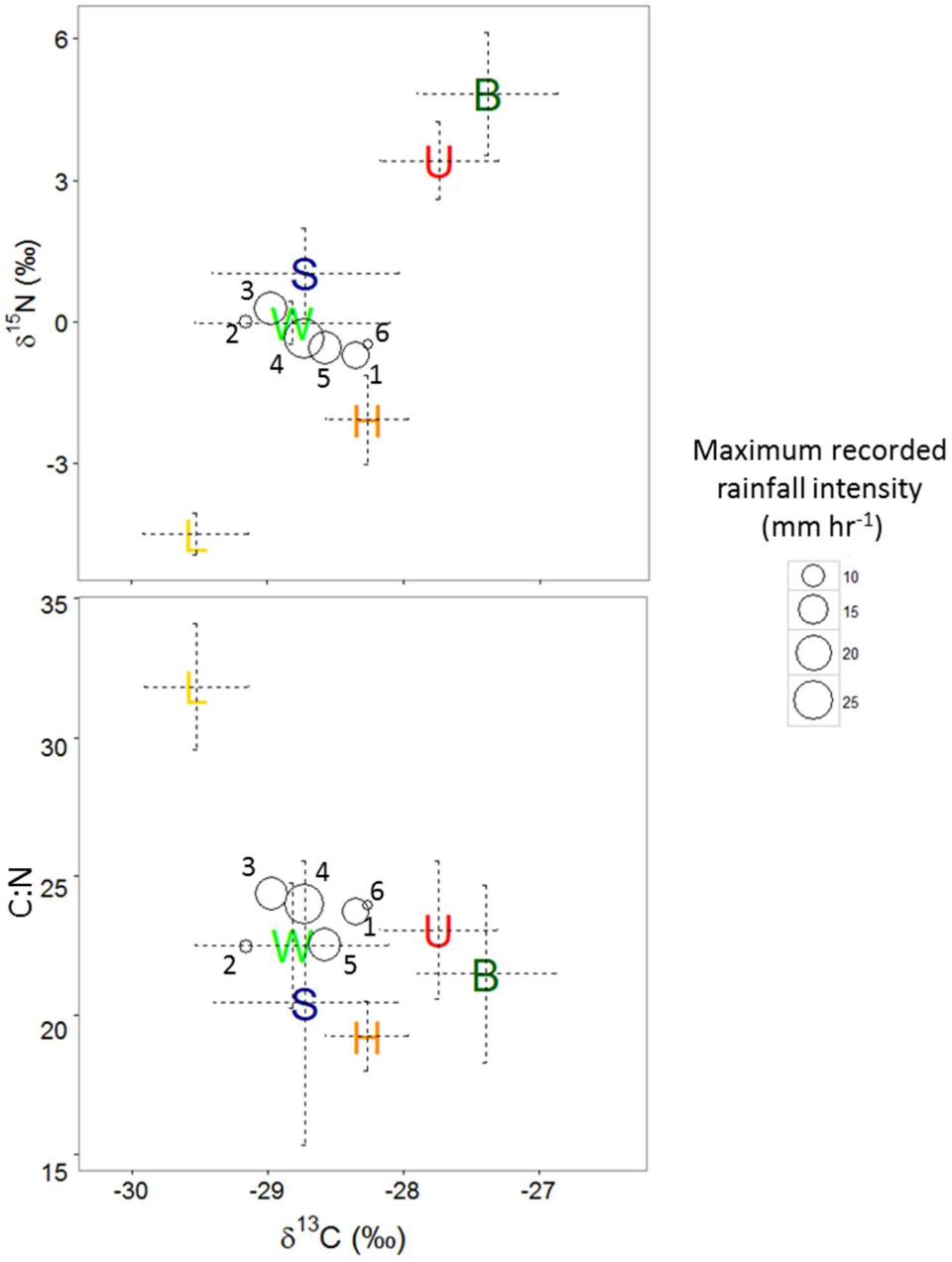

Figure 4.12 Mixing space plots for MPOM, averaged by event across the five sampled locations and sized by maximum precipitation intensity. Events are numbered according to numbers in Table 3.2 and 3.3. Error bars represent standard deviations.

1

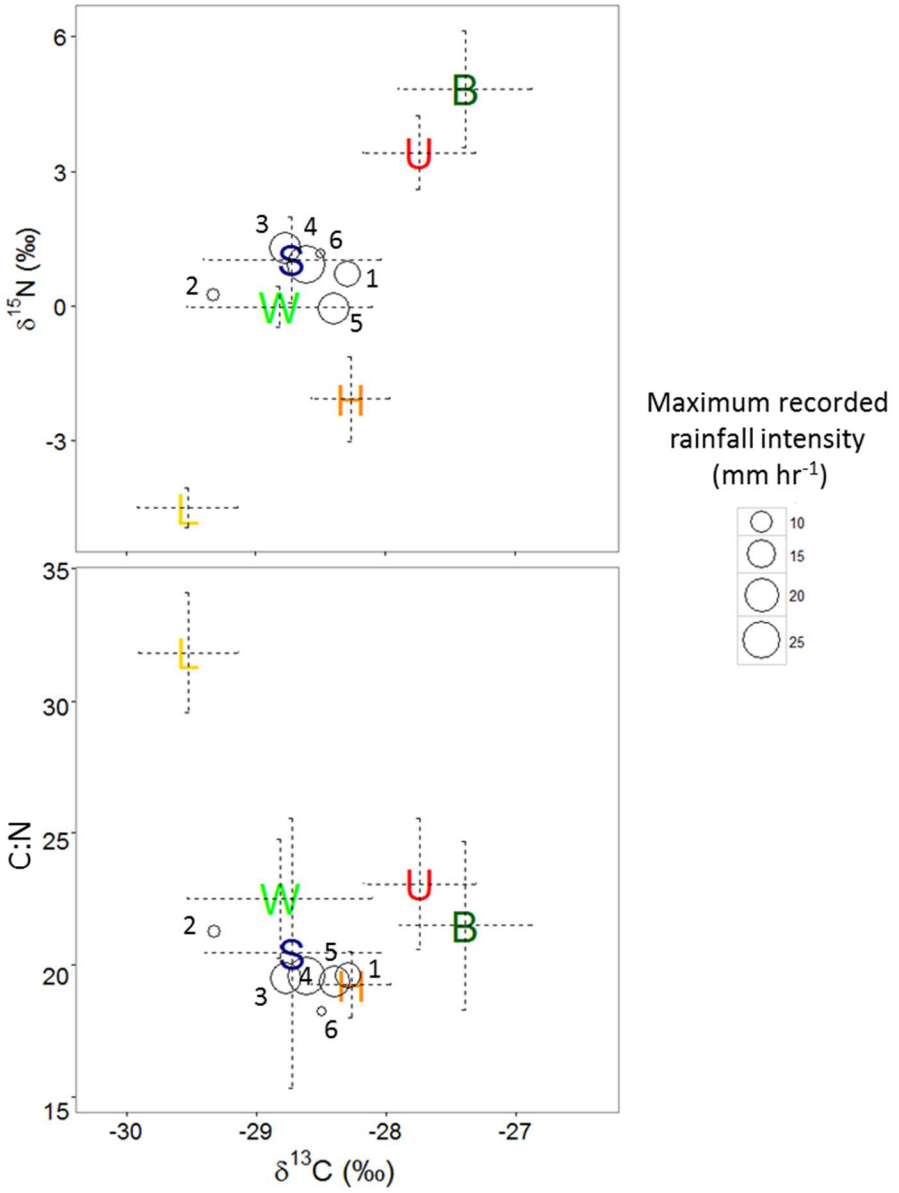

Figure 4.13 Mixing space plots for FPOM, averaged by event across the five sampled locations and sized by maximum precipitation intensity. Events are numbered according to numbers in Table 3.2 and 3.3. Error bars represent standard deviations.

4.5 Quantification of end member contributions to CSS

Implementation of the SIMMR model highlighted several interesting trends in end member contributions for each combination of drainage area and particle size class (Figure 4.14). As discussed in section 4.4, stream bank A and B horizons were combined as one end member due to their indistinguishability in the model mixing space. Upland A horizons were also found to be indistinguishable from the combined stream bank end member during model diagnostics. This end member was assumed to be the least likely to contribute POM to the stream for several reasons:

- The relatively low organic carbon content in upland A horizons (Table 4.1).
- Their greater distance from the stream.
- Their burial below forest floor O horizons.

Combined, these factors make the assumption that A horizons would only contribute a significant proportion of POM to the drainage network under the most extreme conditions defensible. Given the inability of the model to distinguish upland A horizons from stream banks and our assumption that this end member was the least likely to contribute POM, we removed it from model analysis. This had the added benefit of decreasing model uncertainties (Appendix D). However, some posterior distributions, particularly those of wetland contributions, remained relatively wide (Appendix D), suggesting greater variability in their modeled contributions to in-stream POM (Figure 4.14). This could arise from either environmental trends (i.e. different hydrologic or spatial factors leading to more variability in wetlands inputs to POM in our data set) or from greater uncertainty in resolving end members using model parameters. The observation of wide posteriors in sediment fingerprinting studies is consistent with other published literature using similar methods (e.g. Stewart

et al., 2015), and pronounced differences in modeled modes likely represent true differences in the probability of different end members' proportional contributions to POM.

Forest floor litter was found to contribute the largest fraction to CPOM at all drainage locations, but these generally decreased when moving to larger drainage areas (Figure 4.14). The stream bed contributed to a large fraction of FPOM across the network, and this increased at larger drainage areas (i.e moving downstream). However, stream bed contributions to TPOM peaked at the 12 and 30 ha locations due to a greater mass of FPOM contributing to TPOM here.

Generally, stream banks contributed more to POM at the 4.5, 44 and 79 ha locations than they did at the 12 and 30 ha locations. Wetlands consistently contributed a proportionally large amount to TPOM, and this was particularly pronounced at the 12 and 30 ha locations (modes of model outputs were second only to forest floor litter although considerable right-skew was observed in these distributions, Figure 4.14). This pronounced influence resulted from high wetland inputs to FPOM at these locations. The largest drainage location (79 ha) generally had a more homogeneous distribution of end member contributions for all particle size classes when compared to other locations, suggesting a more integrated pool of POM export from the catchment. Humus, however, contributed a large proportion of MPOM at the 79 ha location.

In addition to the spatial trends highlighted above, SIMMR was implemented by aggregating each particle size class across drainage locations and using each of the individual storm events sampled for CSS as treatments (Figure 4.15). This is intended to quantify the patterns observed in Figures 4.8 through 4.13 and elucidate the

hydrologic influences on POM source. The May 01, 2014 exhibited the highest contribution of forest floor litter and second highest contribution of humus to TPOM. The January 19 and April 21, 2015 events had the highest contributions of wetlands and stream beds to TPOM, respectively. Humus contributions to TPOM were highest for the September 30, 2015 event. The July 03, 2015 had the highest rainfall intensity and contributed the most bed material to FPOM. TPOM values were not obtained for the October 03, 2015 event due to a lack of reliable size distribution data.

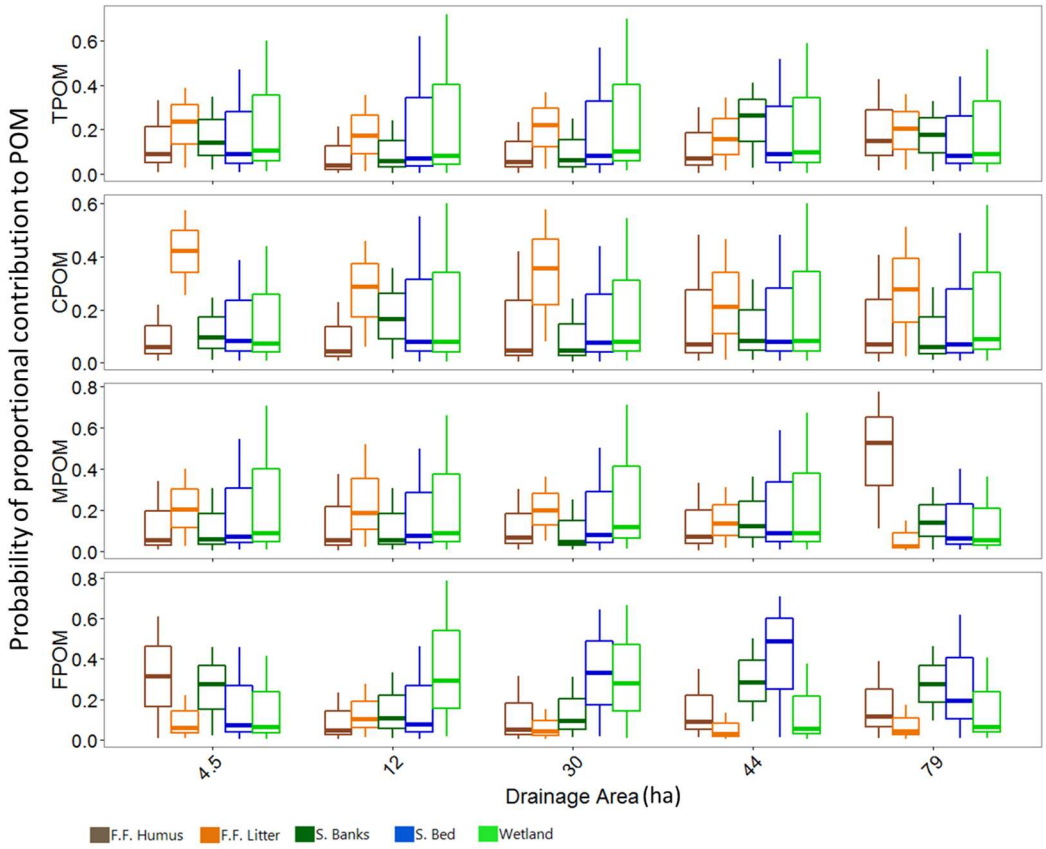

Figure 4.14 Boxplots summarizing posterior probability density distributions from SIMMR outputs aggregated by drainage area (across storm events) to highlight spatial trends. Middle lines represent the mode, or most probable value at the peak of the distribution, hinges represent interquartile ranges and whiskers represent the 95 percent highest probability interval.

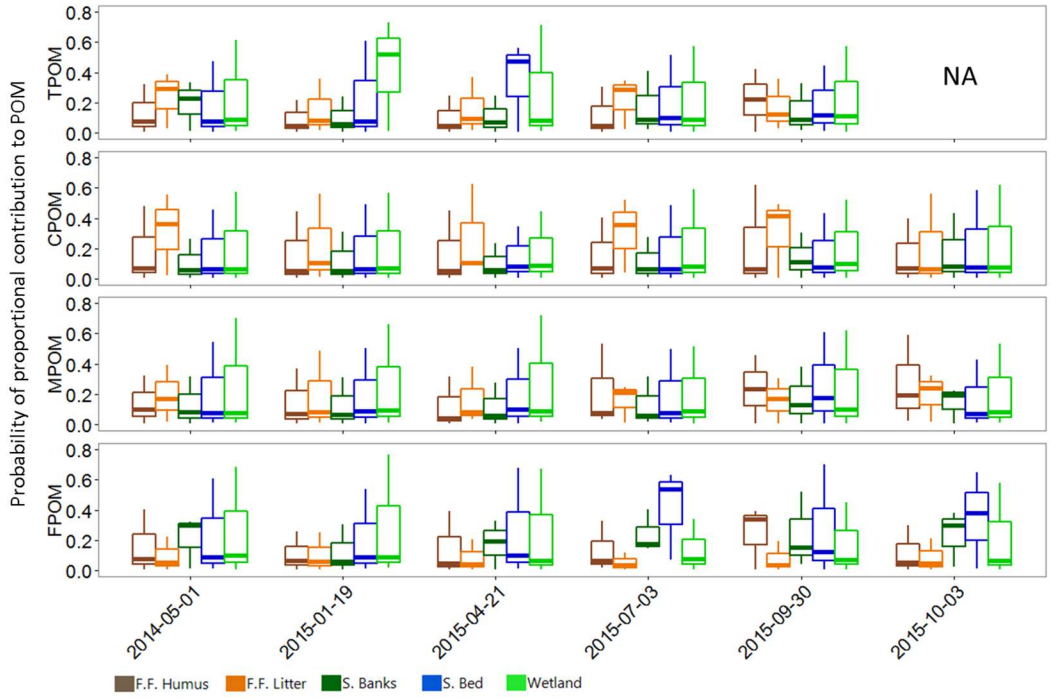

Figure 4.15 Boxplots summarizing posterior probability density distributions from SIMMR outputs aggregated by storm event (across drainage areas) to highlight hydro-climatic trends. Middle lines represent the mode, or most probable value at the peak of the distribution, hinges represent interquartile ranges and whiskers represent the 95 percent highest probability interval.

4.6 Temporal patterns in DSS

All of the events sampled for suspended sediment and POM analysis are displayed in Figures 4.16 through 4.19. POM samples taken at discrete discharges are similar to CSS in that higher flows mobilized POM with a signature centered around the stream bed, wetland, and humus end members at the 12-ha catchment (Figure 4.20 through Figure 4.23), whereas POM from the 79-ha catchment was shifted toward a more diverse assemblage of end members in the mixing space (Figures 4.24 through 4.27). Fifteen total events were sampled for DSS at the 12-ha location and fourteen at the 79-ha location, with a total of nineteen events (Table 3.3.1). Of these, six events produced enough samples with requisite masses for multiple isotopic analyses over the event hydrograph at the 12-ha location and five events produced enough samples at the 79-ha location.

We observed shifts from forest floor litter toward stream beds, wetlands, and humus in the mixing space over the course of the events of January 19, 2015 and September 30, 2015 at the 12-ha location and April 21, 2015 at the 79-ha location event (Figures 4.20, 4.23 and 4.24). Conversely, we observed shifts from outside of the mixing space toward the stream banks, then to humus and the stream beds over the course of the July 3, 2015 event at the 79-ha location (Figure 4.25). This occurred over a complex, double-peaked hydrograph, with high antecedent moisture conditions and the highest recorded rainfall intensity during the study period (Table 3.2.1). Three events generated enough samples with the requisite mass for multiple isotopic analyses but did not display clear patterns in the end member mixing space at different points in the event. These included April 21 and July 27, 2015 at the 12-ha location and September 30, 2015 the 79-ha location. Both events at the 12-ha location did not exhibit sufficient shifts within the mixing space to discern any trend, whereas that at

the 79-ha location fell far outside the end member mixing space, obscuring any observed patterns, although an alternative hypothesis is offered in section 5.5. DSS samples with highly enriched $\delta^{13}C$ at the 79-ha location may indicate a missing end member that was not sampled.

Seven of eleven events (between both locations) that generated enough samples for within-event analysis exhibited a convergence toward the humus end member (Figures 4.28 and 4.29). This was observed at both drainage locations. Interestingly, samples were aligned differently within the mixing space for the two drainage locations. For the 12-ha drainage, the mixing line extends from the litter end member, through the wetland and stream bed to humus (Figure 4.28). At the 79-ha location, we observed wider spread from the wetlands, stream bed, and humus end members toward upland A horizons and stream banks along the x-axis of the isotope mixing space (Figure 4.29). The samples that were more enriched in $\delta^{13}C$ along the x-axis (i.e. close to upland A horizons and stream banks) were all taken during periods of lower discharge, many of which were due to low antecedent moisture conditions, suggesting a missing end member may contribute to DSS along a flowpath that is activated under these conditions. For example, the September 30, 2015 event generated discrete suspended sediment samples at the 79-ha drainage that were very enriched in $\delta^{13}C$ with respect to anything else in our study (-25.95, -25.72, and -22.47, Figure 4.26). These samples fell in the lower quartile of percent C among samples from this site, but had "normal" ranges of $\delta^{15}N$ and C:N with respect to other samples (18.53 to 22.67 and 0.74 to 0.95 ‰, respectively), while CSS had very high carbon values, suggesting the activation of a diversity of sources over the event. This event occurred after an extended period of low baseflow with relatively warm, dry

conditions (antecedent one-week precipitation of 0 mm, Table 3.2), so these samples could indicate an extensively mineralized source that was activated under these conditions.

Hysteresis patterns in DSS were also recorded, as they can elucidate changing POM source over an event. At the 12-ha location, a consistent clockwise hysteresis in POC was noted (Figures 4.20 through 4.23). While clockwise hysteresis in POC was also evident at the 79 ha location, deviations from this pattern were noted. Although the September 30, 2015 exhibited clockwise hysteresis at the 12 ha location, pronounced anticlockwise hysteresis was observed at the 79 ha location (Figure 4.26). This event had the second highest maximum hourly rainfall intensity of the storms sampled throughout the study period (20.22 mm hr^{-1}, Table 3.2) but we observed minimal hydrograph response, presumably due to extremely low antecedent moisture conditions. Additionally, the clockwise pattern observed for the April 21, 2015 event was very weak and could be considered to be a linear response, and the second peak of the October 03, 2015 event displayed a complex hysteresis pattern.

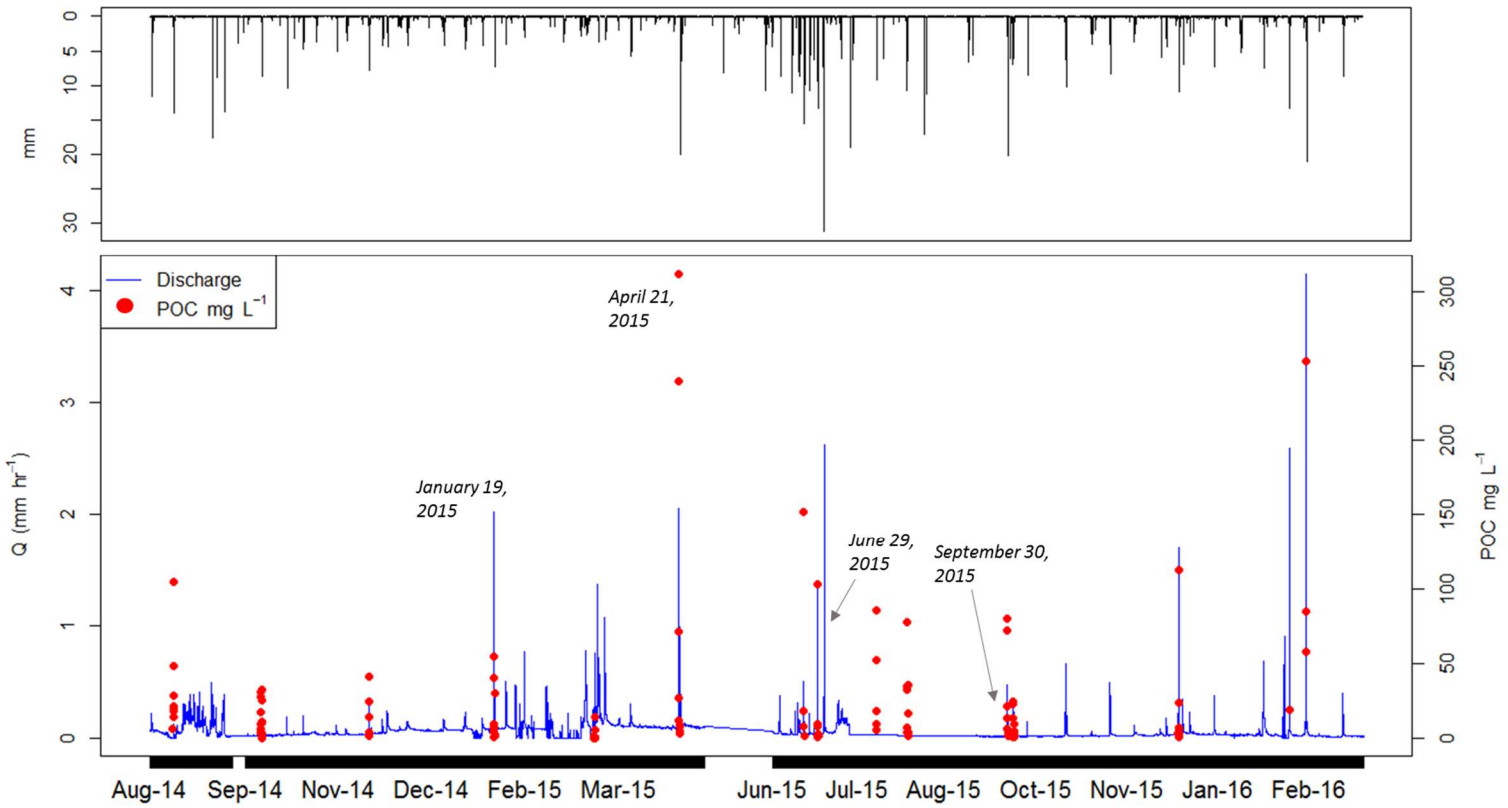

Figure 4.16 Time series plot of all DSS samples from the 12-ha catchment analyzed for POC throughout the study period, including runoff hydrograph (mm hr^{-1}) and rainfall hyetograph (mm). POC concentrations are in mg L^{-1}.

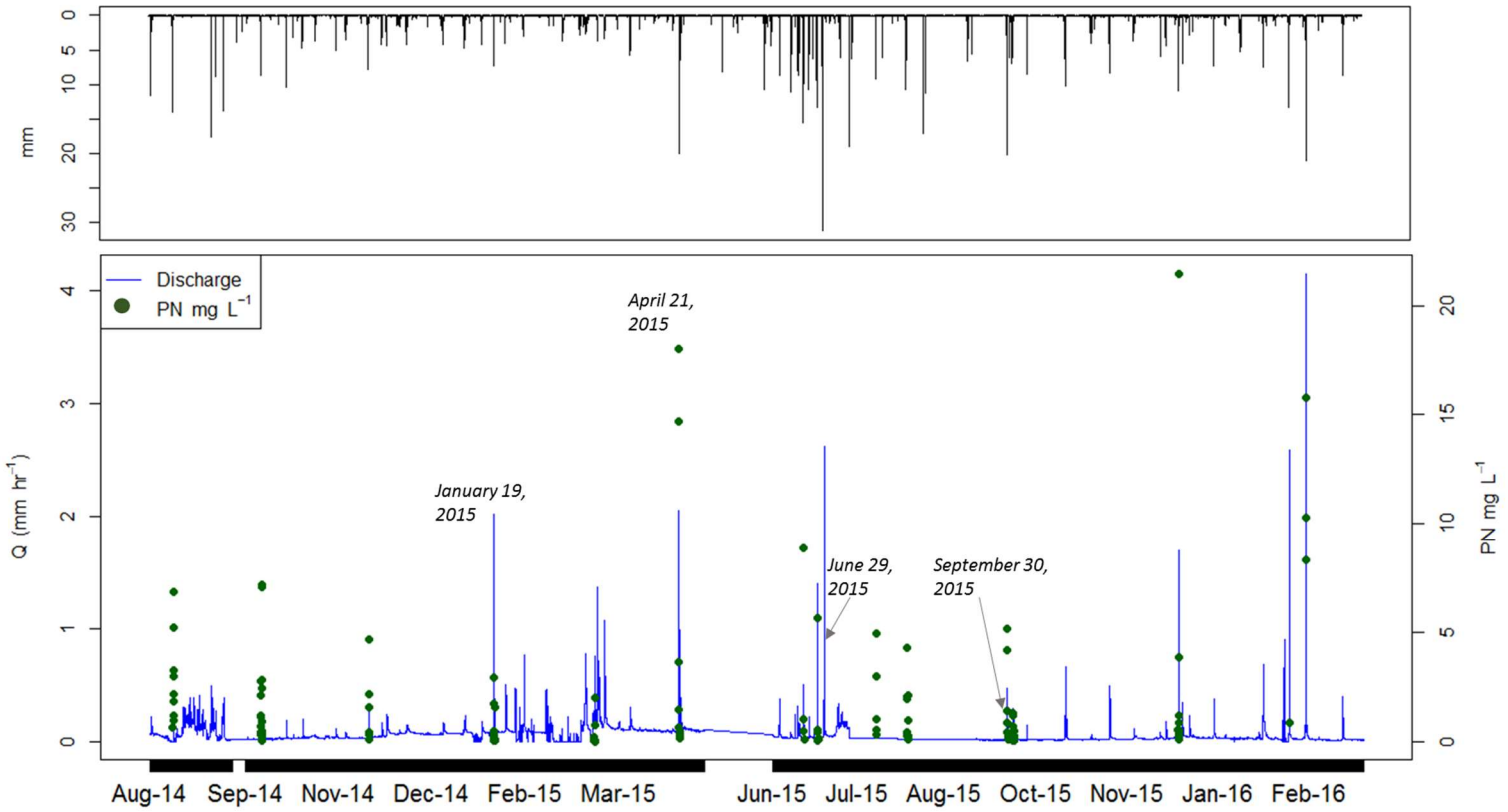

Figure 4.17 Time series plot of all DSS samples from the 12-ha catchment analyzed for PN throughout the study period, including runoff hydrograph (mm hr^{-1}) and hyetograph (mm). PN concentrations are in mg L-1.

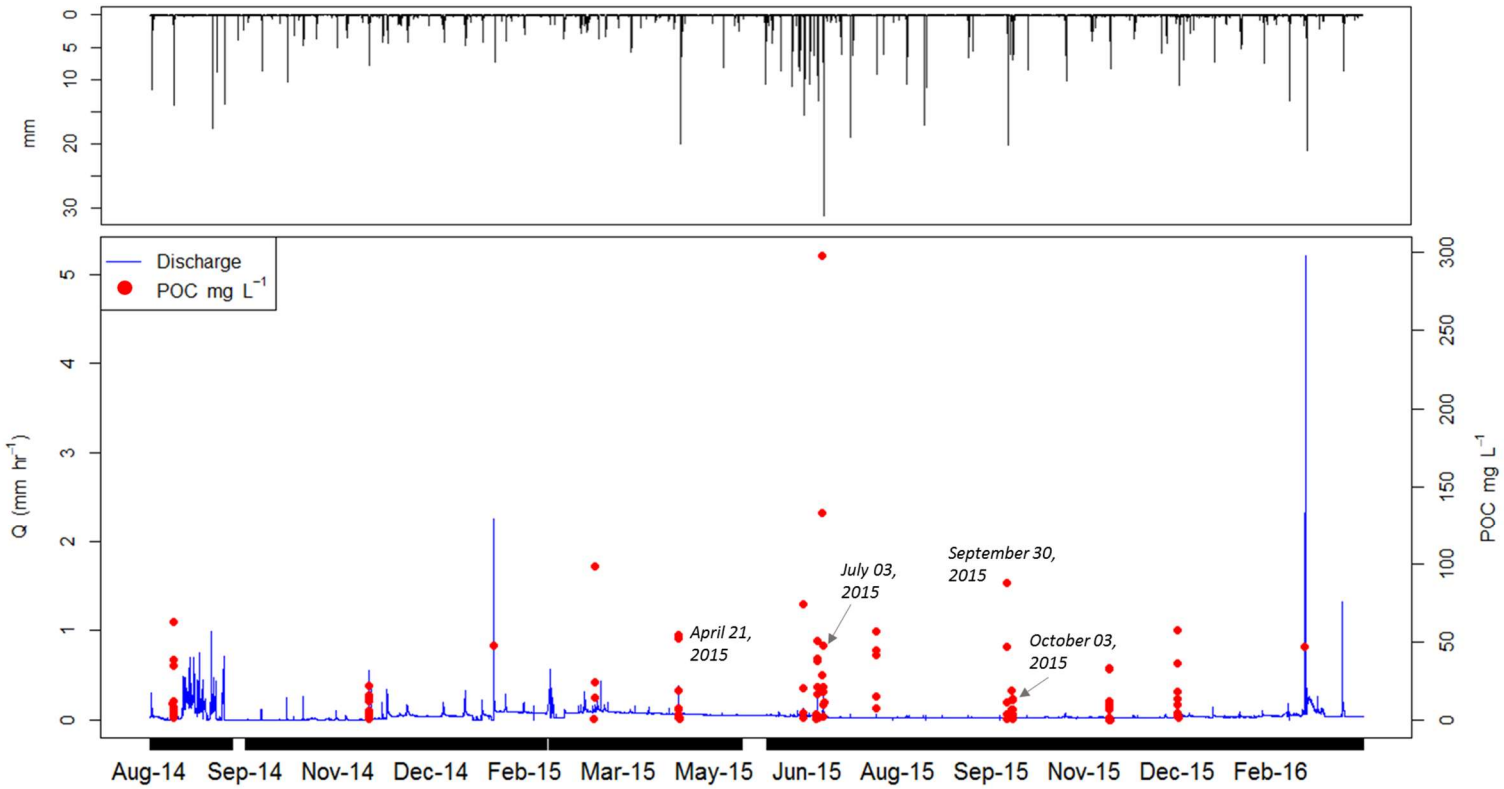

Figure 4.18 Time series plot of all DSS samples from the 79-ha catchment analyzed for POC throughout the study period, including runoff hydrograph (mm hr^{-1}) and hyetograph (mm). POC concentrations are in mg L^{-1}.

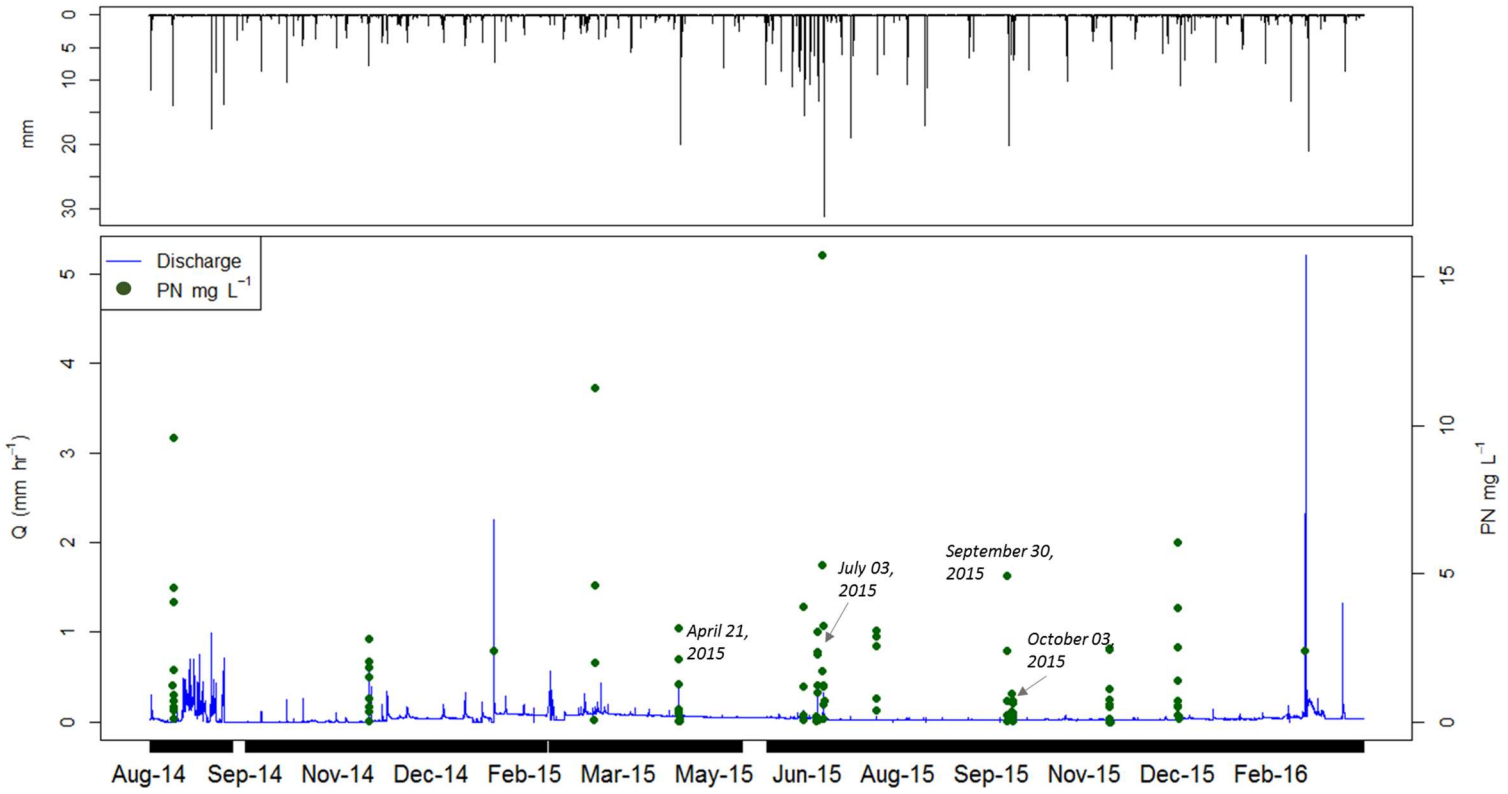

Figure 4.19 Time series plot of all DSS samples from the 79-ha catchment analyzed for PN throughout the study period, including runoff hydrograph (mm hr^{-1}) and hyetograph (mm). PN concentrations are in mg L^{-1}.

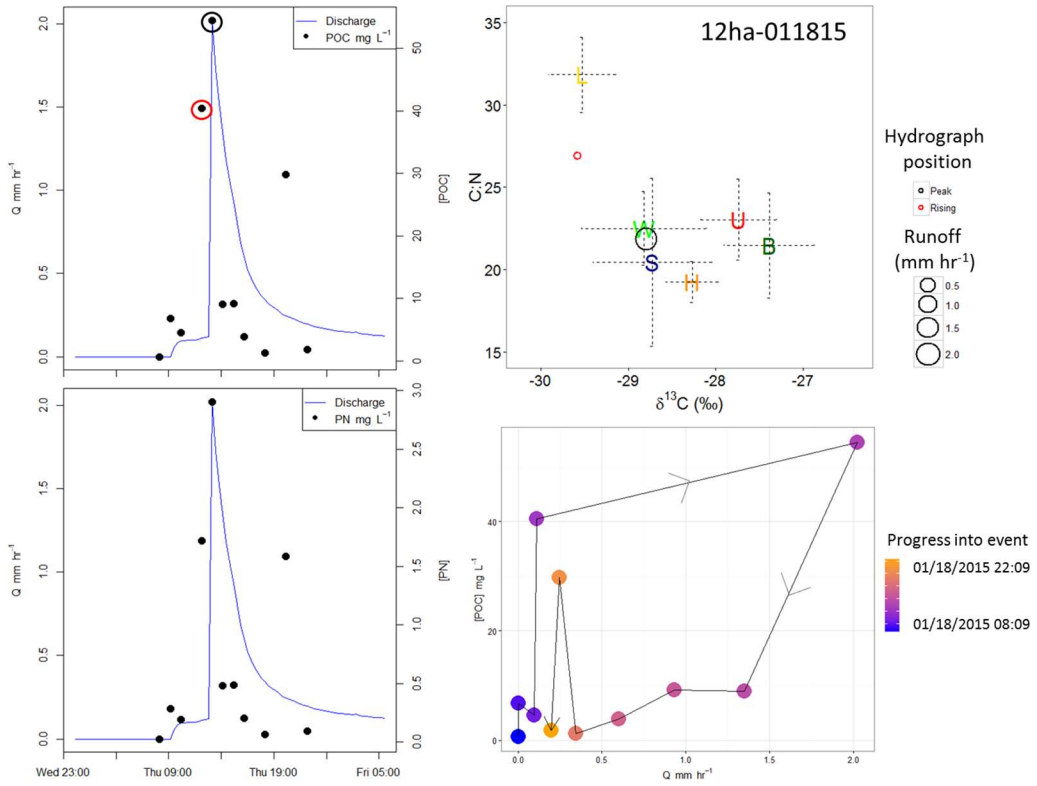

Figure 4.20 Within-event patterns observed in DSS at the 12-ha catchment during the January 19, 2015 event. Two samples in the isotope mixing space indicate shifts from high contributions of the litter end member on the rising limb and a clockwise hysteresis pattern was noted for POC. The second to last sample is a possible outlier. Samples analyzed in the mixing space are circled on the POC hydrograph.

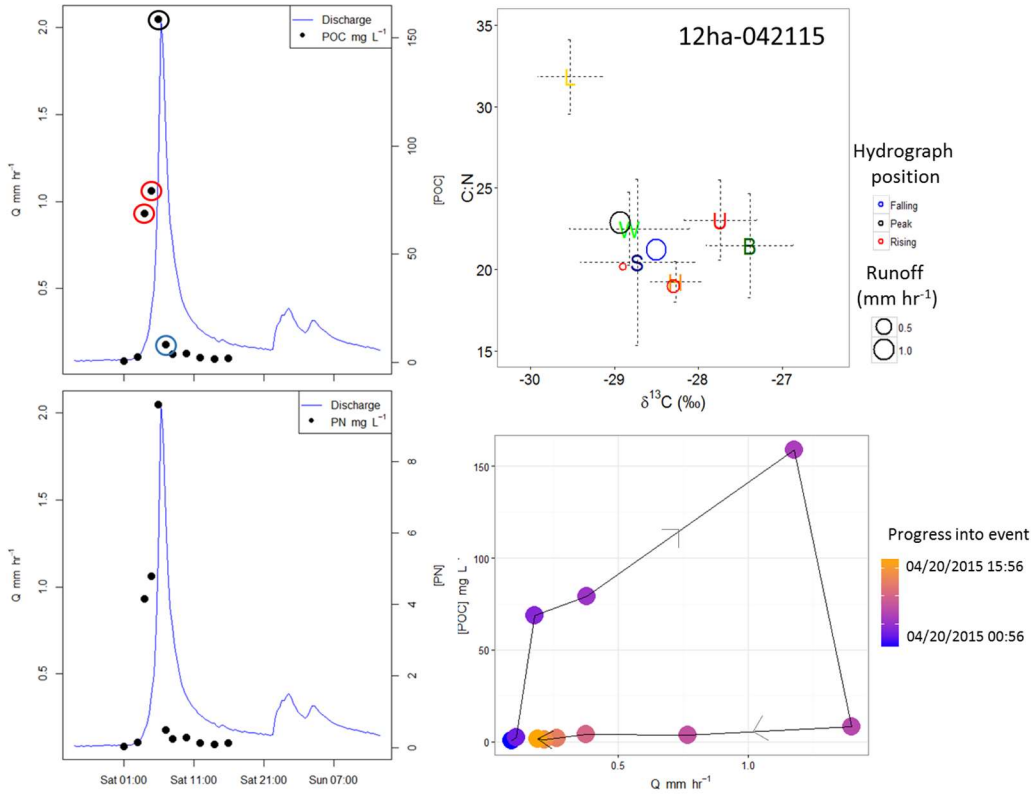

Figure 4.21 Within-event patterns observed in DSS at the 12-ha catchment during the April 21, 2015 event. Four samples in the isotope mixing space suggest shifts from high contributions of the stream bed and humus end members on the rising limb, to dominance of the wetland end member at peak flows to shifts toward stream beds, stream banks and humus on the falling limb. A clockwise hysteresis pattern was noted for POC. Samples analyzed in the mixing space are circled on the POC hydrograph.

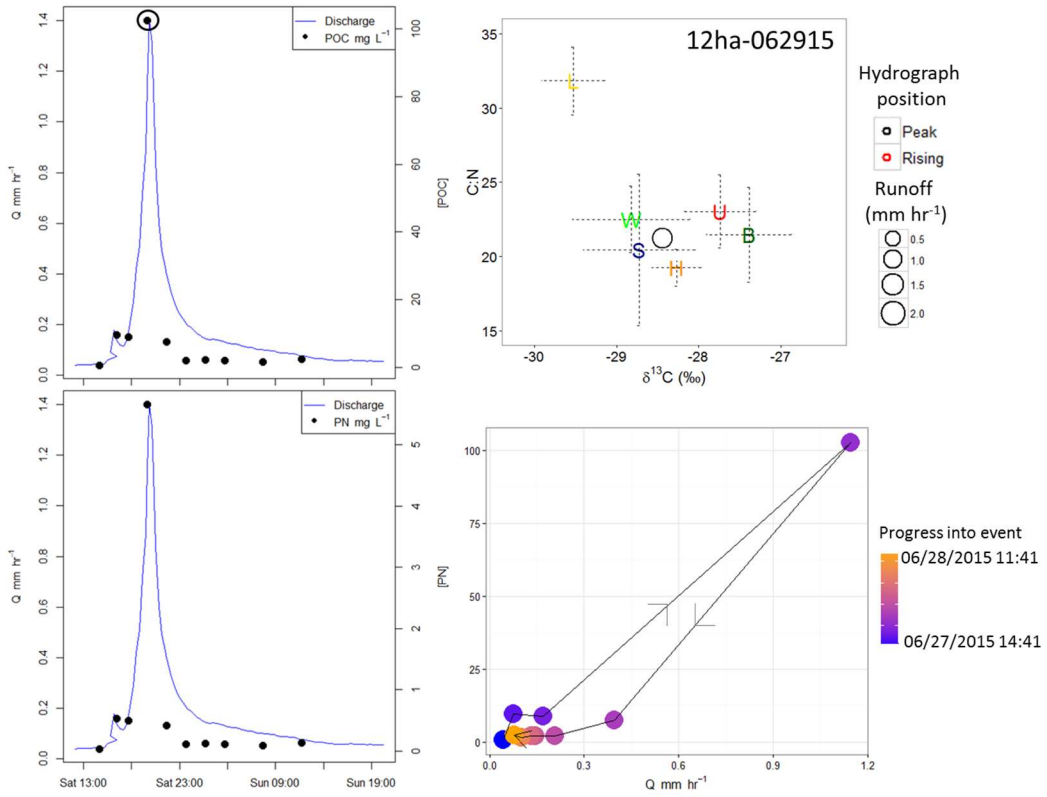

Figure 4.22 Within-event patterns observed in DSS at the 12-ha catchment during the June 29, 2015 event. Two samples in the isotope mixing space suggest shifts from greater contributions of the humus end member on the rising limb to predominantly wetland and stream bed end members at peak flow. A weak clockwise hysteresis pattern was noted for POC. Samples analyzed in the mixing space are circled on the POC hydrograph.

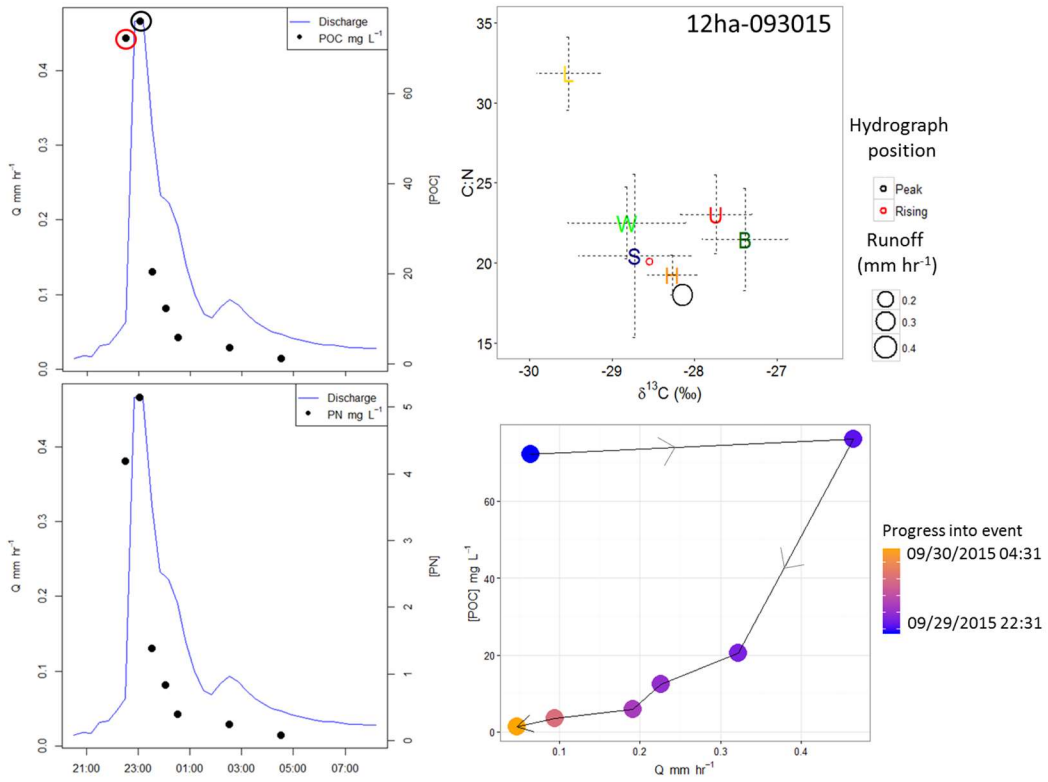

Figure 4.23 Within-event patterns observed in DSS at the 12-ha catchment during the September 30, 2015 event. Two samples in the isotope mixing space suggest shifts from greater contributions of the stream bed end member on the rising limb to predominantly the humus end member at peak flow. A clockwise hysteresis pattern was noted for POC. Samples analyzed in the mixing space are circled on the POC hydrograph.

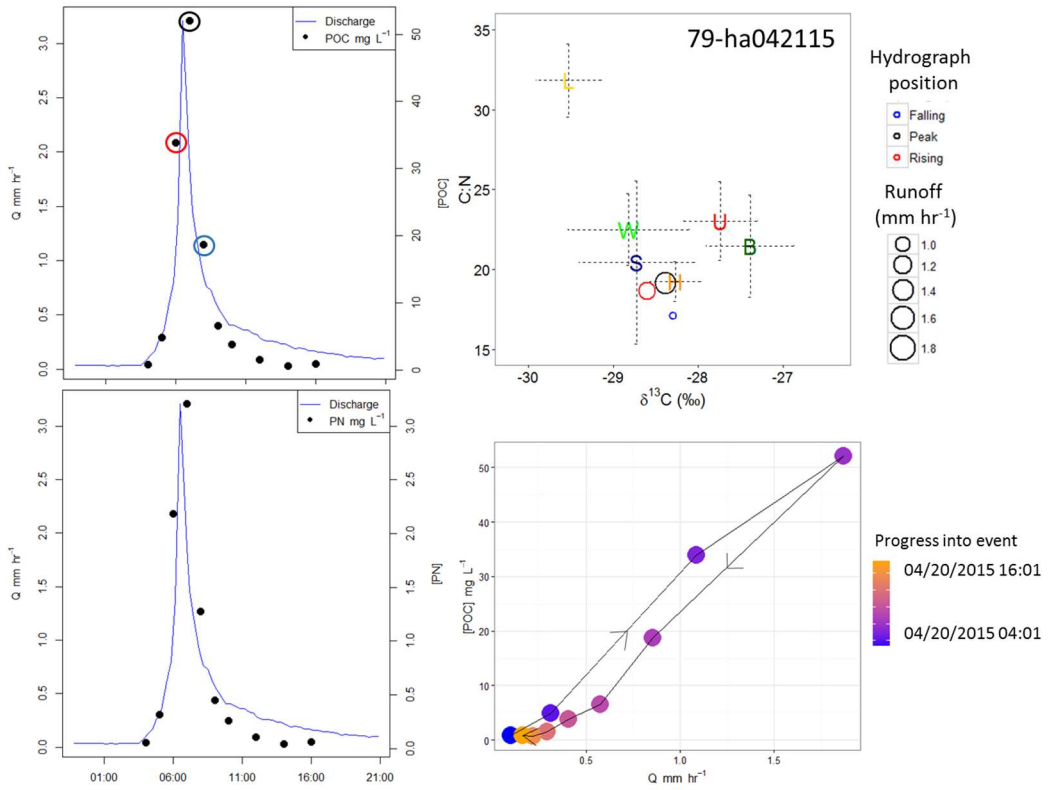

Figure 4.24 Within-event patterns observed in DSS at the 79-ha catchment during the April 21, 2015 event. Three samples in the isotope mixing space suggest shifts from greater contributions of the stream bed end member on the rising limb, to predominantly the humus end member at peak flow and during the falling limb. A weak clockwise hysteresis pattern was noted for POC. Samples analyzed in the mixing space are circled on the POC hydrograph.

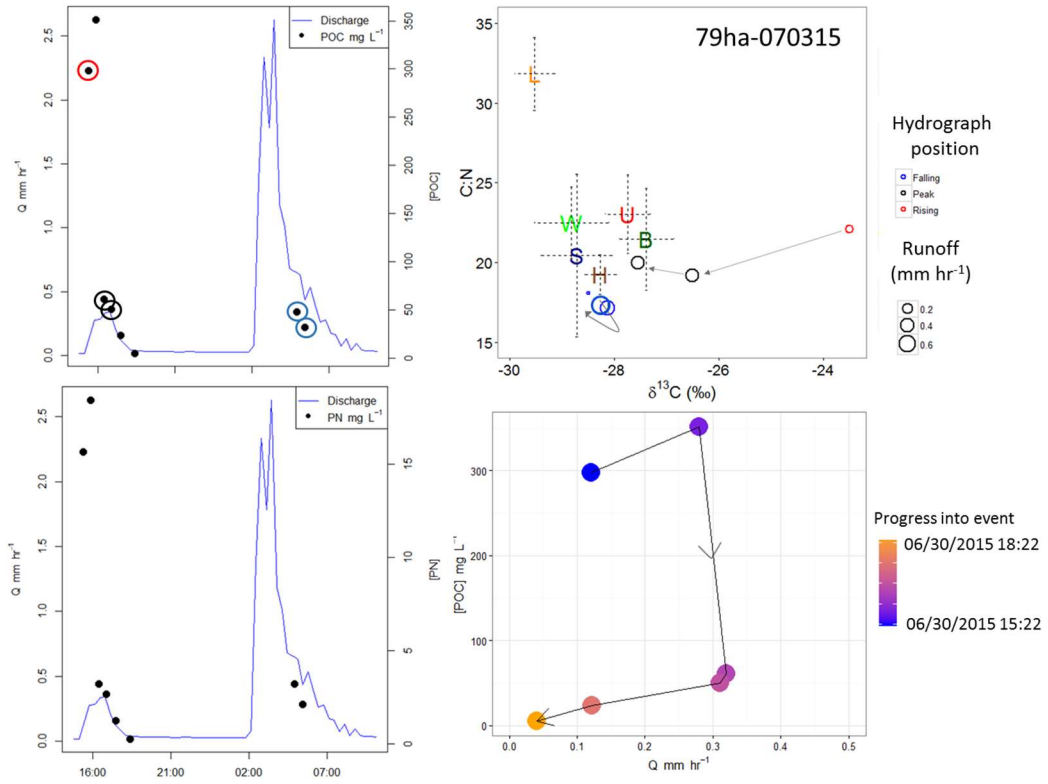

Figure 4.25 Within-event patterns observed in DSS at the 79-ha catchment during the July 03, 2015 event. This event was complex and exhibited multiple hydrograph peaks. Instrument malfunction prevented full sampling of the second, larger, peak. The first peak, however, exhibited clockwise hysteresis. Three samples analyzed for isotopes suggest that the rising limb fell far outside the mixing space, whereas two samples during peak flows resembled the stream bans in character. Samples from the second peak did not exhibit any notable pattern in the mixing space. Samples analyzed in the mixing space are circled on the POC hydrograph.

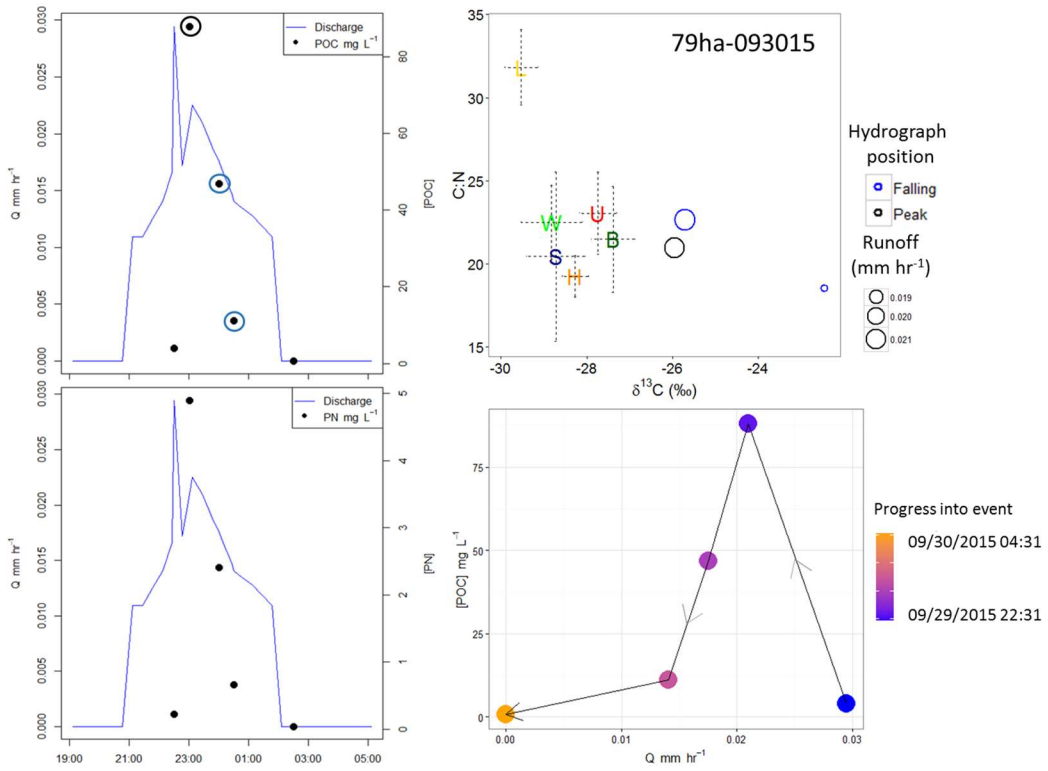

Figure 4.26 Within-event patterns observed in DSS at the 79-ha catchment during the September 30, 2015 event. Anticlockwise hysteresis was noted for POC over the course of this event. Three samples analyzed for isotopes fell far outside the mixing space. Anomalous hydrograph appearance is the result of extremely dry antecedent conditions. Samples analyzed in the mixing space are circled on the POC hydrograph.

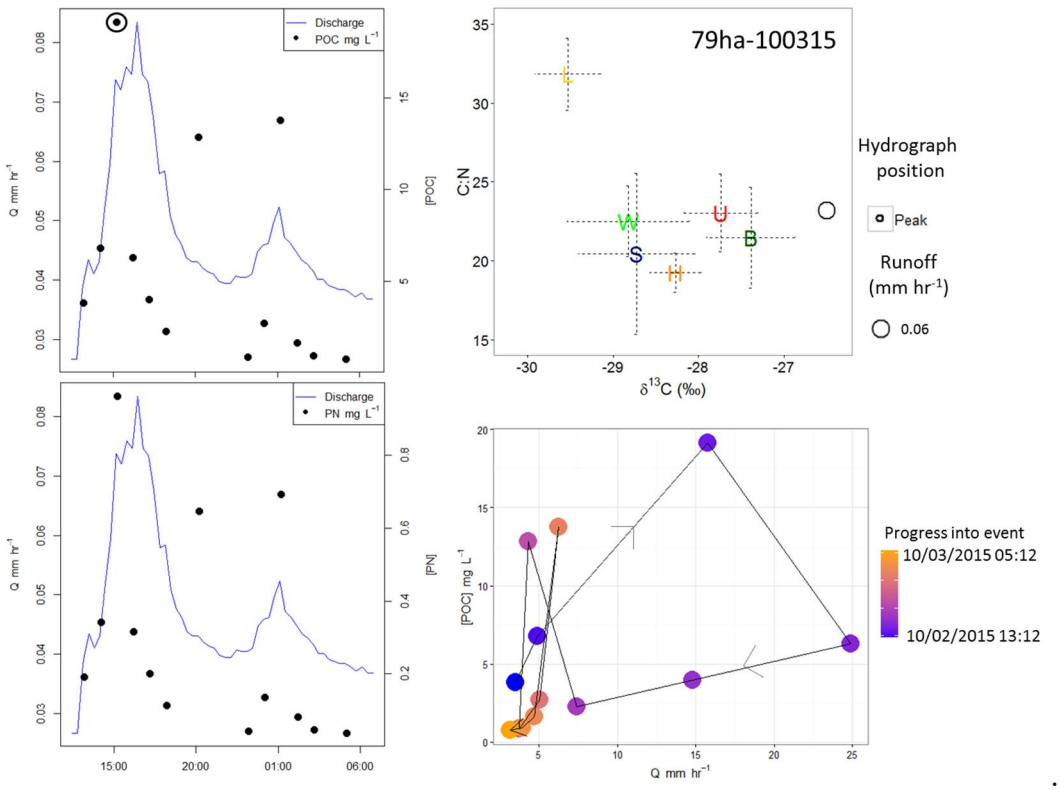

Figure 4.27 Within-event patterns observed in DSS at the 79-ha catchment during the October 03, 2015 event. Complex hysteresis was noted for POC over the course of this event. When considering each hydrograph peak separately, the first peak exhibited clockwise hysteresis, while the second exhibited complex hysteresis. One sample analyzed for isotopes near the peak of the first hydrograph fell just outside the mixing space, but close to the error range of the stream bank end member. Samples analyzed in the mixing space are circled on the POC hydrograph.

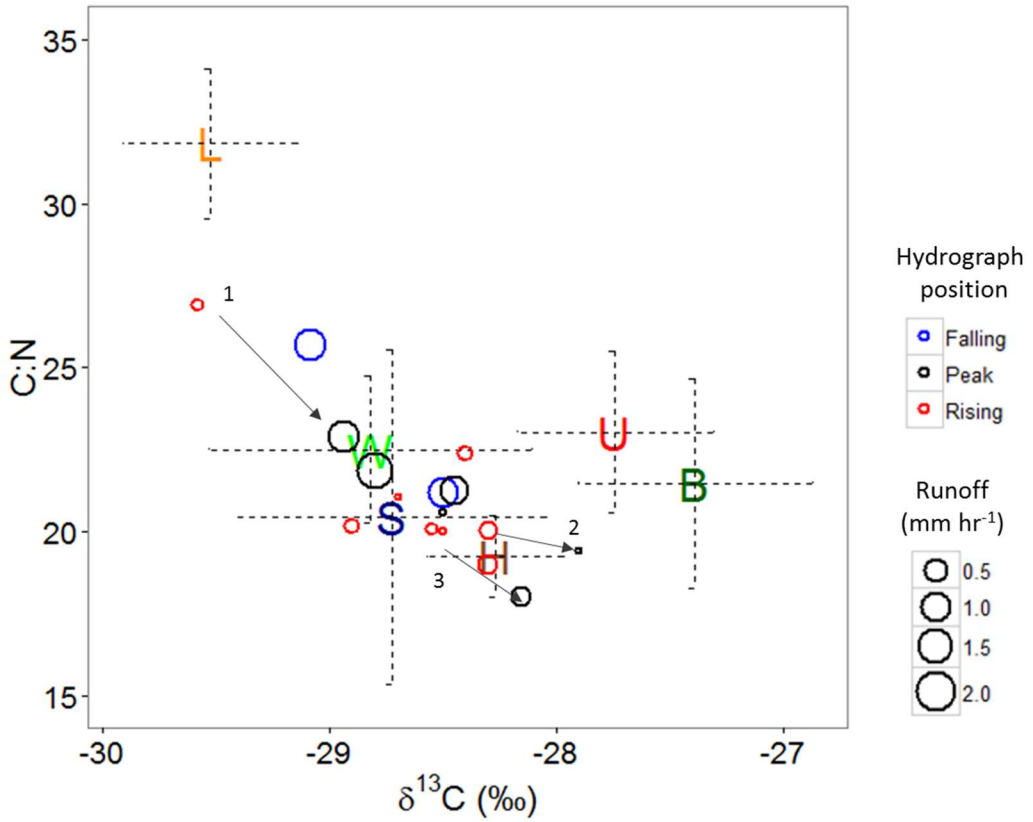

Figure 4.28 All DSS taken at the 12 ha catchment outlet. Events with specific trajectories converging toward the forest floor humus end member include January 19, 2015 (1), August 12, 2015 (2), and September 30, 2015 (3).

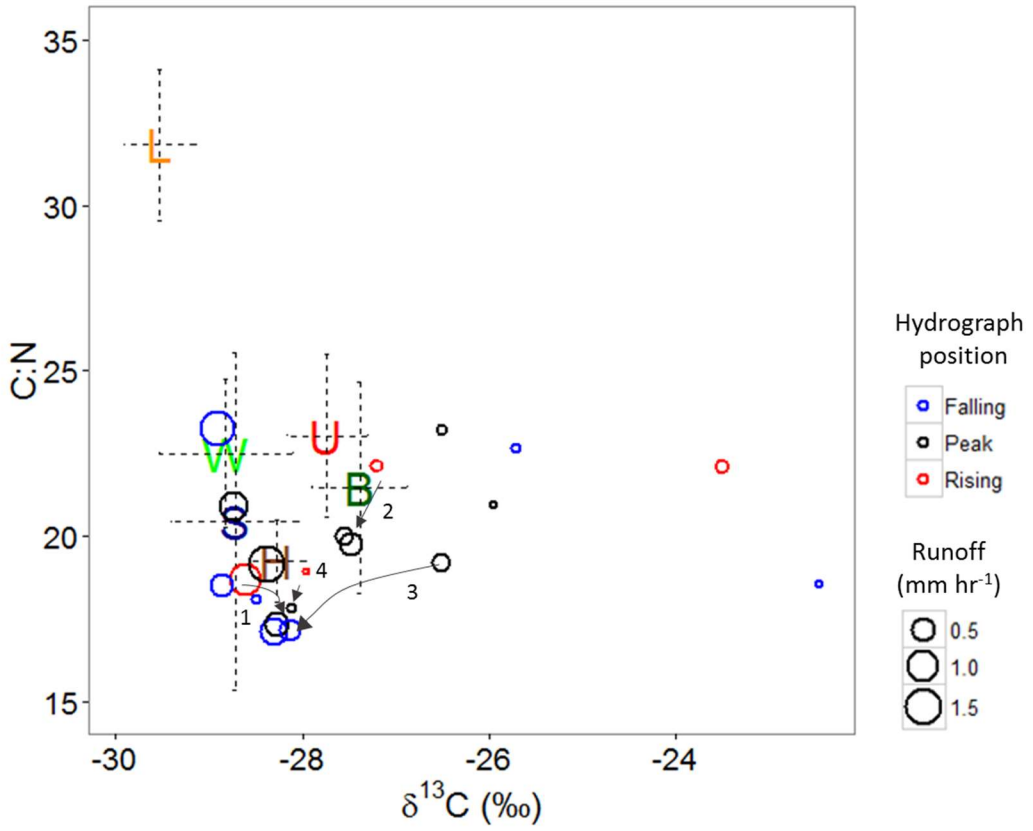

Figure 4.29 All DSS taken at the 79 ha catchment outlet. Events with specific trajectories converging toward the forest floor humus end member include January 19, 2015 (1), June 22, 2015 (2), July 03, 2015 (3), and July 27, 2015 (4).

Table 4.3: Mean POM data for all discrete suspended sediment samples, by hydrograph position and drainage location. The number of samples is indicated by "n".

Hydrograph position	Drainage area (ha)	**% C**	**$\delta^{13}C$**	**% N**	**$\delta^{15}N$**	**C:N (atomic)**	**n**
Rising	12	7.90	-28.65	0.45	0.11	21.22	8
	79	6.57	-26.82	0.37	0.50	20.45	4
Peak	12	7.27	-28.45	0.42	0.19	20.68	6
	79	4.28	-27.40	0.25	0.65	20.12	8
Falling	12	8.04	-28.79	0.40	-0.96	23.44	2
	79	3.20	-27.47	0.17	0.75	22.08	9

Chapter 5

DISCUSSION

5.1 Carbon and nitrogen composition of POM end members

The end member mixing spaces depicted from Figures 4.5 through 4.13 display a clear trajectory in enriching $\delta^{13}C$ and $\delta^{15}N$ across the sampled end members. The isotopically depleted C and N signature of forest floor litter samples is consistent with relatively undecomposed organic matter inputs in the soils literature (Nadelhoffer and Fry, 1988). Enrichment in $\delta^{13}C$ in the humus is associated with $\delta^{15}N$ that remain relatively depleted with respect to the other end members, which likely indicates the preferential respiration of ^{12}C during decomposition of vascular plant litter while N is retained during internal cycling within the soil microbial community.

The isotope ratios observed in wetland and stream bed material suggest colonization of organic matter by microbial communities in which ^{15}N enriches with more accumulation of heterotrophic biomass. Furthermore, decreases in C:N is consistent with humification of organic matter in the wetland, stream bed, and forest floor humus end members. The stream banks and upland A horizon end members consist of organic matter associated with mineral soil matrices; these had the second and third lowest percent C and N, respectively, among end members (Table 4.1.1). Other watershed-scale studies have shown isotopic enrichment (e.g. Jung *et al.*, 2012) in deeper mineral soils. This pattern likely indicates more recalcitrant SOM in these environments. The similarity between stream banks and upland A horizon soils are also interesting because several geomorphic studies (e.g. Donovan *et al.*, 2015, Hupp

et al., 2015, Walter and Merrits, 2008) have noted substantial deposits of "legacy sediment" that was eroded from upland soils and deposited on valley-bottom floodplains following land use changes associated with European settlement of the Eastern U.S. These floodplain deposits, especially in the mid-Atlantic US, have been shown to be important contributors of stream sediment loads via stream bank erosion (Gellis and Noe, 2013).

5.2 End member influence on POM

Mixing model outputs indicate a consistently strong contribution of forest floor litter to CPOM, although this decreased at larger drainage areas (Figure 4.14). Garzon-Garcia *et al*. (2014) suggested up to 70 percent of the carbon in silt-sized sediment could be derived from fresh plant litter and speculated that this may be even great in coarser fractions. While we did not observe litter contributions of the same magnitude to CPOM in our mixing model analysis (Figure 4.14), it's was the most probable contributor to this size fraction, with modes of model outputs ranging from 21 to 42 percent of CPOM regardless of drainage location. Upper limits of 95 percent highest density intervals did range as high as approximately 60 percent for litter contributions to CPOM.

Extensive channel incision was observed in the lower reaches of the catchment (near the 79 ha outlet), and headcut formation was observed near the groundwater seep at the beginning of the 4.5-ha catchment's channel; these likely contribute to the relative importance of recruiting "in-channel" POM compared to other sources such as litter at these locations. This is consistent with mixing model estimates of stream bank contributions which were highest in FPOM at the 4.5, 44 and 79 ha locations. Similarly, a geomorphic study along an incised stream in Australia (Smith and

Dragovich, 2008) found that the dominant sediment source quickly changed from hillslopes to sources within the channel when moving from a second to a third order stream. Recruitment of in-channel material from increasing stream power at larger drainages may mobilize more POM form stream banks and stream beds, increasing its relative importance. This is also consistent with our observations of positive relationships between particle size and catchment drainage area (Figures 4.1 and 4.2), as entrainment of larger particles from these sources takes more energy than that needed to mobilize finer organic particles. Enrichment of $\delta^{13}C$ observed for banks may suggest POM from this source is more recalcitrant in nature as noted above.

Valley-bottom wetlands consistently contributed a substantial amount of POM at all drainage locations in the system. Higher values of TWI, although associated with catchments with more surface-saturated conditions, were not found to be a good predictor of wetland POM estimated by the mixing model. For example, TWI medians and upper quantiles were comparable or lower at the 30 ha drainage location to the two larger drainage locations (Table 3.1.1), but this site exhibited the highest wetland POM inputs. However, the presence of hydric soils (in this case the Galla loam, Table 3.1), especially in the riparian corridor, may play a major role in the recruitment of POM from wetlands at the 12 and 30 ha locations. Ephemeral streams and saturated floodplains were observed throughout the catchment, and these may provide an important conduit through which POM is conveyed from wetlands to the stream during runoff events. Wetlands had a relatively high C:N and depleted $\delta^{13}C$ relative to those of the other end members (Table 4.1), which may indicate the preservation of carbon in anoxic soils. This suggests that wetland environments may serve as an important source of relatively fresh POM to the stream. Other studies have

suggested that the activation of floodplains can replenish labile POM inputs to streams (Atkinson *et al.*, 2009, Jung *et al*., 2014), which can be important for supporting aquatic food webs.

Stream banks and forest floor humus compensated for much of the proportional loss of wetland and stream bed POM contributions observed at larger scales. Humus contributed more to POM at larger drainage areas, especially for MPOM. This may suggest that, when eroded to the channel, this is a highly mobile fraction of POM. Other authors (Wallace *et al.*, 1995) have suggested that CPOM constitutes the least mobile fraction of POM, so the increased mobility throughout the drainage network for POM from this end member, which constitutes a larger proportion of MPOM and FPOM, is a plausible explanation for its greater importance downstream.

It is important to reiterate here that the outlier points from the September 30, 2015 discrete samples had unremarkable C:N values (18.53 to 22.67). We considered the possibility of autochthonous production contributing to POM within our system given the enriched $\delta^{13}C$ in these samples (as aquatic primary production can have a wide range of carbon isotope signatures based on available DIC) observed in these samples, but ruled out the possibility of such a missing end member as lotic algae typically have a C:N lower than 15 (Kendall *et al*., 2001).

It is also worth noting that we only sampled end members during August of 2015. Makundan *et al.* (2013) and Gellis and Noe (2013) suggest that consideration of temporal changes in sediment sources over time might improve model accuracy. Similarly, Gellis and Makundan (2013) suggest that sediment deposits within the stream channel may bias inter-event comparisons. Temporal variability in end

members, especially the stream bed which may partially serve as an integrated signal of other events' deposits, is therefore recognized as a potential source of bias in this study.

5.3 Particle size class and POM composition

A consistent "step" in $\delta^{15}N$ enrichment was observed from CPOM to MPOM to FPOM with a concomitant decrease in C:N across the same particle class gradient. Lower C:N values observed in finer POM classes were similar to those made by Akamatsu *et al*. (2011), Atkinson *et al*. (2009), and Fox and Papanicolaou (2007). This can provide valuable insight into POM source and biogeochemical processing across the three discrete size classes considered in this study. Stream banks and beds contributed disproportionately to FPOM at larger drainage scales. Lower C:N observed in FPOM and these end members may be indicative of recycling of N in benthic environments while carbon is respired. Stream biota play a critical role in processing allochthonous CPOM inputs and to generate an FPOM composition distinct from its initial terrestrial source (Wallace *et al*., 1982). As fungi and bacteria increasingly colonize finer material due to its greater surface area, relatively more nitrogen is retained with their biomass (Tant *et al.*, 2013). While lower aggregate C:N may more closely match the body stoichiometry and nutrient demands of consumers and other heterotrophic microbes, POM quality may decrease with C:N as respiration of labile vascular plant material leaves proportionally more recalcitrant compounds such as lignin and its derivatives (Yoshimura *et al.*, 2008). Isotopic enrichment provides further insight into a more "microbially processed" signature in FPOM. Both $\delta^{13}C$ and $\delta^{15}N$ will enrich when moving up trophic levels, albeit at different rates, so

enrichment may indicate transfer from autotrophic vascular plant matter to heterotrophic fungal and bacterial biomass in the POM pool.

5.4 Alterations to POM composition along the drainage gradient

In addition to our observations of decreasing C:N in smaller particles, the atomic C:N ratios of MPOM and FPOM decreased with increasing drainage area (Figure 4.4). Similar phenomena were reported by Akamatsu *et al*. (2011) and Atkinson *et al*. (2009). These studies were conducted on seston in higher order river systems—our results are unique in that they indicate this phenomenon can even be evident along short headwater reaches where allochthonous inputs dominate.

The similarity of FPOM chemistry to stream beds suggests POM obtains a unique signature in the stream environment, likely from extensive mixing and storage of POM from other end members within the aquatic environment, followed by biotic processing during breakdown to FPOM as suggested in section 5.3. This material may be more recalcitrant, and the proportion of FPOM with this aquatic signature mobilized by stormflows increases at downstream locations.

The percent organic C of all size classes decreased at large drainage areas (Figure 4.3), suggesting a "dilution" of POM by more mineral material. Considering our observations of the highest percent organic C in the coarse size class and observed increases in particle size moving downstream, these opposing trends suggest the decoupling of POM mobilization from that of mineral sediments during transport. Suspension of coarser, sandy sediment downstream likely accounts for increasing particle size distributions (increased skew toward the coarsest sediment fractions accounted for most of the trend than increases in d_{50}, Appendix D). An increased

fraction of FPOM is routed from the stream bed and humus downstream as opposed to CPOM recruited from forest floor litter and/or wetland SOM.

5.5 Hydrologic drivers and the role of storm event magnitude for POM flux, source and composition

Inter-event observations

The storm events with the highest rainfall intensities included those on July 3, 2015, April 21, 2015, and September 30, 2015 (numbers 3, 4, and 5 from CSS-sampled events); these had an aggregate POM signature that was proximal to the stream bed source in the isotope mixing space (Figures 4.12 and 4.13). The May 1, 2014 (event number 1) provides a good contrast to these events, as it was a high discharge event of slightly lower rainfall intensity, with a greater total rainfall extended across a long period of time. Flooding throughout the catchment during this event generated a POM signature shifted closer to the humus end member, suggesting mobilization of forest floor SOM (Figures 4.8 through 4.10). Storms with a high rainfall intensity (e.g. numbers 3, 4 and 5) exhibit sharp hydrographs that may mobilize a large portion of in-channel material. Longer, larger storms (e.g. event number 1) may result in saturation excess runoff, expansion of variable source areas, and mobilization of POM from more distal portions of the catchment (Dhillon and Inamdar, 2014).

The September 30, 2015 event (number 5) was also interesting due to extremely dry antecedent moisture conditions (Table 3.2.1). This event exhibited the highest contributions of forest floor humus to TPOM (Table 4.5.2) and had the highest percent carbon and very enriched $\delta^{13}C$ in CSS. Additionally, DSS POC concentrations were very high relative to runoff peaks (Figures 4.16 and 4.18) and

catchment yields were only low (Table 4.6.2) due to the low total discharge. Carbon stocks can build up in soils due to decreased soil respiration during dry periods (Borken and Matzner, 2009). Dhillon and Inamdar (2014) observed that flow-weighted POC concentrations were exhausted in subsequent events in this catchment, while dry periods allowed carbon stocks to build up. Complimentary observations were made by Bass *et al.* (2014), in which large POC responses were observed in the absence of a major hydrograph response during a storm following an extended dry period. Garzon-Garcia *et al.* (2014) similarly observed higher accumulation of nitrogen in runoff sediments after a dry period an attributed this to the accumulation of plant material in sediment matrices under such conditions. Together, these results suggest that rewetting pulses after droughts can mobilize disproportionate amounts of POM from soils stocks.

The January 19, 2015 event (number 2) also offers some interesting comparisons to other events given its relatively high antecedent moisture conditions and runoff ratio (Table 3.2.2). POC concentrations were relatively low relative to runoff peaks for this event (Figures 4.16 and 4.18). Other authors (Gellis and Noe, 2013) have indicated that freeze-thaw processes during winter storms cause erosion of sediment and POM from stream banks to occur more readily. We did not observe this here (Figure 4.15), but rather that a "sharp" hydrograph resulting from wet and frozen soils flushed a large proportion of wetland and stream bed POM from the network.

Intra-event observations at two catchment scales

Consistent clockwise hysteresis patterns were observed in the 12-ha catchment (Figures 4.20 through 4.23). This is in agreement with the observations of predominantly clockwise hysteresis in POC made by Dhillon and Inamdar (2014) and

in PN (Inamdar *et al*., 2015) in the same catchment, and suggests POM sources proximal to the stream. Rapid increases in stream power may scour the sandy stream bed and shunt out POM stored in the bed matrix similar to the observations made by Larsen *et al*. (2015).

However, POM displayed variable patterns within the mixing space over the course of these high-flow events, suggesting hysteresis alone is insufficient to elucidate POC source under different hydrologic conditions. For the January 19, 2015 event (Figure 4.20), a shift from close proximity to litter samples to a signature closer to that of wetlands and stream beds was observed for DSS. While this event was of a moderate rainfall intensity compared to the others here, it had the highest runoff ratio of any sampled event, presumably due to high antecedent moisture (Table 3.1) and frozen soils. Rapid generation of overland flow may have contributed litter material from the catchment, followed by a flush of stream bed and wetland POM closer to the hydrograph peak. The event sampled on June 29, 2015 (Figure 4.22), had the highest maximum rainfall intensity and catchment yield of POC (Table 3.1). DSS shifted from proximity to the humus end member to the stream bed in the isotope mixing space; similarly, this event had high antecedent moisture so runoff may have eroded forest floor material followed by stream bed mobilization during higher flows.

A valuable contrast was observed during the September 30, 2015 event, which was of the second highest rainfall intensity of the six events sampled for CSS but produced minimal runoff. While clockwise hysteresis was still observed at the 12-ha location, two DSS samples shifted from the stream bed toward the humus end member in the isotope mixing space. Antecedent moisture was extremely low, and the hydrograph response, runoff ratio, and POC yield were all small relative to the other

events suggesting flow on the rising limb was generated from sources proximal to the channel and forest humus contributions increased as the catchment "wetted up". A similar response in the mixing space was observed for an event sampled during on August 12, 2015 after a period of low baseflow, which was not depicted on hydrograph plots due to a "flatline" in the discharge record. Such variable responses despite high rainfall intensity point to the importance of antecedent moisture conditions in controlling POM source in forested catchments.

The April 21, 2015 event exhibited clockwise hysteresis in POC over the hydrograph without a consistent pattern in the isotope mixing space (Figure 4.21). Four DSS samples shifted within the error range of the stream bed end member, although a shift toward the humus end member was observed for the second sample on the rising limb and a shift toward the wetland end member was observed at peak flow. Nevertheless, these changes were small and this event likely indicates the mobilization of predominantly in-channel POM.

Four storm events analyzed for intra-event patterns at the 79 ha catchment outlet displayed more complex results than those from the 12 ha catchment. The April 21, 2015 event exhibited a weak clockwise hysteresis in POC, with three DSS samples displaying a trajectory from the stream bed toward the humus end member. Three other events including July 03, 2015, September 30, 2015 and October 03, 2015 generated DSS that fell outside the conceptual mixing space due to highly enriched $\delta^{13}C$ (Figures 4.25 through 4.27). We speculate that these may represent a missed signature of the stream banks for several reasons:

- Stream banks had the most enriched $\delta^{13}C$ of any end member sampled.

- Our sampling regime did not include the bank of the second order stream, which may have a different isotopic signature and elemental composition due to changes in geomorphic processes (Figure 3.2)

- The riparian corridor immediately surrounding stream channels have very high biological activity and redoximorphic characteristics that can lead to high spatial heterogeneity (Harvey & Gooseff, 2015) and could enrich $\delta^{13}C$ in the end member signature.

- Observations of highly incised banks along these stream reaches suggest active bank erosion is a major contributor to sediments in this watershed.

The July 03, 2015 event exhibited depletion in $\delta^{13}C$ from outside the bank end member toward humus over the course of the first hydrograph peak of the event (Figure 4.25). This may indicate bank erosion during the rising limb of the event hydrograph to peak flow, where proportionally more fine upland POM dominates the material in suspension on the falling limb. A similar process was noted by Landers and Sturm (2013), who identified increased contributions of fine particles from upland environments over the progression of storm events using in-situ sensors. DSS from the second peak fell in the vicinity of the stream bed and humus end members and did not exhibit a clear pattern. The September 30, 2015 event at this drainage location was the only sampled event to exhibit anticlockwise hysteresis in POC concentrations (Figure 4.26). This occurred after an extremely dry period with low baseflow and had minimal hydrograph response and runoff ratios given the moderately high rainfall intensity (Table 3.2.1). Bass *et al.* (2011) similarly observed a considerable flux of DOC and POC in the absence of a large hydrograph response during a rewetting event following a drought. It is likely that minimal overland flow was generated during this event, and that anticlockwise hysteresis resulted from a lagged response in the requisite stream power for bank and bed erosion. DSS moved further outside of the mixing space as flows increased, supporting the idea of a missed stream bank end

member with a highly enriched $\delta^{13}C$. Ziegler *et al*. (2014) observed a similar process, in which clockwise hysteresis was typically noted between discharge and total suspended solids (TSS), but large storms during dry months deviated from this pattern. The subsequent event on October 03, 2015 returned to clockwise hysteresis, and DSS remained in the region of highly enriched $\delta^{13}C$ outside of the mixing space.

Finally, we observed a consistent trend in decreasing C:N and $\delta^{13}C$ converging toward the humus end member over the course of storm events at both the 12-ha and 79-ha catchment outlet (Figures 4.28 and 4.29). Humus was found to be a major contributor to FPOM at the 4.5-ha catchment and especially to MPOM at the 79-ha catchment outlet. The increased presence of humus at the largest catchment outlet and later in storm events may suggest that while stream bed and stream bank material are flushed earlier in an event, POM from the forest floor along receding portions of hydrographs continues to be discharged through the catchment.

Chapter 6

SUMMARY AND CONCLUSIONS

High discharge storm events play a critical role in mobilizing terrestrial POM in headwater systems and subsidizing the nutrient and energy flows to downstream aquatic ecosystems. While the size distributions of POM in aquatic environments has been shown to have important biogeochemical ramifications, few studies have explicitly sought to identify unique catchment sources of the different sizes of POM mobilized under storm conditions. We explored the variability in the total organic C and N content, isotopic quality, and abundance of three discrete particle size classes of POM at multiple sampling locations, the source of POM to the stream vary among particle sizes, and the influence of rainfall intensity and total discharge on POM source. This was conducted by targeted sampling of large storm events at five drainage locations within a forested 79 ha catchment in the Mid-Atlantic region of the United States. Suspended sediments were analyzed for particle size distributions and stable isotopes of C and N and quantitative and conceptual mixing model analyses were implemented to trace POM source. We found that:

1. Litter contributions decrease from coarser to finer POM and are largely replaced by stream beds, stream banks and humus. This suggests a transition from relatively more labile fractions in CPOM to more recalcitrant material during microbial decomposition in aquatic environments.

2. Fresh plant litter inputs decrease at larger drainage areas and are largely replaced by stream banks, stream beds and humus.

3. Increases in particle size along with decreases in the carbon content of the coarse particle size class at larger drainage areas indicate that more mineral sediment is recruited downstream. Coarser total sediments are likely the result of higher stream power, and bed and bank erosion, where carbon-rich fractions are predominantly recruited from forest floor environments at all drainage areas.

4. The relative abundance of wetland soils appears to exert a strong control on fluvial POM composition at the headwater locations.

5. POM of all three particle size classes was mobilized from the forest floor in larger proportions during a very high discharge event of moderate rainfall intensity. A differential response was observed during higher intensity events in which a greater proportion of CPOM was sourced forest floor end members but MPOM and FPOM were mobilized in greater proportions from the stream bed and wetland end members.

6. Mixing space analysis suggests contributions of terrestrial humus increased as storm events progressed. This was observed for multiple storm events.

High intensity rainfall events are predicted to increase in both frequency and intensity throughout the Northeastern United States, and extensive flushing of POM from headwaters to larger drainage networks has the potential to alter biogeochemical nutrient and energy balances and to affect downstream water quality. This is of particular concern in the Mid-Atlantic, where erosion of nutrient-rich legacy channel sediment deposits is a well-documented water quality concern.

Given our observations, we speculate that periods of dry weather followed by high-intensity precipitation mobilize a large fraction of stream bed and stream bank material, while protracted high-flow events or storms following periods of high antecedent moisture may activate floodplains or other more distal sources. It is important to consider this in the context of forested catchments, as areas with high impervious surface coverage and/or compacted soils may quickly generate overland flow during high-intensity events, exhibiting different dynamics in POM mobilization.

The in-stream POM that is rapidly mobilized by these events may be more refractory as suggested by its enriched isotopic signatures. These conditions may deter biotic degradation of POM and, in combination with low C:N of channel material, allow for conservative transport of proportionally more PN through longer reaches of a drainage basin. Conversely, high antecedent moisture conditions or protracted rainfall events may generate saturation flows that contribute more labile POM from forested environments.

REFERENCES

Akamatsu, F., Kobayashi, S., Amano, K., Nakanishi, S., & Oshima, Y. (2011), Longitudinal and seasonal changes in the origin and quality of transported particulate organic matter along a gravel-bed river. *Hydrobiologia*, 669(1), 183–197. doi:10.1007/s10750-011-0682-8

Alvarez-Cobelas, M., Angeler, D. G., Sánchez-Carrillo, S., & Almendros, G. (2010). A worldwide view of organic carbon export from catchments. *Biogeochemistry*, 107(1-3), 275–293. http://doi.org/10.1007/s10533-010-9553-z

Angradi, T. R. (2015). Trophic linkages in the lower Colorado River: multiple stable isotope evidence, *Journal of the North American Benthological Society,* 13(4), 479–495.

Atkinson, C. L., Golladay, S. W., Opsahl, S. P., & Covich, A. P. (2009), Stream discharge and floodplain connections affect seston quality and stable isotopic signatures in a coastal plain stream. *Journal of the North American Benthological Society*, 28(2), 360–370. doi:10.1899/08-102.1

Bass, A. M., Bird, M. I., Liddell, M. J., & Nelson, P. N. (2011), Fluvial dynamics of dissolved and particulate organic carbon during periodic discharge events in a steep tropical rainforest catchment. *Limnology and Oceanography*, 56(6), 2282–2292. doi:10.4319/lo.2011.56.6.2282

Bass, A. M., Munksgaard, N. C., Leblanc, M., Tweed, S., & Bird, M. I. (2014), Contrasting carbon export dynamics of human impacted and pristine tropical catchments in response to a short-lived discharge event. *Hydrological Processes*, 28(4), 1835–1843. doi:10.1002/hyp.971

Bianchi, T., & Bauer, J. (2011). *Particulate organic carbon cycling and transformation*. *Treatise on estuarine and coastal …* (Vol. 5). Elsevier Inc. http://doi.org/10.1016/B978-0-12-374711-2.00503-9

Borken, W., & Matzner, E. (2009). Reappraisal of drying and wetting effects on C and N mineralization and fluxes in soils. *Global Change Biology*, *15*(4), 808–824. http://doi.org/10.1111/j.1365-2486.2008.01681.x

Brym, A., Paerl, H. W., Montgomery, M. T., Handsel, L. T., Ziervogel, K., & Osburn, C. L. (2014). Optical and chemical characterization of base-extracted particulate organic matter in coastal marine environments. *Marine Chemistry*, *162*, 96–113. http://doi.org/10.1016/j.marchem.2014.03.006

Buss, S. R., Cai, Z., Cardenas, B., Fleckenstein, J., Hannah, D. M., Hepell, K., … Wood, P. (2009). *The Hyporheic Handbook A handbook on the groundwater – surface water interface and hyporheic zone for environment managers* Integrated catchment science programme Science report : SC050070.

Carey, A. E., Gardner, C. B., Goldsmith, S. T., Lyons, W. B., & Hicks, D. M. (2005), Organic carbon yields from small, mountainous rivers, New Zealand. *Geophysical Research Letters*, 32(15), 1–5. http://doi.org/10.1029/2005GL023159

Caverly, E., Kaste, J. M., Hancock, G. S., & Chambers, R. M. (2013), Dissolved and particulate organic carbon fluxes from an agricultural watershed during consecutive tropical storms. *Geophysical Research Letters*, 40(19), 5147–5152. doi:10.1002/grl.50982

Clifford, N. J., Richards, K. S., Brown, R. a., & Lane, S. N. (1995). Laboratory and field assessment of an infrared turbidity probe and its response to particle size and variation in suspended sediment concentration. *Hydrological Sciences Journal*, *40*(6), 771–791. http://doi.org/10.1080/02626669509491464

Cole, J. J., Prairie, Y. T., Caraco, N. F., McDowell, W. H., Tranvik, L. J., Striegl, R. G., Duarte, C.M., Kortelainen, P., Downing, J.A., Middleburg, J.J., & Melack, J. (2007), Plumbing the Global Carbon Cycle: Integrating Inland Waters into the Terrestrial Carbon Budget. *Ecosystems*, 10(1), 172–185. http://doi.org/10.1007/s10021-006-9013-8

Committee on Extreme Weather Events and Climate Change Attribution. (2016). *Attribution of Extreme Weather Events in the Context of Climate Change*. http://doi.org/10.17226/21852

Cordova, J. M., Rosi-Marshall, E. J., Tank, J. L., & Lamberti, G. a. (2008). Coarse particulate organic matter transport in low-gradient streams of the Upper Peninsula of Michigan. *Journal of the North American Benthological Society*, *27*(3), 760–771. http://doi.org/10.1899/06-119.1

Correll, D. L., Jordan, T. E., & Weller, D. E. (1999). Transport of nitrogen and phosphorus from rhode river watersheds during storm events. *Water Resources Research*, *35*(8), 2513. http://doi.org/10.1029/1999WR900058

Cory, R. M., & Mcknight, D. M. (2005). Fluorescence Spectroscopy Reveals Ubiquitous Presence of Oxidized and Reduced Quinones in Dissolved Organic Matter Fluorescence Spectroscopy Reveals Ubiquitous Presence of Oxidized and Reduced Quinones in Dissolved Organic Matter. *Environmental Science & Technology*, *39*(21), 8142–8149. http://doi.org/10.1021/es0506962

Czuba, J. A., & Foufoula-Georgiou, E. (2014). A network-based framework for identifying potential synchronizations and amplifications of sediment delivery in river basins. *Water Resources Research*, *50*, 3826–3851. http://doi.org/10.1002/2013WR014227.Received

Davis, C. M., & Fox, J. F. (2009). Sediment Fingerprinting: Review of the Method and Future Improvements for Allocating Nonpoint Source Pollution. *Journal of Environmental Engineering*, *135*(7), 490–504. http://doi.org/10.1061/(ASCE)0733-9372(2009)135:7(490)

Dhillon, G. S., & Inamdar, S. (2013), Extreme storms and changes in particulate and dissolved organic carbon in runoff: Entering uncharted waters? *Geophysical Research Letters*, 40(7), 1322–1327. doi:10.1002/grl.50306

Dhillon, G. S., & Inamdar, S. (2014), Storm event patterns of particulate organic carbon (POC) for large storms and differences with dissolved organic carbon (DOC), *Biogeochemistry*, 118(1-3), 61–81. doi:10.1007/s10533-013-9905-6

Donovan, M., Miller, A., Baker, M., & Gellis, A. (2015). Sediment contributions from floodplains and legacy sediments to Piedmont streams of Baltimore County, Maryland. *Geomorphology*, *235*, 88–105. http://doi.org/10.1016/j.geomorph.2015.01.025

Dyer, K.R., Manning, A.J. (1999). Observation of the size, settling velocity and effective density of flocs, and their fractal dimensions. *Journal of Sea Research* 41, 87–95.

Estapa, M. L., Mayer, L. M., & Boss, E. (2012), Rate and apparent quantum yield of photodissolution of sedimentary organic matter. *Limnology and Oceanography*, 57(6), 1743–1756. http://doi.org/10.4319/lo.2012.57.6.1743

Etheridge, J. R., Birgand, F., & Burchell, M. R. (2014). Quantifying nutrient and suspended solids fluxes in a constructed tidal marsh following rainfall: The value of capturing the rapid changes in flow and concentrations. *Ecological Engineering*. http://doi.org/10.1016/j.ecoleng.2014.05.021

Etheridge, J. R., Birgand, F., Osborne, J. a., Osburn, C. L., Ii, M. R. B., & Irving, J. (2014). Using in situ ultraviolet-visual spectroscopy to measure nitrogen, carbon, phosphorus, and suspended solids concentrations at a high frequency in a brackish tidal marsh. *Limnology and Oceanography: Methods*, *12*, 10–22. http://doi.org/10.4319/lom.2014.12.10

Ford, W. I., Fox, J. F., & Rowe, H. (2015), Impact of extreme hydrologic disturbance upon the sediment carbon quality in agriculturally impacted temperate streams. *Ecohydrology*, 8(3), 438–449. doi:10.1002/eco.1514

Fox, J. F. & Papanicolaou, A. N. (2007), The Use of Carbon and Nitrogen Isotopes to Study Watershed Erosion Processes. *Journal of the American Water Resources Association*, 43(4), 1047–1064. doi:10.1111/j.1752-1688.2007.00087.x

Gabor, R. S., Burns, M. a., Lee, R. H., Elg, J. B., Kemper, C. J., Barnard, H. R., & McKnight, D. M. (2015). Influence of Leaching Solution and Catchment Location on the Fluorescence of Water-Soluble Organic Matter. *Environmental Science & Technology*, 150309144001005. http://doi.org/10.1021/es504881t

Galuszka, A., Migaszewski, Z. M., & Namiesnik, J. (2015). Moving your laboratories to the field - Advantages and limitations of the use of field portable instruments in environmental sample analysis. *Environmental Research*, *140*, 593–603. http://doi.org/10.1016/j.envres.2015.05.017

Garzon-garcia, A., Olley, J. M., & Bunn, S. E. (2014), Controls on carbon and nitrogen export in an eroding catchment of south-eastern Queensland, Australia. *Hydrological Processes*, doi:10.1002/hyp.10192

Gellis, A. C., & Mukundan, R. (2013), Watershed sediment source identification: tools, approaches, and case studies. *Journal of Soils and Sediments*, 13(10), 1655–1657. http://doi.org/10.1007/s11368-013-0778-z

Gellis A.C. & Noe, G.B.(2013). Sediment source analysis in the Linganore Creek watershed, Maryland, USA, using the sediment fingerprinting approach: 2008 to 2010. *Journal of Soils and Sediments*, *13*: 1735–1753. doi. 10.1007/s11368-013-0771-6

Gellis, A.C., Noe, G.B., Clune, J.W., Myers, M.K., Hupp, C.R., Schenk, E.R., and Schwarz, G.E. (2015), Sources of fine- grained sediment in the Linganore Creek watershed, Frederick and Carroll Counties, Maryland, 2008–10: *U.S. Geological Survey Scientific Investigations Report, 2014–5147*, 56 p., http://dx.doi.org/10.3133/sir20145147

Gippel, C. J. (1989). The use of turbidimeters in suspended sediment research. *Hydrobiologia*, *176-177*(1), 465–480. http://doi.org/10.1007/BF00026582

Griffiths, N. A., Tank, J. L., Royer, T. V, Rosi-marshall, E. J., Whiles, R., Chambers, C. P., … Chambers, P. (2015). Rapid Decomposition of Maize Detritus in Agricultural Headwater Streams. *Ecological Applications*, *19*(1), 133–142.

Guenet, B., Danger, M., Harrault, L., Allard, B., Jauset-Alcala, M., Bardoux, G., … Lacroix, G. (2013). Fast mineralization of land-born C in inland waters: first experimental evidences of aquatic priming effect. *Hydrobiologia*, *721*(1), 35–44. http://doi.org/10.1007/s10750-013-1635-1

Hancock, G. J., & Revill, A. T. (2013). Erosion source discrimination in a rural Australian catchment using compound-specific isotope analysis (CSIA). *Hydrological Processes*, *27*(6), 923–932. http://doi.org/10.1002/hyp.9466

Harvey, J., & Gooseff, M. (2015), River corridor science: Hyrologic exchange and ecological consequences from bedforms to basins. *Water Resources Research*, 1–30. http://doi.org/10.1002/2015WR017617.

Hirsch, R.M. (2012), Flux of Nitrogen, Phosphorous, and Suspended Sediment from the Susquehanna River Basin to the Chesapeake Bay during Tropical Storm Lee, September 2011, as an Indicator of the Effects of Reservoir Sedimentation on Water Quality. USGS Scientific Investigations Report 2012-5185.

Hope, D., Billett, M. F., & Cresser, M. S. (1994), A review of the export of carbon in river water: Fluxes and processes. *Environmental Pollution*, 84, 301–324.

Horowitz, A. J. (2008), Determining annual suspended sediment and sediment-associated trace element and nutrient fluxes. *Science of the Total Environment*, 400(1-3), 315–343. doi:10.1016/j.scitotenv.2008.04.022

Hupp, C. R., Noe, G. B., Schenk, E. R., & Benthem, A. J. (2013). Recent and historic sediment dynamics along Difficult Run, a suburban Virginia Piedmont stream. *Geomorphology*, *180-181*, 156–169. http://doi.org/10.1016/j.geomorph.2012.10.007

Inamdar, S., Dhillon, G., Singh, S., Parr, T., & Qin, Z. (2015). Particulate nitrogen exports in stream runoff exceed dissolved nitrogen forms during large tropical storms in a temperate, headwater, forested watershed. *Journal of Geophysical Research: Biogeosciences*, *120*(8), 1548–1566. http://doi.org/10.1002/2015JG002909

Jastram, J. D., Zipper, C. E., Zelazny, L. W., & Hyer, K. E. (2010). Increasing Precision of Turbidity-Based Suspended Sediment Concentration and Load Estimates. *Journal of Environment Quality*, *39*(4), 1306. http://doi.org/10.2134/jeq2009.0280

Jeong, J.-J., Bartsch, S., Fleckenstein, J. H., Matzner, E., Tenhunen, J. D., Lee, S. D., … Park, J.-H. (2012), Differential storm responses of dissolved and particulate organic carbon in a mountainous headwater stream, investigated by high-frequency, in situ optical measurements. *Journal of Geophysical Research*, 117(G3), G03013. doi:10.1029/2012JG001999

Jung, B. J., Lee, H. J., Jeong, J. J., Owen, J., Kim, B., Meusburger, K., … Park, J. H. (2012), Storm pulses and varying sources of hydrologic carbon export from a mountainous watershed. *Journal of Hydrology*, 440-441, 90–101. http://doi.org/10.1016/j.jhydrol.2012.03.030

Jung, B.-J., Jeanneau, L., Alewell, C., Kim, B., & Park, J.-H. (2014), Downstream alteration of the composition and biodegradability of particulate organic carbon in a mountainous, mixed land-use watershed. *Biogeochemistry*, 122(1), 79–99. doi:10.1007/s10533-014-0032-9

Jung, B.-J., Lee, J.-K., Kim, H., & Park, J.-H. (2014), Export, biodegradation, and disinfection byproduct formation of dissolved and particulate organic carbon in a forested headwater stream during extreme rainfall events. *Biogeosciences*, 11(21), 6119–6129. doi:10.5194/bg-11-6119-2014

Karl, T.R., Knight, R.W. (1998) Secular trends of precipitation amount, frequency, and intensity in the United States. *Bull Am Meteorological Society,* 79(2):231–241.

Karl, T.R., J. M. Melillo, T.C. Peterson, and S. J.Hassol (2009), Global climate change impacts in the United States, University Press, Cambridge.

Kaushal, S. S., Mayer, P. M., Vidon, P. G., Smith, R. M., Pennino, M. J., Newcomer, T. a., … Belt, K. T. (2014), Land Use and Climate Variability Amplify Carbon, Nutrient, and Contaminant Pulses: A Review with Management Implications. *JAWRA Journal of the American Water Resources Association*, 50(3), 585–614. doi:10.1111/jawr.12204

Kendall, C., Silva, S. R., & Kelly, V. J. (2001), Carbon and nitrogen isotopic compositions of particulate organic matter in four large river systems across the United States. *Hydrological Processes*, 15(7), 1301–1346. doi:10.1002/hyp.216

Koiter, A. J., Lobb, D. a., Owens, P. N., Petticrew, E. L., Tiessen, K. H. D., & Li, S. (2013), Investigating the role of connectivity and scale in assessing the sources of sediment in an agricultural watershed in the Canadian prairies using sediment source fingerprinting. *Journal of Soils and Sediments*, 13(10), 1676–1691. doi:10.1007/s11368-013-0762-7

Laceby, J. P., Olley, J., Pietsch, T. J., Sheldon, F., & Bunn, S. E. (2015). Identifying subsoil sediment sources with carbon and nitrogen stable isotope ratios. *Hydrological Processes*, *29*(8), 1956–1971. http://doi.org/10.1002/hyp.10311

Landers, M. N., & Sturm, T. W. (2013), Hysteresis in suspended sediment to turbidity relations due to changing particle size distributions. *Water Resources Research*, 49(9), 5487–5500. doi:10.1002/wrcr.20394

Larsen, L., Harvey, J., Skalak, K., & Goodman, M. (2015). Fluorescence-based source tracking of organic sediment in restored and unrestored urban streams. *Limnology and Oceanography*, n/a–n/a. http://doi.org/10.1002/lno.10108

Lawler, D. M., Petts, G. E., Foster, I. D. L., & Harper, S. (2006). Turbidity dynamics during spring storm events in an urban headwater river system: The Upper Tame, West Midlands, UK. *Science of The Total Environment*, *360*(1-3), 109–126. http://doi.org/10.1016/j.scitotenv.2005.08.032

Leopold, L. B., M. G. Wolman, and J. P. Miller, 1964. *Fluvial processes in geomorphology*. W. H. Freeman and Company: San Francisco.

Lohse, K. a., Brooks, P. D., McIntosh, J. C., Meixner, T., & Huxman, T. E. (2009). Interactions Between Biogeochemistry and Hydrologic Systems. *Annual Review of Environment and Resources*, *34*(1), 65–96. http://doi.org/10.1146/annurev.environ.33.031207.111141

Lu, Y. H., Canuel, E. a., Bauer, J. E., & Chambers, R. M. (2014), Effects of watershed land use on sources and nutritional value of particulate organic matter in temperate headwater streams. *Aquatic Sciences*, 76(3), 419–436. doi:10.1007/s00027-014-0344-9

Mukundan, R., Walling, D. E., Gellis, A. C., Slattery, M. C., & Radcliffe, D. E. (2012). Sediment Source Fingerprinting: Transforming From a Research Tool to a Management Tool 1. *JAWRA Journal of the American Water Resources Association*, *48*(6), 1241–1257. doi: 10.1007/s11368-013-0778-z

Martínez-Carreras, N., Schwab, M. P., Klaus, J., & Hissler, C. (2016). In situ and high frequency monitoring of suspended sediment properties using a spectrophotometric sensor. *Hydrological Processes*, n/a–n/a. http://doi.org/10.1002/hyp.10858

Marttila, H., & Kløve, B. (2015). Spatial and temporal variation in particle size and particulate organic matter content in suspended particulate matter from peatland-dominated catchments in Finland. *Hydrological Processes*, *29*(6), 1069–1079. http://doi.org/10.1002/hyp.10221

Maryland State Climatologist Office Data Page. (n.d.) . Retrieved from http://metosrv2.umd.edu/~climate/cono/norm.html

Mayer, M., Joye, B., & Aller, C. (1998), Importance of suspended participates in riverine delivery of bioavailable nitrogen to coastal zones, Global Biogeochemical Cycles 12(4), 573–579.

Mengistu, S. G., Creed, I. F., Webster, K. L., Enanga, E., & Beall, F. D. (2014). Searching for similarity in topographic controls on carbon, nitrogen and phosphorus export from forested headwater catchments. *Hydrological Processes*, *28*(8), 3201–3216. http://doi.org/10.1002/hyp.9862

Miller, J., Sinclair, J., & Walsh, D. (2015). Controls on Suspended Sediment Concentrations and Turbidity within a Reforested, Southern Appalachian Headwater Basin. *Water*, *7*(6), 3123–3148. http://doi.org/10.3390/w7063123

Mukundan, R., Walling, D. E., Gellis, A. C., Slattery, M. C., & Radcliffe, D. E. (2012), Sediment Source Fingerprinting: Transforming From a Research Tool to a Management Tool 1. *JAWRA Journal of the American Water Resources Association*, 48(6), 1241–1257. doi:10.1111/j.1752-1688.2012.00685.x

Mutema, M., Chaplot, V., Jewitt, G., Chivenge, P., & Bloschl, G. (2015), Annual water, sediment, nutrient, and organic carbon fluxes in river basins: A global meta-analysis as a function of scale. *Water Resources Research*, 51, 8949–8972. http://doi.org/10.1002/2014WR016259

Nadelhoffer, K. J., & Fry, B. (1988). Controls on natural nitrogen-15 and carbon-13 abundances in forest soil organic matter. *Soil Science Society of America* Journal 52(5):1633-1640.

Osburn, C. L., Handsel, L. T., Mikan, M. P., Paerl, H. W., & Montgomery, M. T. (2012). Fluorescence tracking of dissolved and particulate organic matter quality in a river-dominated estuary. *Environmental Science & Technology*, *46*(16), 8628–36. http://doi.org/10.1021/es3007723

Parnell, A. (2016), SIMMR, A Stable Isotope Mixing Model (Version 0.3). Available from https://cran.r-project.org/web/packages/simmr/index.html.

Pellerin, B. A., Stauffer, B. A., Young, D. A., Sullivan, D. J., Bricker, S. B., Walbridge, M. R., … Shaw, D. M. (2016). Emerging Tools for Continuous Nutrient Monitoring Networks: Sensors Advancing Science and Water Resources Protection. *Journal of the American Water Resources Association*, *20460*. http://doi.org/10.1111/1752-1688.12386

Raymond, P. A., Saiers, J. E., & Sobczak, W. V. (2015). Hydrological and biogeochemical controls on watershed dissolved organic matter transport: Pulse-shunt concept. *Ecology*, *89*(10), 150728163409002. http://doi.org/10.1890/14-1684.1

Sharp, Z. (2007) *Stable Isotope Geochemistry*. Pearson: New Jersey.

Singh, S., Inamdar, S., Mitchell, M., & McHale, P. (2013). Seasonal pattern of dissolved organic matter (DOM) in watershed sources: influence of hydrologic flow paths and autumn leaf fall. *Biogeochemistry*, *118*(1-3), 321–337. http://doi.org/10.1007/s10533-013-9934-1

Smith, H. G., & Dragovich, D. (2008). Improving precision in sediment source and erosion process distinction in an upland catchment, south-eastern Australia. *CATENA*, *72*(1), 191–203. http://doi.org/10.1016/j.catena.2007.05.013

Stelzer, R. S., Heffernan, J., & Likens, G. E. (2003), The influence of dissolved nutrients and particulate organic matter quality on microbial respiration and biomass in a forest stream. *Freshwater Biology*, 48(11), 1925–1937. http://doi.org/10.1046/j.1365-2427.2003.01141.x

Stewart, H. A., Massoudieh, A., & Gellis, A. (2015). Sediment source apportionment in Laurel Hill Creek, PA, using Bayesian chemical mass balance and isotope fingerprinting. *Hydrological Processes*, *29*(11), 2545–2560. http://doi.org/10.1002/hyp.10364

Tank, J. L., Rosi-Marshall, E. J., Griffiths, N. a., Entrekin, S. a., & Stephen, M. L. (2010). A review of allochthonous organic matter dynamics and metabolism in streams. *Journal of the North American Benthological Society*, *29*(1), 118–146. http://doi.org/10.1899/08-170.1

Tant, C. J., Rosemond, A. D., & First, M. R. (2013), Stream nutrient enrichment has a greater effect on coarse than on fine benthic organic matter. *Freshwater Science*, 32(4), 1111–1121. http://doi.org/10.1899/12-049.1

Vannote, R. L., Minshall, G. W., Cummins, K. W., Sedell, J. R., & Cushing, C. E. (1980). The River Continuum Concept. *Canadian Journal of Fisheries and Aquatic Sciences*, *37*(1), 130–137. http://doi.org/10.1139/f80-017

Wallace, J. B., Webster, J. R., Cuffney, T. F., Url, S., Wallace, J. B., Webster, J. R., & Cuffney, T. F. (1982). International Association for Ecology Stream Detritus Dynamics : Regulation by Invertebrate Consumers, *53*(2), 197–200. http://doi.org/0029-8549/82/0053/0197/SOl.OO

Wallace, J. B., Whiles, M. R., Webster, J. R., Cuffney, T. F., Lugthart, G. J., & Chung, K. (1993), Dynamics of Inorganic Particles in Headwater Streams - Linkages with Invertebrates. *Journal of the North American Benthological Society*, 12(2), 112–125. http://doi.org/10.2307/1467341

Walter, R. C., & Merritts, D. J. (2008). Natural streams and the legacy of water-powered mills. *Science (New York, N.Y.)*, *319*(5861), 299–304. http://doi.org/10.1126/science.1151716

Webster, J. R., & Meyer, J. L. (1997). Stream organic matter budgets-introduction. *Journal of the North American Benthological Society*, *16*(1), 5–13. Retrieved from journals.

Wohl, E., Bledsoe, B. P., Jacobson, R. B., Poff, N. L., Rathburn, S. L., Walters, D. M., & Wilcox, a. C. (2015). The Natural Sediment Regime in Rivers: Broadening the Foundation for Ecosystem Management. *BioScience*, *65*(4), 358–371. http://doi.org/10.1093/biosci/biv002

Wood, P. J. (1997). Biological Effects of Fine Sediment in the Lotic Environment. *Environmental Management*, *21*(2), 203–217. http://doi.org/10.1007/s002679900019

Wotton, R.S. (1994), *The Biology of Particles in Aquatic Systems*, (Second Edition), CRC Press : Boca Raton, Florida.

Yoshimura, C., Gessner, M. O., Tockner, K., & Furumai, H. (2008), Chemical properties, microbial respiration, and decomposition of coarse and fine particulate organic matter. *Journal of the North American Benthological Society*, 27(3), 664–673. http://doi.org/10.1899/07-106.1

Yoshimura, C., & Fujii, M. (2010). Instream release of dissolved organic matter from coarse and fine particulate organic matter of different origins. *Biogeochemistry, 100* (1), 151–165. http://doi.org/10.1007/sl0533-010-9412-y

Zhang, Q., Brady, D. C., Boynton, W. R., & Ball, W. P. (2015), Long-Term Trends of Nutrients and Sediment from the Nontidal Chesapeake Watershed: An Assessment of Progress by River and Season. *Journal of the American Water Resources Association*, 51(6), 1534–1555. http://doi.org/10.1111/1752-1688.12327

Ziegler, A. D., Benner, S. G., Tantasirin, C., Wood, S. H., Sutherland, R. a., Sidle, R. C., … Fox, J. M. (2014). Turbidity-based sediment monitoring in northern Thailand: Hysteresis, variability, and uncertainty. *Journal of Hydrology*, *519*, 2020–2039. http://doi.org/10.1016/j.jhydrol.2014.09.010

Ziegler, A., Benner, S., Kunkel, M., Phang, V., Lupascu, M., & Tanasarin, C. (2016). Particulate carbon and nitrogen dynamics in a headwater catchment in Northern Thailand : Hysteresis , high yields , and hot spots. *Hydrological Processes*, n/a–n/a. http://doi.org/10.1002/hyp.10840

Appendix A

COMPLIMENTARY AND ONGOING WORK

This study sought to quantify source contributions to storm event POM fluxes from a headwater catchment across a range of particle sizes, drainage areas and hydrologic conditions. Complementary ongoing work to provide a more detailed description of variability in POM molecular composition with the same factors and to better characterize POC fluxes using high resolution sensors are described in this section.

Several other ongoing and potential studies could further strengthen this work. Fluorescence analysis of extracted dissolved organic matter and sediment incubations may help to elucidate potential impacts of POM on receiving water quality. Analysis of radioisotope activity of carbon (^{14}C) in conjunction with stable isotopes could draw inferences about the relative ages of POM of different sizes or from different sources, and give further insight into the aquatic processing of POM. Finally, use of available synoptic storm calendars from the state climatologist records could be used to generate more detailed descriptions of storm types (e.g. summer convective cells, northeasters, etc.) and ultimately link them to the magnitude and sources of POM fluxes.

A.1 Molecular biomarkers

Organic biomarkers (Bianchi and Bauer, 2011) have also been implemented as environmental tracers in this study to characterize the POM sources. Additionally, such biomarkers can also provide important insights into the state of degradation and

relative bioavailability of POM. Subsamples from the same set of events used for isotopes have been analyzed for biomarkers for the 12 and 79 ha drainage locations. POM samples were analyzed via THM-GC-MS for a total of 116 compounds by Dr. Laurent Jeanneau from the University of Rennes in France. Due to the diversity of these organic compounds, these were summarized into four main families: carbohydrates, small organic acids, fatty acids, and aromatic alcohols and acids (or phenolic-like compounds). Much of this work is still evolving and Dr. Jeanneau will be taking the lead in drafting the research manuscript.

Preliminary results using biomarkers as tracers qualitatively suggest similar trends to those observed in our isotope mixing model, although exact proportions of end member contributions vary. Specifically, proportional contributions of litter decrease while stream beds, wetlands, and humus increase, respectively, when moving from CPOM to MPOM to FPOM. These results also suggest that proportionally less POM is routed from leaf litter while more comes from the stream bed when comparing larger to smaller drainage areas. However, one important difference is that biomarker data suggest high-discharge, low-rainfall intensity events (such as that on May 01, 2014) mobilize proportionally more stream bed material and less forest floor material when compared to low-discharge, high-rainfall intensity events (such as that on September 30, 2015), contrary to our findings. DSS samples distributed across the hydrograph for one event (April 21, 2015, 12-ha location) were analyzed and, similar to our isotopic analyses, suggest increased contributions from humus during hydrograph recession.

In addition to reinforcing our isotope-based mixing model results, an important goal in incorporating molecular biomarkers was to make inferences about the

composition and ecological role of POM of different size classes transported under various hydrologic conditions. While this research is ongoing, we have made a few relevant, preliminary observations. First, the proportion of the organic pool composed of carbohydrates is negatively correlated with $\delta^{13}C$, and were higher in CPOM. Second, the proportional presence of phenolic compounds is negatively correlated with atomic C:N , and is higher in FPOM. As carbohydrates are generally considered bioavailable, and phenolics in natural environments largely comprise lignin degradation byproducts and humic macromolecules, these support our inference that CPOM from wetlands and forest floor litter is more labile than FPOM from in-stream end members as discussed in section 5.2 and 5.3. These results are summarized in a multivariate space and are presented in Figure A1.

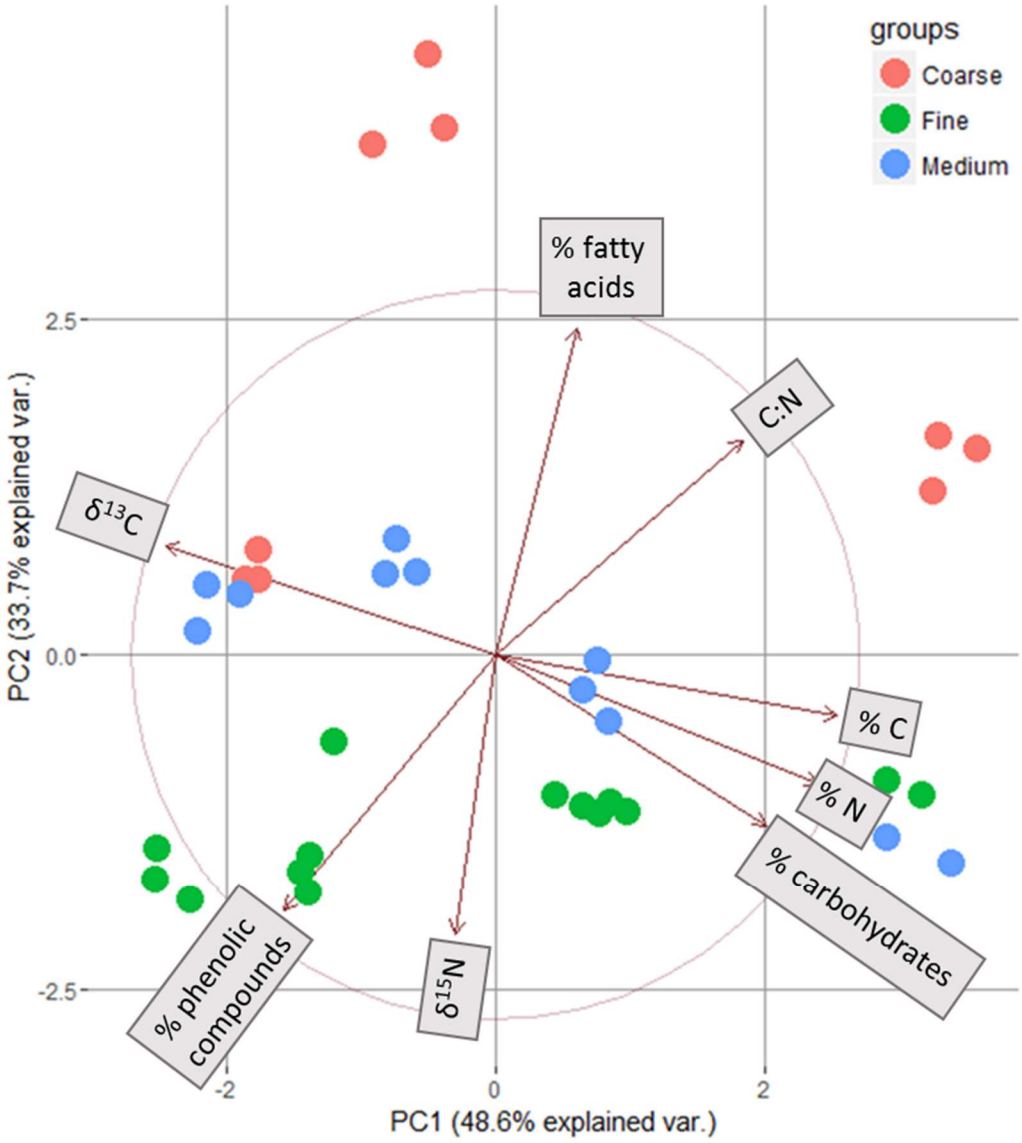

Figure A1 Evaluation of CSS POM particle classes in multivariate PCA space. Relationships between elemental, isotope, and molecular composition (mass percent of compounds detected and identified as fatty acids, phenolic compounds, or carbohydrates) are displayed.

A.2 Measurements of POC using *in-situ* sensors

Reliable sensors for the continuous *in-situ* measurement of water quality are gaining popularity because of the ability to make high-resolution measurements that may be cost- or logistically-prohibitive otherwise. Such measurements are providing new insights into hydrologic drivers of ecologically-important solutes such as nitrate (Galuszka *et al.,* 2015, Pellerin *et al.,* 2016). Several recent studies have indicated that optical sensors can be used to reproducibly estimate concentrations of different particulate parameters, and that such measurements may be useful for assessing long term loads, trends, within-event patterns, and source dynamics in parameters such as POC (Bass *et al.*, 2011, Etheridge *et al.*, 2014, Jeong *et al.,* 2012, Martínez-Carreras *et al.,* 2016).

We deployed two optical sensors (spectro::lyser, s::can Messtechnik GmbH, Vienna, Austria) at the intensive 12 and 79 ha monitoring locations in our catchment. POC measurements from DSS are being compared to sensor estimates (calculated as TOC minus DOC). The development of a reliable calibration relating laboratory measurements to sensor estimates of POC has yielded mixed results thus far. Correlations between laboratory and sensor values are significant at the 12 ha site after the removal of three outliers, although they are not as strong as the relationships reported in other studies (Figure B1). There is no statistically significant correlation at the 79 ha location. This could be for several reasons including (but not limited to):

- Lower and more variable organic content of particles at the 79 ha location
- Coarser particle size distributions at the 79-ha location (optical turbidity meters are less sensitive to coarser particle size distributions, Clifford *et al.*, 1995, Gippel, 1989, Jastram *et al*., 2010)

- Inadequate resolution of sensor measurements to capture changes in POC concentrations between validation grab samples
- Inadequacy of a linear model to capture relationships between POC concentrations and measured optical properties at our site
- Other potential limitations of sampling or measurements of POC in DSS samples that generate a bias or reduce precision

Several steps are currently being undertaken to assess these possibilities and attempt to develop a robust calibration. These include interpolation of POC samples to the exact time point of the sensor readings, development of multivariate calibrations similar to those employed by Etheridge *et al.* (2014), comparisons of sensor readings to POC grab samples across multiple study sites, and a laboratory experiment examining differences in sensor responses to a factorial of multiple suspended sediment concentrations, percent organic C content, provenance, and size classes. After the development of a robust calibration, we hope to complement our analysis of POC sources with high-resolution measurements of POC concentrations across event hydrographs. These may generate new insights into hysteresis patterns or "hot moments" during sampled events, and will provide data for events that may not have been sampled otherwise.

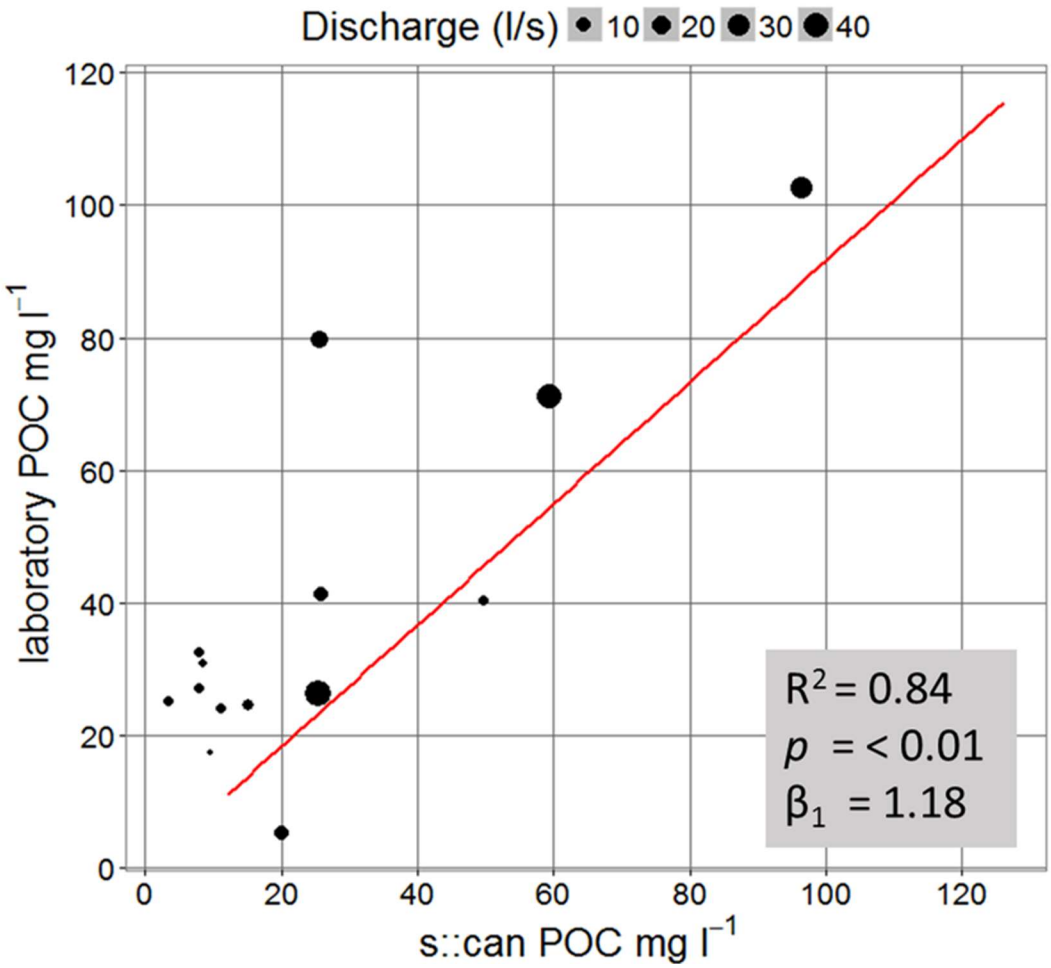

Figure A2 Relationship between POC as measured by the s::can spectro::lyser and in grab samples at the 12-ha drainage monitoring location.

Appendix B

AUXILIARY INFORMATION ON CATCHMENT GEOSPATIAL ATTRIBUTES

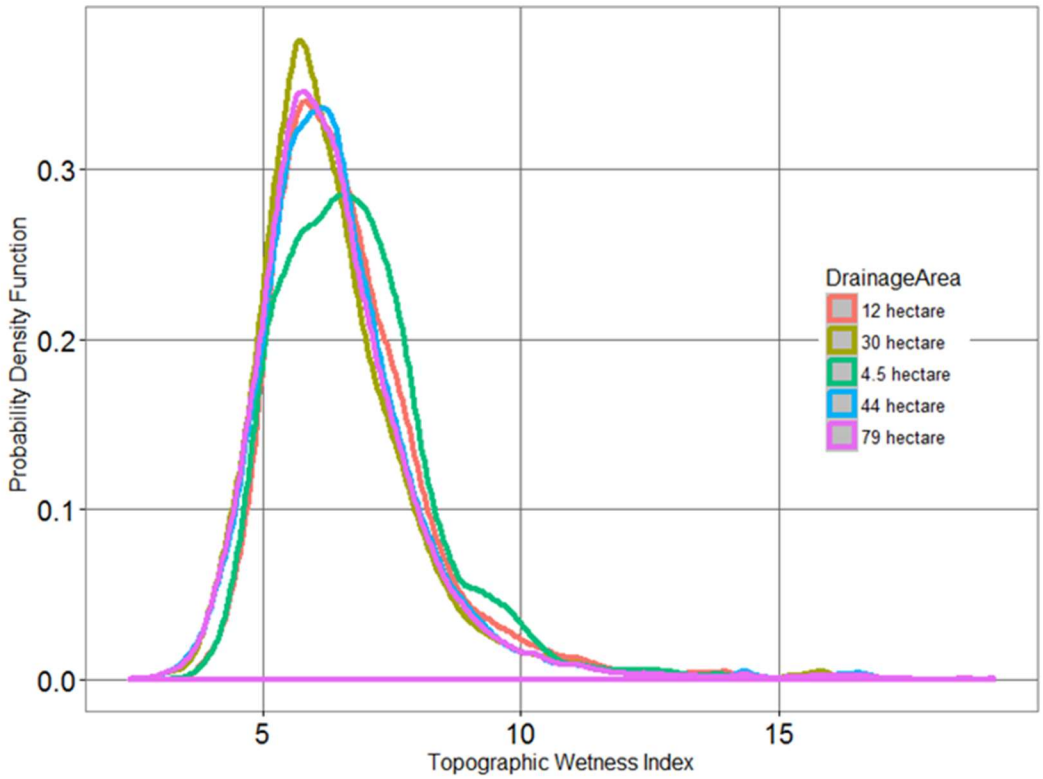

Figure B1: Probability density functions of the topographic wetness index calculated for each sampling location.

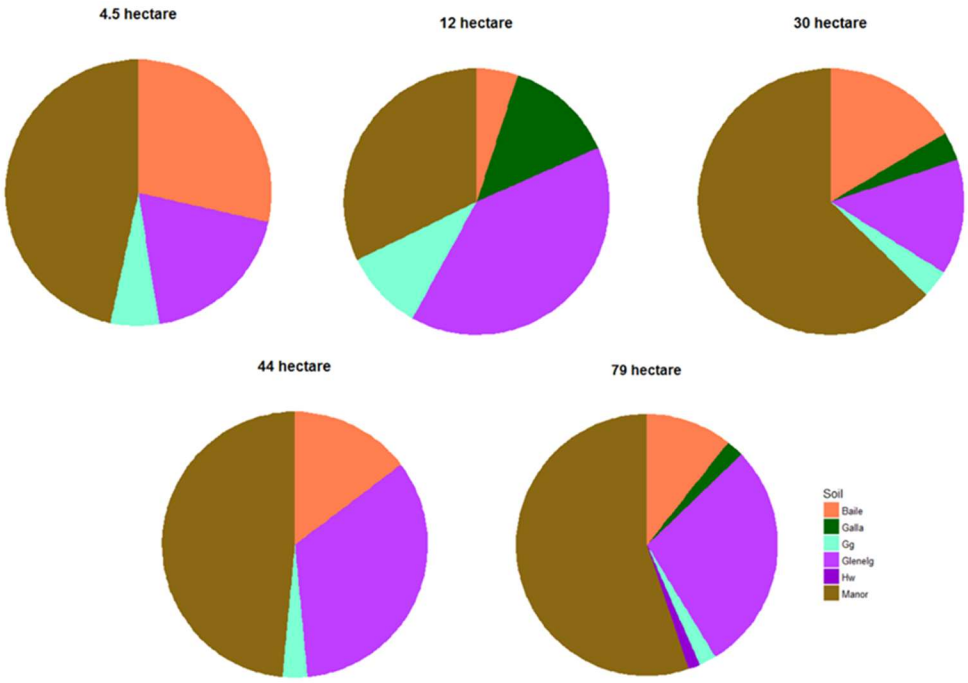

Figure B2: Summary of soil series by catchment area. Baile is an upland silty loam, Galla is a very OM-rich valley-bottom soil, Glenelg is a dense, clayey soil, and Manor is an upland loam.

Table B1: Buffer analysis of catchment geospatial attributed potentially related to POM source and transport. Analysis was conducted using a 50-meter radius around the stream channel.

	4.5 ha	**12 ha**	**30 ha**	**44 ha**	**79 ha**
Topographic wetness index					
10 %	4.94	5.21	4.58	4.59	4.61
25 %	5.56	5.83	5.39	5.33	5.35
50 (med)	6.96	6.61	6.34	6.27	6.31
75 %	8.18	7.84	7.59	7.42	7.51
90 %	9.80	9.10	8.80	8.79	8.81
Slope (%)					
10 %	2.38	2.91	3.32	3.32	3.32
25 %	3.88	4.09	5.44	5.32	5.39
50 (med)	8.40	7.73	9.77	8.54	8.95
75 %	11.79	11.63	14.81	13.25	13.86
90 %	14.05	14.60	19.34	17.94	18.70
Soil Series coverage (%)					
Baile	4.87	20.67	36.30	32.79	31.82
Galla	NA	30.28	10.26	NA	3.38
Glenelg	12.32	12.05	4.08	26.90	17.12
Gg	NA	NA	NA	NA	NA
Hw	NA	NA	NA	NA	4.27
Manor	82.81	37.00	49.36	40.31	43.41

Appendix C

OUTPUT DISTIBUTIONS FROM SIMMR MODEL ANALYSIS

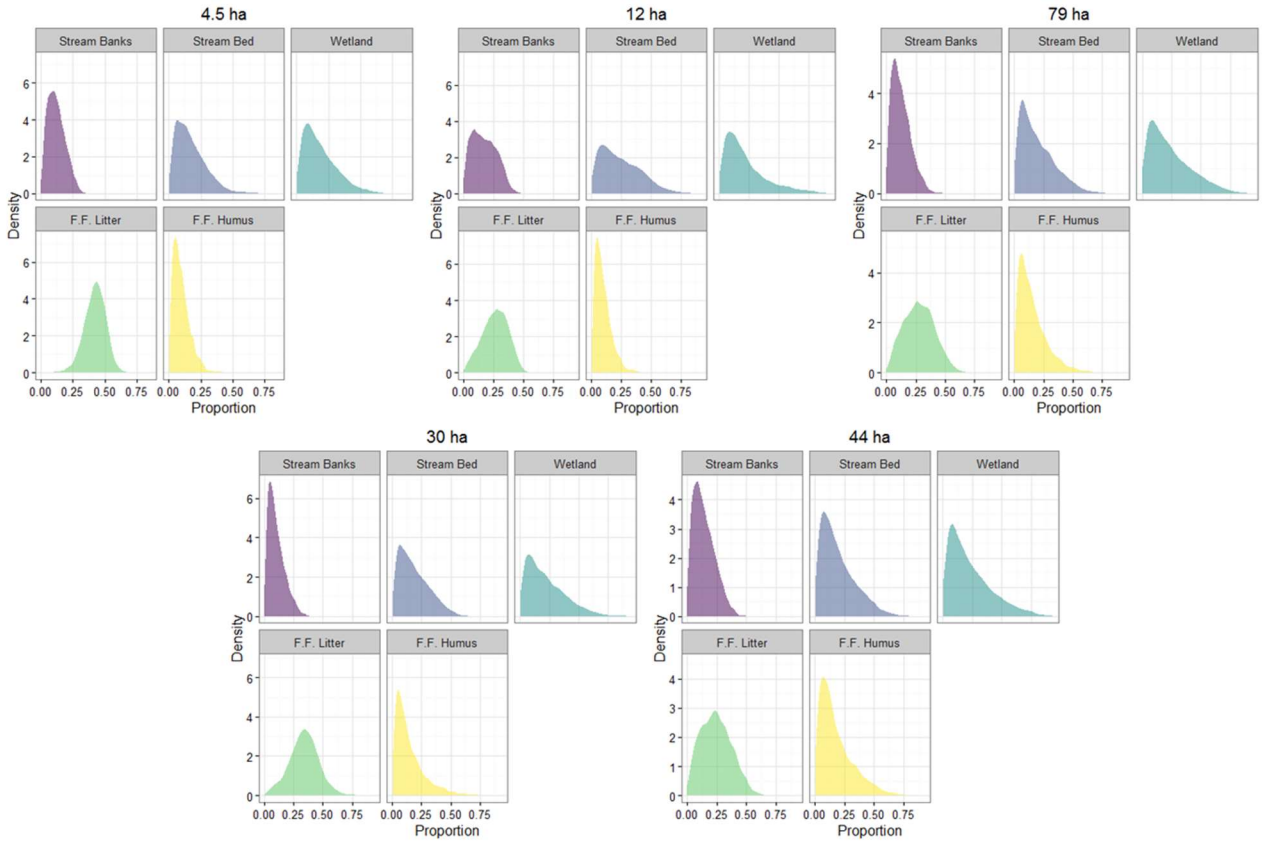

Figure C1: SIMMR posterior probability density distributions of proportional end member contributions to CPOM for each drainage location averaged across six events.

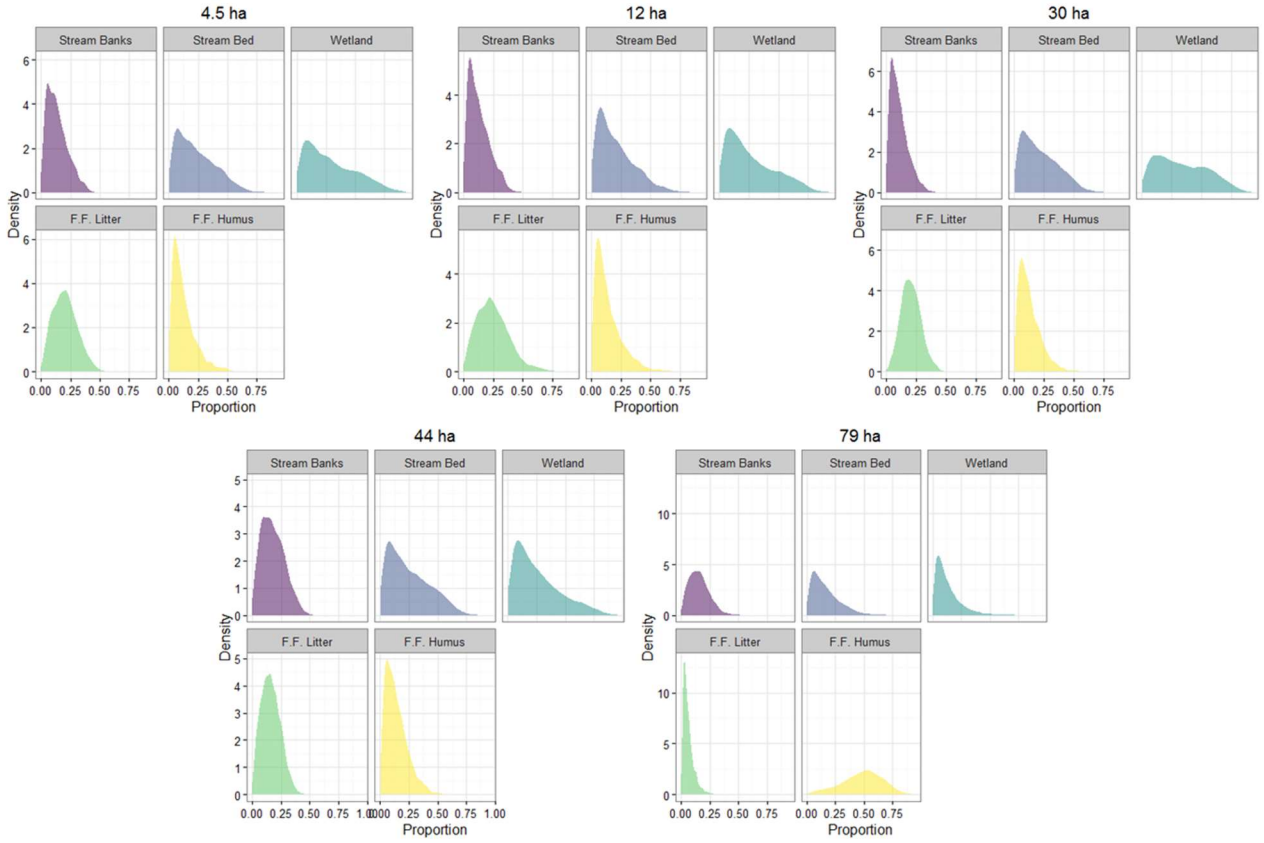

Figure C2: SIMMR posterior probability density distributions of proportional end member contributions to MPOM for each drainage location averaged across six events.

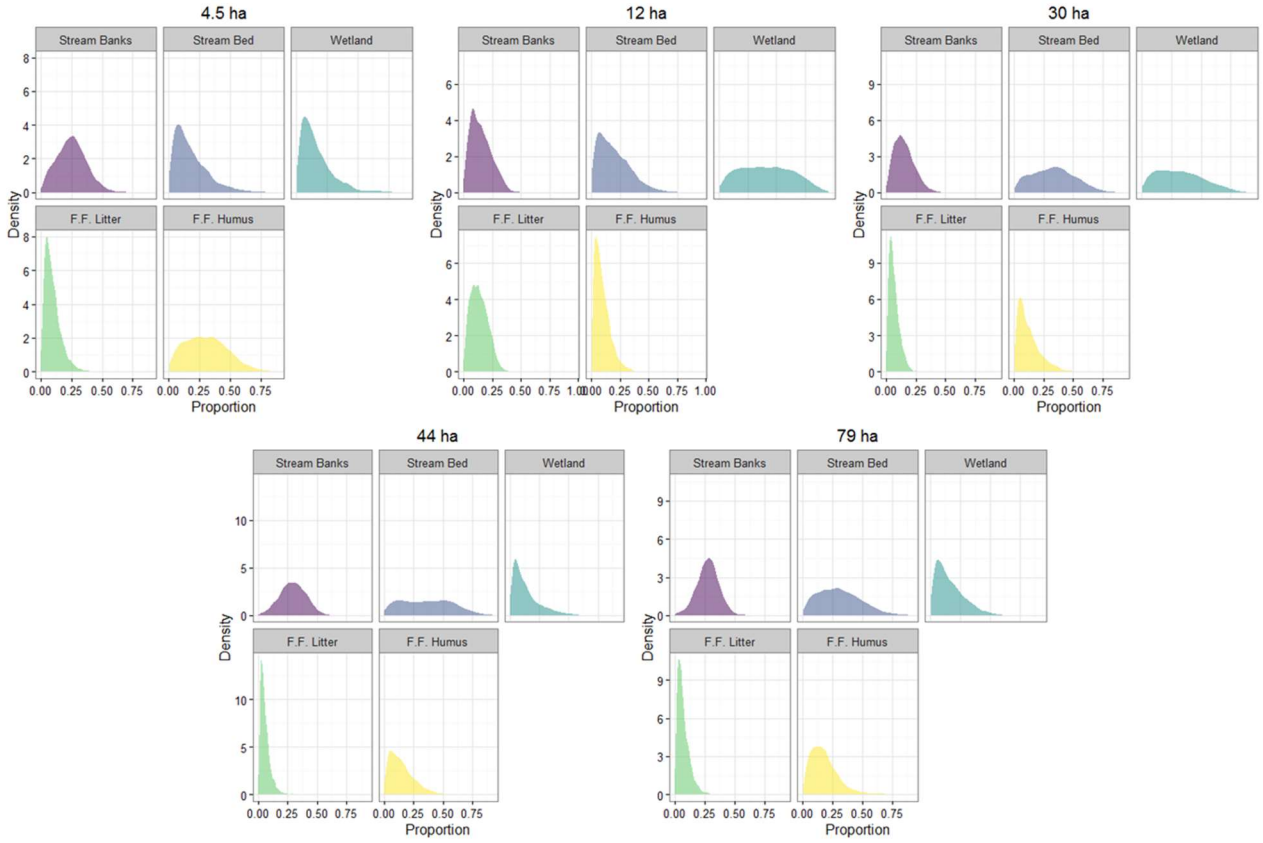

Figure C3: SIMMR posterior probability density distributions of proportional end member contributions to FPOM for each drainage location averaged across six events.

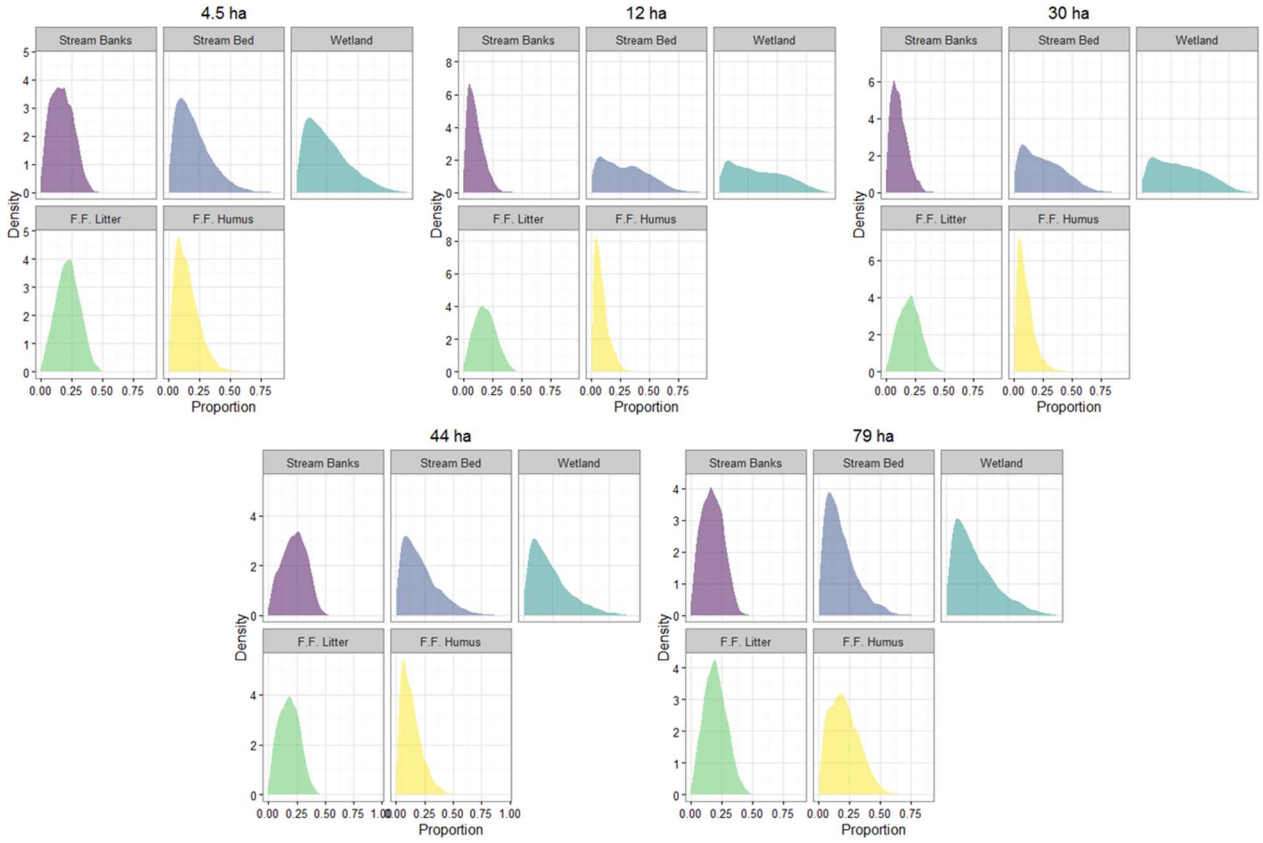

Figure C4: SIMMR posterior probability density distributions of proportional end member contributions to TPOM for each drainage location averaged across six events.

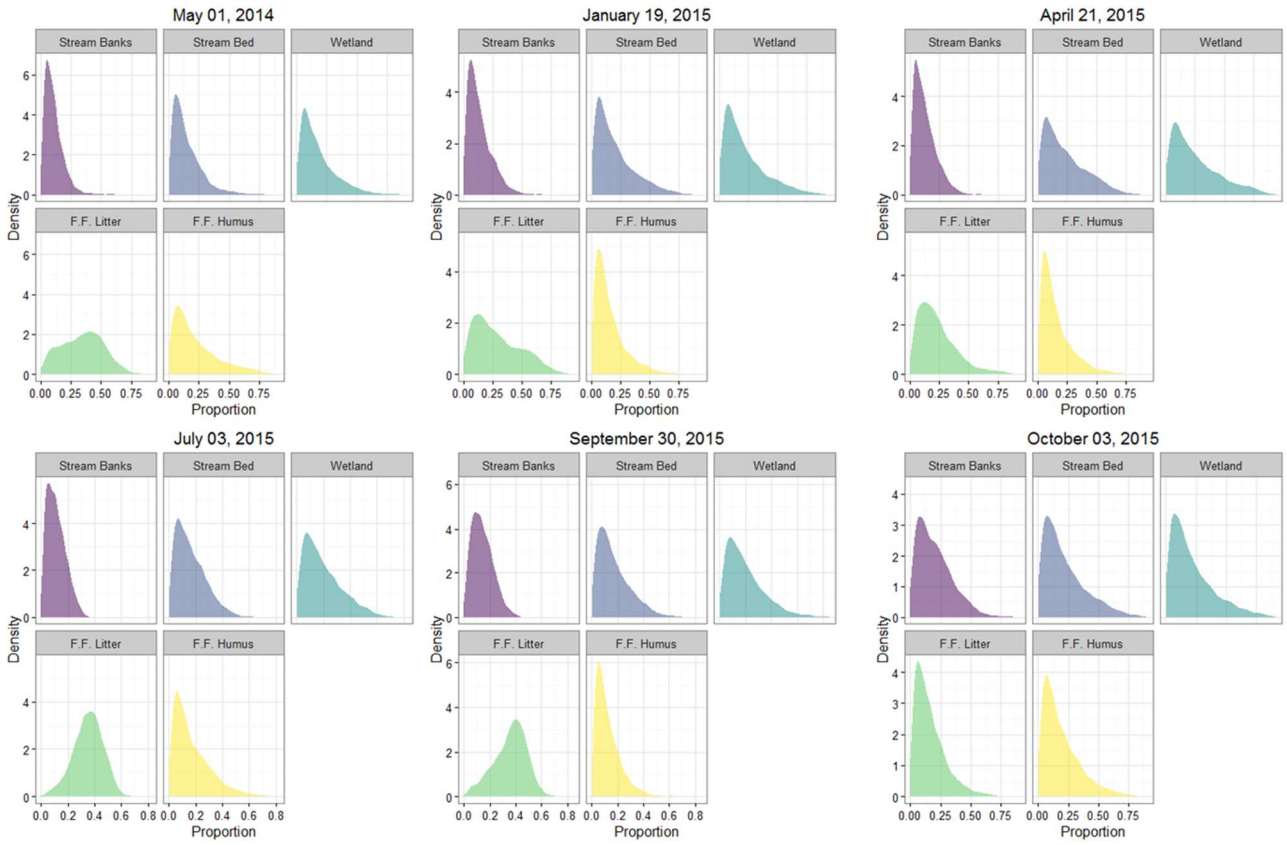

Figure C5: SIMMR posterior probability density distributions of proportional end member contributions to CPOM for each event averaged across five locations.

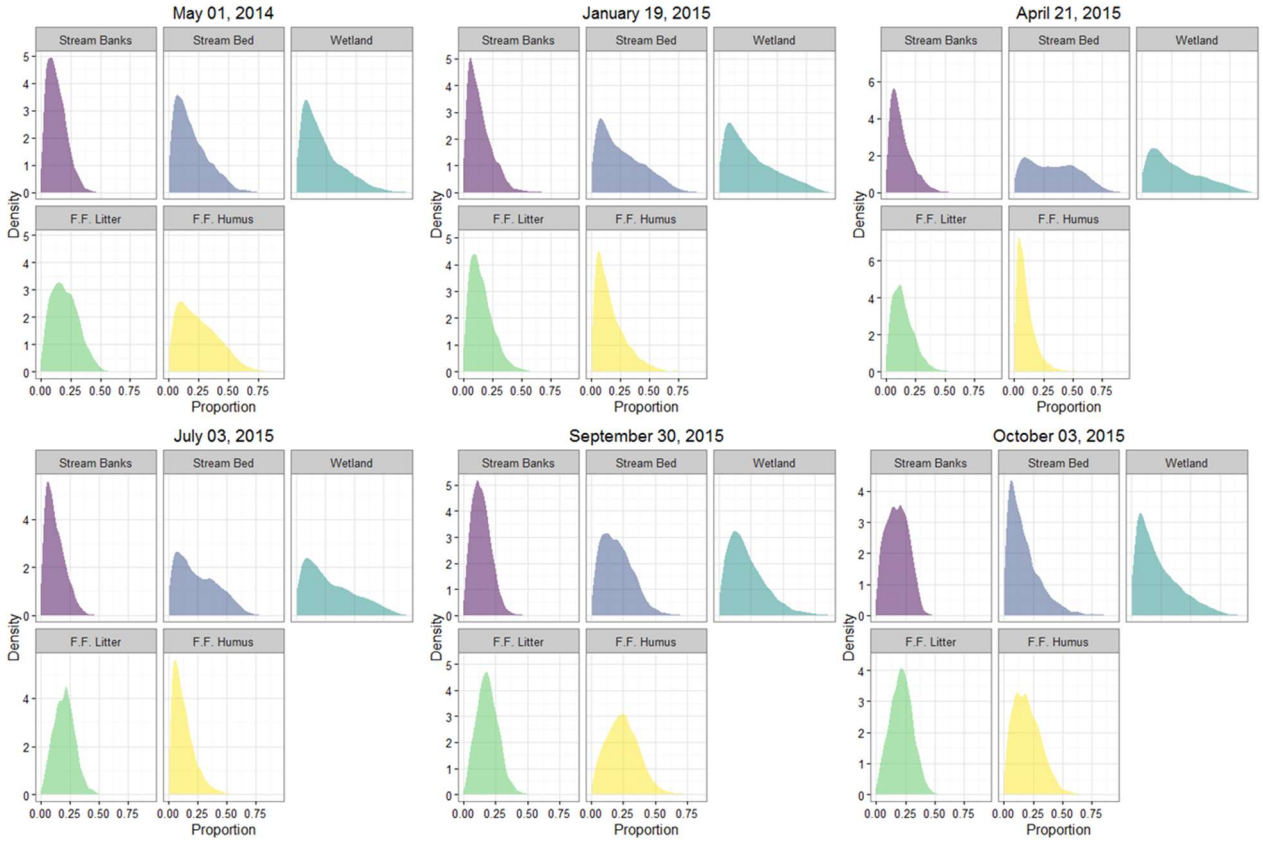

Figure C6: SIMMR posterior probability density distributions of proportional end member contributions to MPOM for each event averaged across five locations.

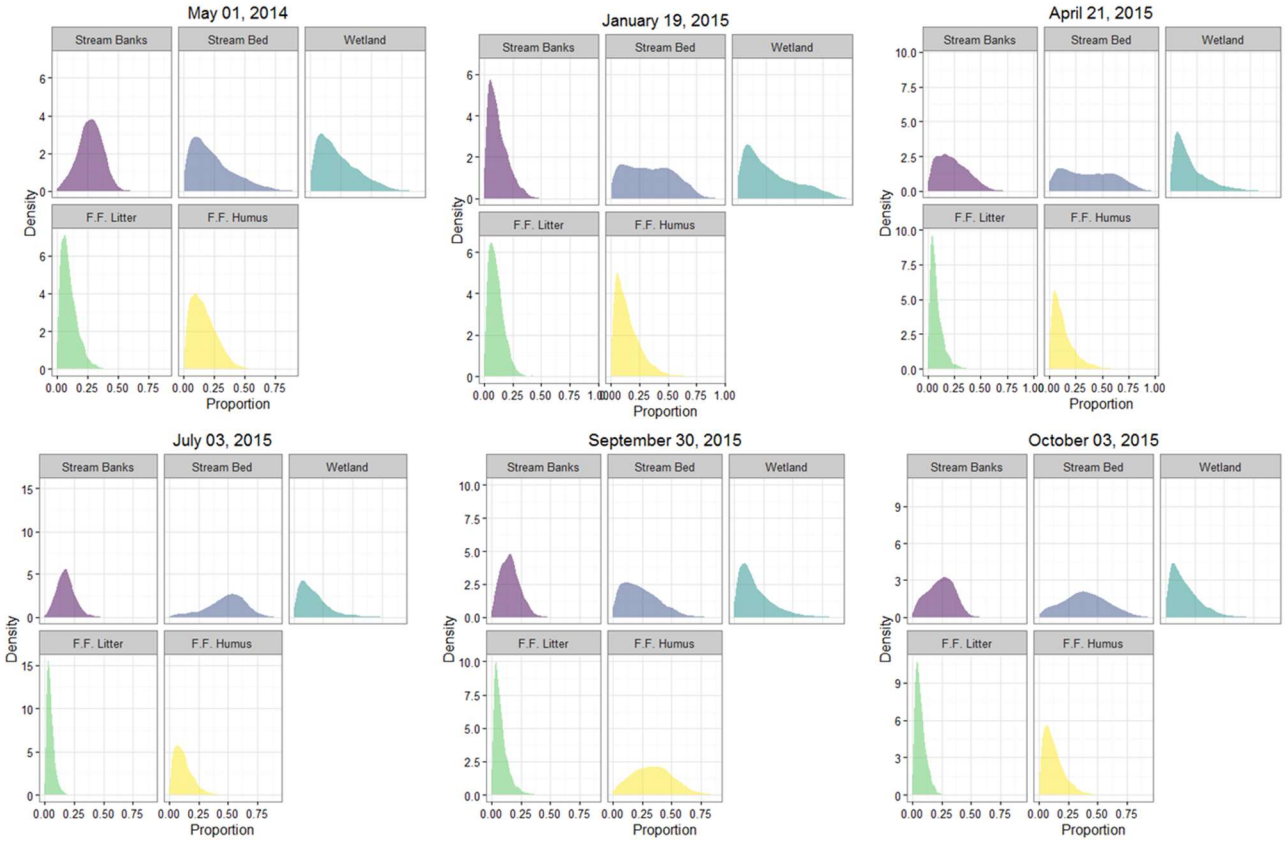

Figure C7: SIMMR posterior probability density distributions of proportional end member contributions to FPOM for each event averaged across five locations.

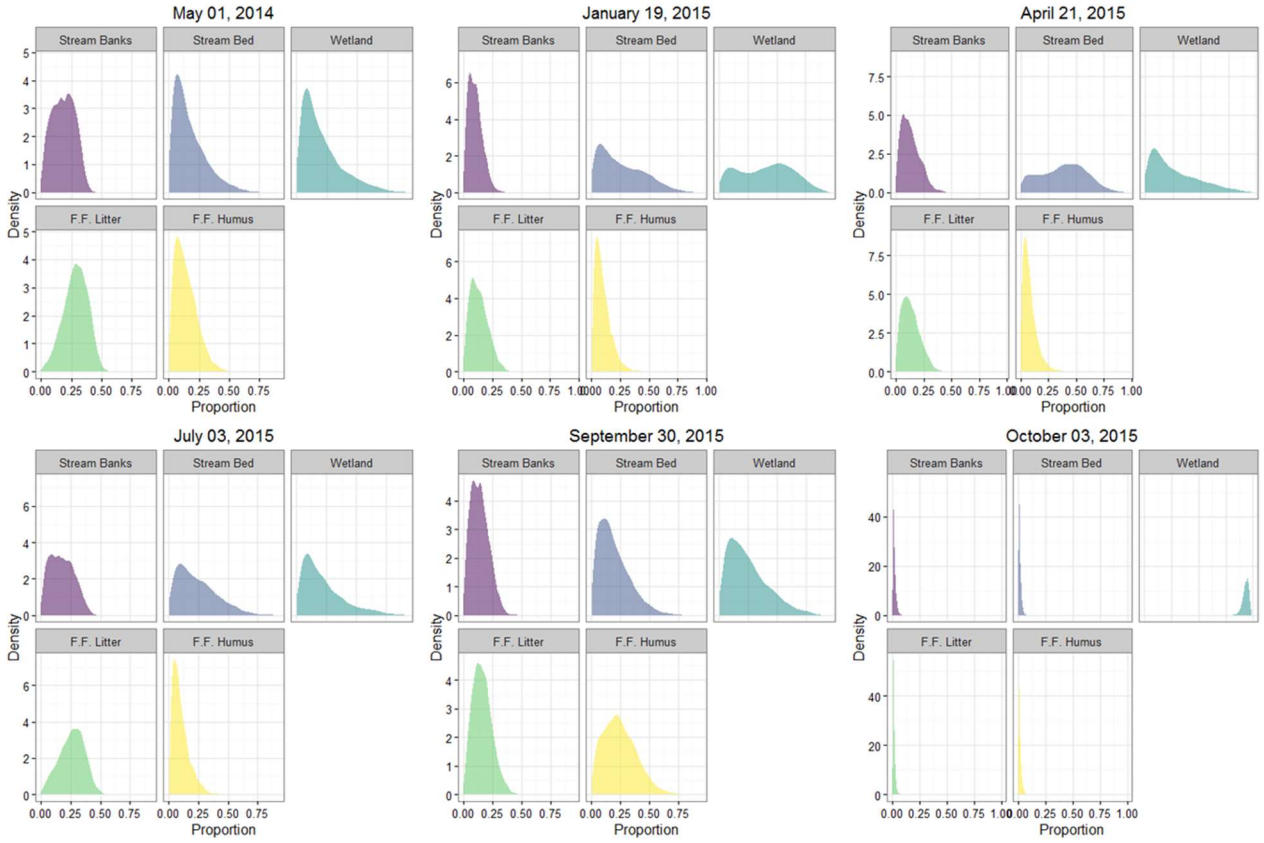

Figure C8: SIMMR posterior probability density distributions of proportional end member contributions to TPOM for each event averaged across five locations.

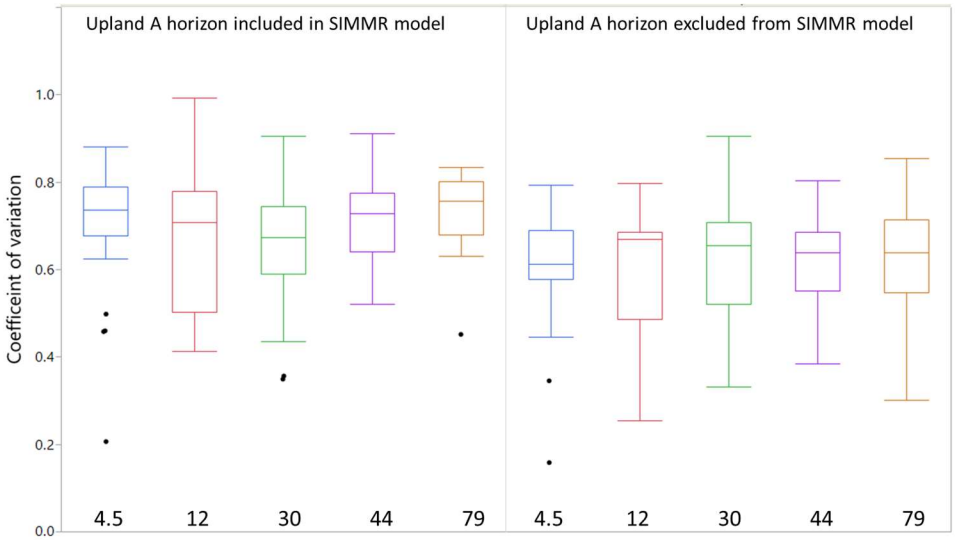

Figure C4 Distribution of coefficients of variation for each end member's contribution to total POM and POM of each size class at each drainage location. CV's of posterior distributions were generally lower when the model was run without upland A horizons, indicating this decreased model uncertainty.

Table C1: Statistics of SIMMR posterior distributions estimating POM source by particle size class for storm events 1 through 3. C.I. represents the 95 % credible interval.

		5/1/2014			1/19/2015			4/21/2015		
Size class	End Member	Mode	95 % CI Lower	95 % CI Upper	Mode	95 % CI Lower	95 % CI Upper	Mode	95 % CI Lower	95 % CI Upper
TPOM	F.F. Humus	0.073	0.006	0.324	0.049	0.004	0.214	0.044	0.008	0.243
TPOM	F.F. Litter	0.29	0.028	0.385	0.082	0.019	0.359	0.094	0.018	0.366
TPOM	Stream Bank	0.229	0.011	0.334	0.057	0.008	0.24	0.067	0.006	0.247
TPOM	Stream Bed	0.073	0.005	0.476	0.074	0.003	0.611	0.472	0.004	0.56
TPOM	Wetland	0.085	0.009	0.614	0.521	0.011	0.733	0.082	0.011	0.712
CPOM	F.F. Humus	0.07	0.006	0.481	0.054	0.005	0.446	0.053	0.004	0.453
CPOM	F.F. Litter	0.364	0.023	0.553	0.106	0.012	0.561	0.107	0.104	0.627
CPOM	Stream Bank	0.055	0.007	0.263	0.054	0.006	0.31	0.055	0.008	0.233
CPOM	Stream Bed	0.062	0.006	0.458	0.064	0.007	0.491	0.081	0.008	0.347
CPOM	Wetland	0.065	0.006	0.571	0.068	0.006	0.565	0.089	0.007	0.445
MPOM	F.F. Humus	0.097	0.004	0.323	0.069	0.004	0.37	0.043	0.007	0.317
MPOM	F.F. Litter	0.168	0.019	0.389	0.081	0.011	0.488	0.083	0.035	0.379
MPOM	Stream Bank	0.079	0.004	0.318	0.061	0.007	0.31	0.058	0.006	0.277
MPOM	Stream Bed	0.073	0.009	0.545	0.085	0.003	0.502	0.098	0.005	0.502
MPOM	Wetland	0.075	0.011	0.7	0.095	0.011	0.66	0.088	0.016	0.717
FPOM	F.F. Humus	0.076	0.004	0.403	0.061	0.005	0.257	0.047	0.004	0.392
FPOM	F.F. Litter	0.053	0.006	0.222	0.055	0.006	0.249	0.043	0.005	0.202
FPOM	Stream Bank	0.296	0.01	0.321	0.056	0.007	0.306	0.194	0.008	0.328
FPOM	Stream Bed	0.087	0.011	0.607	0.086	0.01	0.537	0.096	0.013	0.676
FPOM	Wetland	0.096	0.006	0.683	0.087	0.016	0.768	0.062	0.007	0.671

Table C2: Statistics of SIMMR posterior distributions estimating POM source by particle size class for storm events 4-6. C.I. represents the 95 % credible interval.

		7/3/2015			9/30/2015			10/3/2015		
Size class	End Member	Mode	95 % CI Lower	95 % CI Upper	Mode	95 % CI Lower	95 % CI Upper	Mode	95 % CI Lower	95 % CI Upper
TPOM	F.F. Humus	0.047	0.047	0.047	0.224	0.006	0.423	0.008	x	x
TPOM	F.F. Litter	0.285	0.285	0.285	0.123	0.026	0.358	0.007	x	x
TPOM	Stream Bank	0.089	0.089	0.089	0.087	0.014	0.329	0.008	x	x
TPOM	Stream Bed	0.1	0.1	0.1	0.117	0.009	0.442	0.007	x	x
TPOM	Wetland	0.09	0.09	0.09	0.109	0.008	0.572	0.952	x	x
CPOM	F.F. Humus	0.067	0.067	0.067	0.062	0.008	0.619	0.067	0.005	0.395
CPOM	F.F. Litter	0.358	0.358	0.358	0.415	0.008	0.49	0.061	0.003	0.559
CPOM	Stream Bank	0.061	0.061	0.061	0.108	0.008	0.302	0.082	0.007	0.434
CPOM	Stream Bed	0.064	0.064	0.064	0.074	0.005	0.433	0.074	0.006	0.585
CPOM	Wetland	0.079	0.079	0.079	0.099	0.008	0.521	0.074	0.007	0.618
MPOM	F.F. Humus	0.077	0.077	0.077	0.234	0.007	0.457	0.19	0.02	0.588
MPOM	F.F. Litter	0.213	0.213	0.213	0.169	0.008	0.301	0.242	0.015	0.319
MPOM	Stream Bank	0.059	0.059	0.059	0.127	0.008	0.378	0.195	0.007	0.222
MPOM	Stream Bed	0.073	0.073	0.073	0.173	0.006	0.607	0.067	0.01	0.428
MPOM	Wetland	0.088	0.088	0.088	0.101	0.004	0.623	0.081	0.009	0.533
FPOM	F.F. Humus	0.061	0.061	0.061	0.39	0.006	0.337	0.054	0.007	0.298
FPOM	F.F. Litter	0.032	0.032	0.032	0.036	0.004	0.19	0.045	0.006	0.21
FPOM	Stream Bank	0.174	0.174	0.174	0.152	0.04	0.522	0.296	0.021	0.378
FPOM	Stream Bed	0.539	0.539	0.539	0.121	0.008	0.703	0.379	0.012	0.651
FPOM	Wetland	0.073	0.073	0.073	0.072	0.005	0.448	0.065	0.008	0.582

Table C3: Statistics of SIMMR posterior distributions estimating POM source by particle size class for the 4.5, 12 and 20 ha locations. C.I. represents the 95 % credible interval.

		4.5 ha			12 ha			30 ha		
Size class	End Member	Mode	95 % CI Lower	95 % CI Upper	Mode	95 % CI Lower	95 % CI Upper	Mode	95 % CI Lower	95 % CI Upper
TPOM	F.F. Humus	0.093	0.009	0.331	0.04	0.004	0.212	0.056	0.005	0.234
TPOM	F.F. Litter	0.236	0.03	0.389	0.174	0.012	0.354	0.221	0.024	0.369
TPOM	Stream Bank	0.143	0.021	0.347	0.061	0.004	0.243	0.062	0.005	0.248
TPOM	Stream Bed	0.091	0.009	0.471	0.07	0.005	0.62	0.085	0.005	0.569
TPOM	Wetland	0.109	0.011	0.599	0.084	0.005	0.72	0.103	0.015	0.7
CPOM	F.F. Humus	0.059	0.007	0.219	0.045	0.007	0.228	0.049	0.005	0.419
CPOM	F.F. Litter	0.424	0.254	0.573	0.288	0.059	0.458	0.357	0.08	0.576
CPOM	Stream Bank	0.098	0.011	0.246	0.166	0.014	0.356	0.048	0.006	0.242
CPOM	Stream Bed	0.083	0.008	0.387	0.079	0.006	0.551	0.076	0.004	0.439
CPOM	Wetland	0.073	0.008	0.44	0.079	0.004	0.599	0.08	0.007	0.543
MPOM	F.F. Humus	0.054	0.006	0.34	0.055	0.003	0.376	0.069	0.008	0.301
MPOM	F.F. Litter	0.203	0.024	0.4	0.189	0.021	0.522	0.202	0.049	0.364
MPOM	Stream Bank	0.061	0.005	0.308	0.057	0.009	0.306	0.048	0.007	0.251
MPOM	Stream Bed	0.073	0.01	0.544	0.078	0.006	0.497	0.082	0.004	0.501
MPOM	Wetland	0.089	0.006	0.708	0.09	0.007	0.663	0.12	0.011	0.71
FPOM	F.F. Humus	0.316	0.01	0.607	0.048	0.005	0.233	0.051	0.004	0.314
FPOM	F.F. Litter	0.059	0.006	0.221	0.103	0.013	0.275	0.041	0.004	0.151
FPOM	Stream Bank	0.277	0.022	0.458	0.106	0.008	0.333	0.093	0.012	0.311
FPOM	Stream Bed	0.071	0.003	0.459	0.076	0.004	0.461	0.333	0.015	0.643
FPOM	Wetland	0.064	0.005	0.412	0.293	0.016	0.787	0.278	0.009	0.664

Table C4: Statistics of SIMMR posterior distributions estimating POM source by particle size class for the 44 and 79 ha locations. C.I. represents the 95 % credible interval.

		44 ha			79 ha		
Size class	End Member	Mode	95 % CI Lower	95 % CI Upper	Mode	95 % CI Lower	95 % CI Upper
TPOM	F.F. Humus	0.071	0.006	0.301	0.15	0.018	0.427
TPOM	F.F. Litter	0.158	0.016	0.343	0.204	0.021	0.361
TPOM	Stream Bank	0.263	0.029	0.41	0.178	0.014	0.329
TPOM	Stream Bed	0.09	0.011	0.517	0.083	0.011	0.439
TPOM	Wetland	0.101	0.005	0.589	0.093	0.007	0.561
CPOM	F.F. Humus	0.071	0.007	0.481	0.069	0.004	0.407
CPOM	F.F. Litter	0.212	0.01	0.467	0.278	0.026	0.51
CPOM	Stream Bank	0.083	0.011	0.315	0.059	0.011	0.283
CPOM	Stream Bed	0.079	0.007	0.481	0.069	0.008	0.488
CPOM	Wetland	0.083	0.007	0.602	0.091	0.009	0.593
MPOM	F.F. Humus	0.073	0.004	0.331	0.528	0.112	0.778
MPOM	F.F. Litter	0.137	0.017	0.312	0.027	0.003	0.15
MPOM	Stream Bank	0.124	0.015	0.361	0.14	0.006	0.309
MPOM	Stream Bed	0.09	0.006	0.587	0.063	0.006	0.399
MPOM	Wetland	0.087	0.008	0.675	0.053	0.007	0.364
FPOM	F.F. Humus	0.088	0.011	0.35	0.116	0.01	0.387
FPOM	F.F. Litter	0.028	0.005	0.135	0.042	0.005	0.174
FPOM	Stream Bank	0.286	0.091	0.5	0.274	0.095	0.461
FPOM	Stream Bed	0.486	0.012	0.709	0.195	0.009	0.617
FPOM	Wetland	0.056	0.004	0.374	0.066	0.007	0.407

Appendix D

PARTICLE SIZE DISTRIBUTIONS BY DRAINAGE LOCATION FOR SELECTED EVENTS

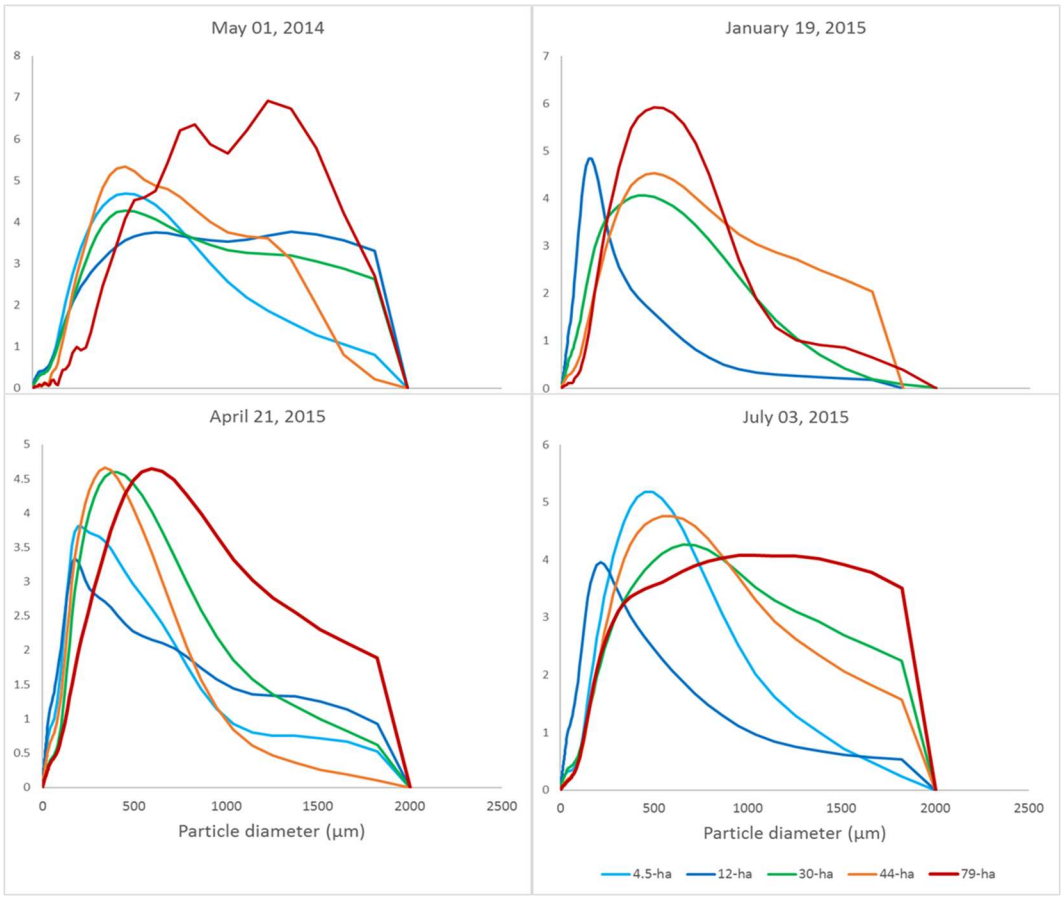

Figure D1: Probability distributions of particle size measured by laser diffraction at five drainage areas for four events.

Appendix E

POC YIELDS BY STORM EVENT METRICS

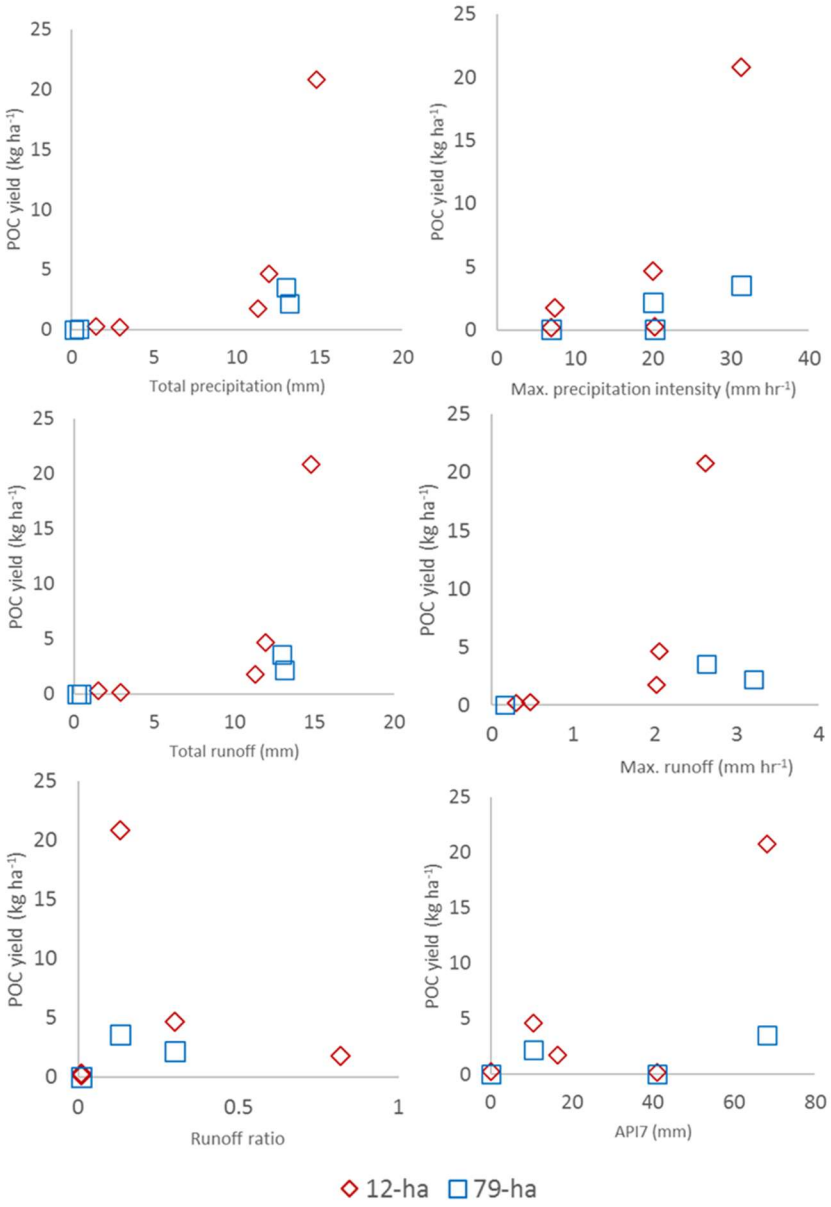

Figure E1 POC yields for the 12- and 79-ha catchments plotted against events' hydro-climatic metrics.